

#1

Document N^o 21100-70004
Revision Date ~~OCT 01 1999~~
Release Date: _____



16665 Space Center Boulevard
Houston, TX 77058

**RTIEE:
ROBOTIC TANK INSPECTION
END EFFECTOR**

**RECEIVED
JAN 05 2001
OSTI**

Contract Number:
DE-AR21-93MC30363

Final Report
For period July 1995-July 1999

For: U.S. Department of Energy

Prepared by:

Rachel Landry
Rachel Landry, Project Engineer

Approved by:

Reg Beer
Reg Beer, Project Manager

Reg Beer for
Kent Copeland, Program Manager

ACQUISITION & ASSISTANCE
1999 OCT - 8 A 11: 04
USDOE-FETC

PROCESSED FROM BEST AVAILABLE COPY

Disclaimer

This work was performed for the Federal Energy Technology Center (FETC) and sponsored by the US Department of Energy, Office of Technology Development.

Reference herein to any specific commercial product, process, or service by trade name, trademark, manufacturer, or otherwise, does not constitute or imply its endorsement by the United States Government or Oceaneering Space Systems.

DISCLAIMER

This report was prepared as an account of work sponsored by an agency of the United States Government. Neither the United States Government nor any agency thereof, nor any of their employees, make any warranty, express or implied, or assumes any legal liability or responsibility for the accuracy, completeness, or usefulness of any information, apparatus, product, or process disclosed, or represents that its use would not infringe privately owned rights. Reference herein to any specific commercial product, process, or service by trade name, trademark, manufacturer, or otherwise does not necessarily constitute or imply its endorsement, recommendation, or favoring by the United States Government or any agency thereof. The views and opinions of authors expressed herein do not necessarily state or reflect those of the United States Government or any agency thereof.

DISCLAIMER

Portions of this document may be illegible in electronic image products. Images are produced from the best available original document.

Change Log					
Rev. Ltr. Change Nº	Justification and Description of Change	Affected Pages	Effectivity (Serial Nº)	Release Date	Change Approval (Initial & Date)
IR	Initial Release	All		OCT 01 1999	

Note of Appreciation

OSS would like to extend its appreciation to Maria Vargas of FETC for supporting OSS in these endeavors. OSS would also like to thank the operators at INEEL for their guidance and expertise in deploying the RTIEE, especially into the radioactive storage tank in February 1999. Thanks especially to Cal Christensen, Mike Anderson, Brad Griebenow, and Chris Brown of INEEL and Allan Pardini of Hanford.

Abstract

The objective of this contract between Oceaneering Space Systems (OSS) and the Department of Energy (DoE) was to provide a tool for the DoE to inspect the inside tank walls of underground radioactive waste storage tanks in their tank farms. Some of these tanks are suspected to have leaks, but the harsh nature of the environment within the tanks precludes human inspection of tank walls. As a result of these conditions only a few inspection methods can fulfill this task. Of the methods available, OSS chose to pursue Alternating Current Field Measurement (ACFM), because it does not require clean surfaces for inspection, nor any contact with the surface being inspected, and introduces no extra by-products in the inspection process (no coupling fluids or residues are left behind).

The tool produced by OSS is the Robotic Tank Inspection End Effector (RTIEE), which is initially deployed on the tip of the Light Duty Utility Arm (LDUA). The RTIEE combines ACFM with a color video camera for both electromagnetic and visual inspection. The complete package consists of an end effector, its corresponding electronics and software, and a user's manual to guide the operator through an inspection. The system has both coarse and fine inspection modes and allows the user to catalog defects and suspected areas of leakage in a database for further examination, which may lead to emptying the tank for repair, decommissioning, etc.). The following is an updated report to OSS document OSS-21100-7002, which was submitted in 1995.

During the course of the contract, two related subtasks arose, the Wall and Coating Thickness Sensor and the Vacuum Scarifying and Sampling Tool Assembly. The first of these subtasks was intended to evaluate the corrosion and wall thinning of 55-gallon steel drums. The second was retrieved and characterized the waste material trapped inside the annulus region of the underground tanks on the DoE's tank farms. While these subtasks were derived from the original intent of the contract, the focus remains on the RTIEE.

Table of Contents

Change Log	i
Abstract	iii
Table of Contents.....	iv
List of Figures.....	iv
1.0 Introduction.....	1
1.1 RTIEE: Robotic Tank Inspection End Effector	1
1.2 Wall and Coating Thickness Sensor	4
1.3 VSSTA: Vacuum Scarifying Sampling Tool Assembly.....	5
1.4 Summary	5
2.0 Objective.....	6
3.0 Operational Overview	7
3.1 RTIEE	7
3.2 VSSTA.....	12
4.0 Contract Milestones/Accomplishments.....	15
4.1 RTIEE	15
4.2 VSSTA.....	21
5.0 Future Applications.....	22
Appendix A: Original Draft Final Report for Robotic End Effector for Inspection of Storage Tanks.....	A-1
Appendix B: Wall and Coating Thickness Sensor Measurement Test Summary	B-1
Introduction	B-1
Test Description.....	B-2
Conclusions	B-5

List of Figures

Figure 1.1.1: Photo of Robotic Tank Inspection End Effector.....	2
Figure 1.1.2 (a)	2
Figure 1.1.2 (b).....	3
Figure 1.2:	4
Figure 3.1.1: Software As It Appears Upon Startup of the System.....	8
Figure 3.1.2 (a):	9
Figure 3.1.2 (b).....	9
Figure 3.1.3 (a)	10
Figure 3.1.3 (b).....	10
Figure 3.1.4:	11
Figure 3.2.1 (e-i).....	13
Figure 4.1.1: Robotic End Effector Powered Up on LDUA at Hanford.....	15
Figure 4.1.2 (a)	16
Figures 4.1.2 (b).....	17
Figure 4.1.3 (a)	18
Figure 4.1.3 (b).....	19

Figure 4.1.3 (c)	18
Figure 4.1.3 (d)	19
Figure 4.1.3 (e)	19
Figure 4.1.3 (f).....	20
Figure 4.1.3 (g).....	20
Figure B-1: Test Configuration for wall thickness measurement.....	B-2
Figure B-2:	B-3
Figure B-3:	B-4
Figure B-4:	B-5

1.0 Introduction

Oceanering Space Systems (OSS) entered into a contract (DE-AR21-93MC30363) with the Department of Energy (DoE) in October 1993 to develop a robotic end effector for non-destructive evaluation (NDE) and visual inspection of underground waste storage tanks. This report is an update to submittal (OSS-21100-7002), to reflect the end effector modifications/evolution and two recent subtasks, which materialized under the same contract. These subtasks were the Wall and Coating Thickness Sensor and the Vacuum Scarifying Sampling Tool Assembly (VSSTA). The previous report is included as an appendix.

1.1 RTIEE: Robotic Tank Inspection End Effector

The Robotic Tank Inspection End Effector (RTIEE) project was initiated in 1993 in a contract between OSS and the DoE to inspect radioactive waste tanks at various waste storage sites. During the five-year duration of the project, the scope was redefined from detecting small surface breaking defects, such as pits and cracks in stainless and carbon steel tank walls, to larger defects of the same type, which were of greater concern due to tank leakage issues. The electromagnetic inspection method used in RTIEE remained unchanged, so any description or definition of this method may be understood by referring to the previous report, OSS document number 21100-70002 (Appendix A).

The current defect sizing range is from a minimum of 0.25" in length by 0.25" deep to a maximum of 2.5" in length by 0.125" deep. Accuracy requirements for the entire range are about 10%. Cracks outside this range (smaller and larger) can be detected, but are outside the model's range in the current algorithm implementation and thus cannot be sized reliably. Smaller or larger defects can be sized using a different sensor coil configuration, and in the first generation of RTIEE, the flaws detected and sized were as small as 0.125" long by 0.125" deep. The end effector has also been radiation hardened for exposure up to 1.0×10^6 rad and has an operational temperature range of 0 to 50° C. Additionally, it is slightly positively pressurized (less than 1 psi) to perform inspections below the liquid waste level.

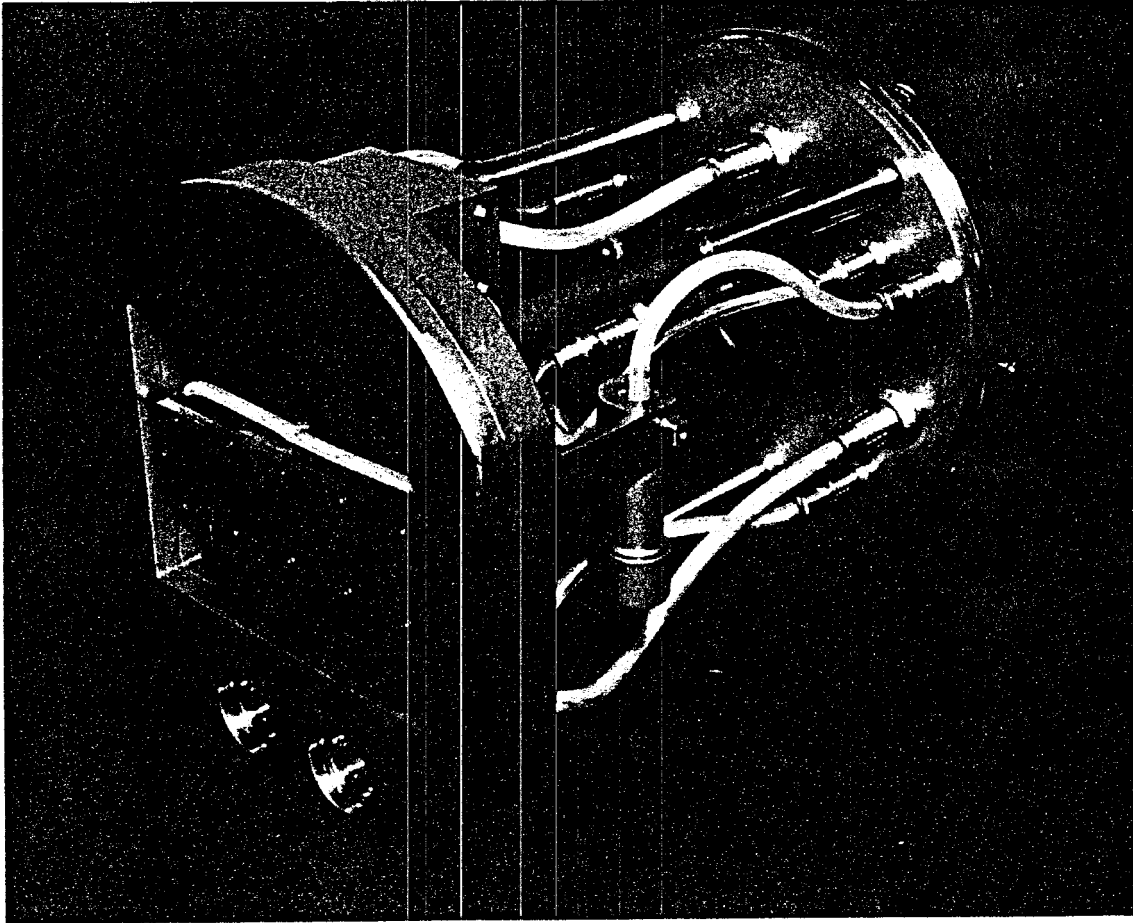


Figure 1.1.1: Photo of Robotic Tank Inspection End Effector

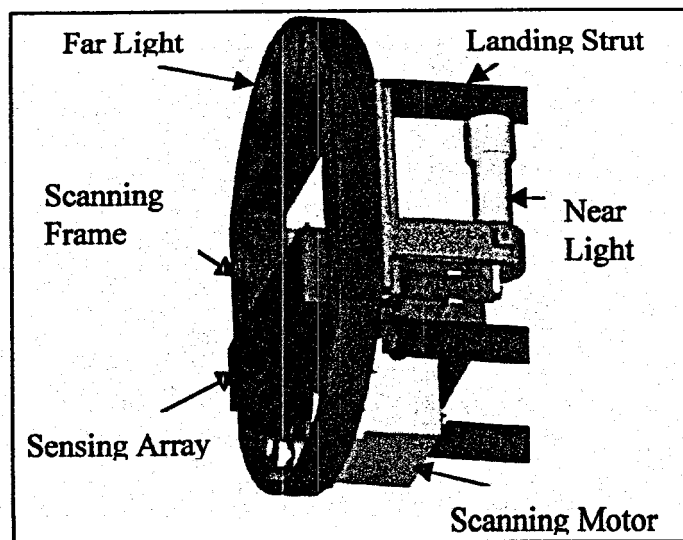


Figure 1.1.2 (a)

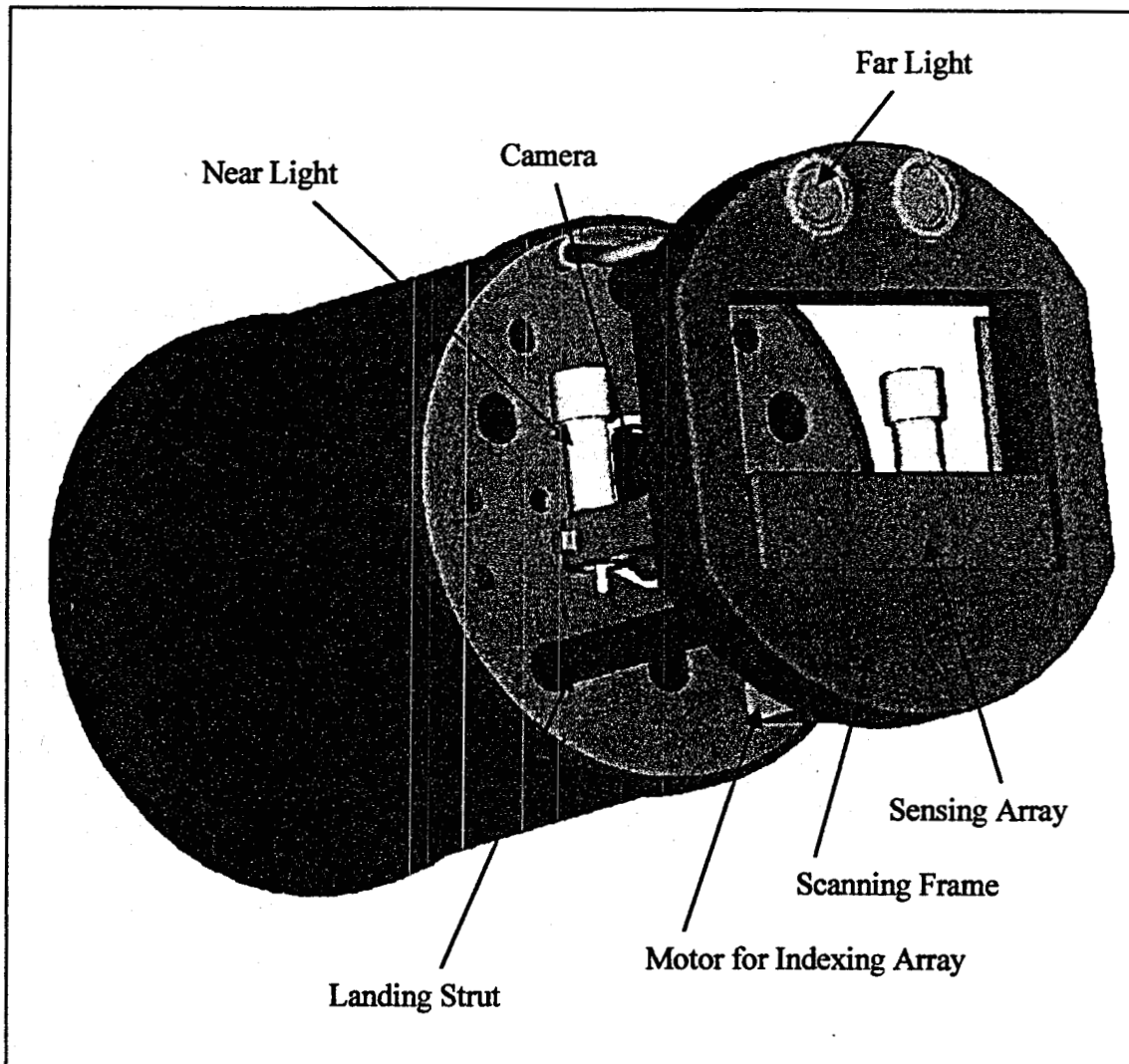


Figure 1.1.2 (b)

Figure 1.1.2: RTIEE 3-dimensional model showing the end effector's current configuration. The RTIEE has an outside diameter of 10.5", is 19.4" in length, and weighs approximately 45 lbs. (a) The front pancake-shaped portion of the end effector is the scanning frame. The front face of the frame has been removed here so that some of the inner components of the cable drive assembly can be seen. Visible here are the scanning sensor head (containing the arrays of sensing/inducting coils), the motor driving the cable motion, and the near and far light locations. Also inside the scanning frame are the three standoff sensors (not shown) in a triangular configuration. (b) The larger view shows the entire end effector without connectors. The large cylinder contains the color camera and its controller, along with other electronics, such as the multiplexing and standoff sensor circuitry. These electronics are radiation hardened Mil-spec parts. For more information, refer to Appendix A.

1.2 Wall and Coating Thickness Sensor

The first subtask within the RTIEE DOE contract was a wall and coating thickness sensor. The purpose of this sensor system was to determine wall thickness and coating thickness of metal samples. The test summary for this system is included as Appendix B. The sensor was based on the same general principle as ACFM, using electromagnetic induction and eddy current decay as an indicator of the thickness of stainless steel, carbon steel, and aluminum.

The scope of this effort was to evaluate the corrosion and/or general wall thinning of metal barrels of waste at a DOE waste storage site. The barrels are 55-gallon drums, some of which contain unknown wastes (contaminated equipment/protective garments, chemicals/by-products in liquid and solid form, etc.), residing in large warehouse-type storage locations. The system was in prototype stages and analytical models were under evaluation for the 55-gallon drum application, however the task was put on hold as RTIEE became a higher priority. The prototype unit consists of an ACFM "sensor gun" connected by umbilical to a portable battery-powered computer for collecting and storing inspection data. The ACFM "sensor gun" consists of the ACFM sensor electronics embedded within an automobile timing light. The tip of the "sensor gun" is to be placed against a barrel in order to collect the ACFM signal data. Analysis of the data would be performed by saving it to disk and importing it later into a database such as Excel for plotting. There was speculation that a final working unit could be as small and compact as possible, and that the computer could be incorporated into some type of backpack for ease of use and transport.

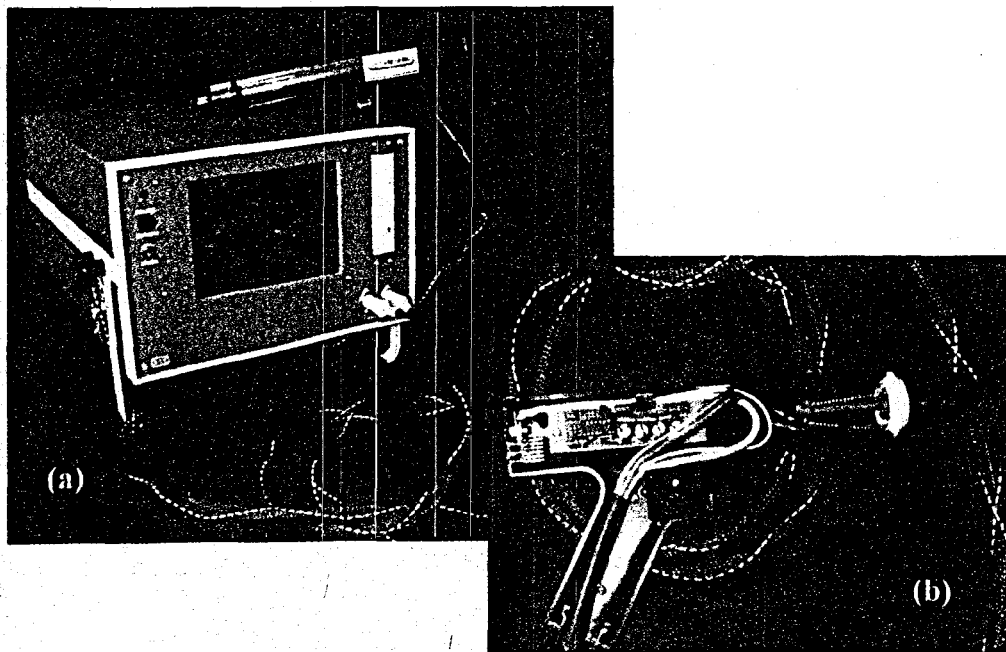


Figure 1.2:

Figure 1.2: Photographs of (a) 55-gallon drum inspection prototype unit. The pulsed eddy current sensor/inductor coils reside in the (b) gun-shaped housing for data collection. The coils (one coaxial inside the other) are spring-biased to maintain constant contact as they are pressed against the barrel to be inspected. It should be noted that contact is not needed for inspection,

however, a consistent standoff distance from the sample material is necessary for quantitative analysis of surface defects. The actual inspection process is activated when the trigger is pulled. The LEDs at the back of the "inspection gun" are status indicators to let the user know the operational state of the tool during an inspection. For example, they would allow the user to determine when the equipment is ready to collect data and when data is being collected. They also indicate whether or not its coils remain in good contact while data is being taken, and when the data collection for a given location is complete; i.e., contact has been maintained continuously for an adequate amount of time to collect reliable data. See Appendix B for experimentation results.

1.3 VSSTA: Vacuum Scarifying Sampling Tool Assembly

The second of these subtasks is a sampling tool successfully deployed to collect waste in the annulus region of the large underground storage tanks at the Savannah River site. The annulus is the area between the inner and outer storage tank walls. The radioactive material in this region is described as 'salt cake'. For this application, a tool was needed to reach the floor of the annulus region. The resulting sampling tool designed and manufactured by OSS is made of eight (8) segments of aluminum pipe, which are assembled piecewise by operators at the tank farm and lowered into the tank. The tool has a camera mounted on the outside of the bottom segment to look down into the annulus as the tube is inserted. This is both for maneuvering the long tool and for visually assessing the general condition of the tank annulus. On the bottom segment of the tool are a scraping mechanism, some flaps to ensure that particulate remain trapped inside the tube as it is collected, and a cup to hold the captured salt cake particles. Each segment has o-rings and vacuum grease in the joint interfaces to allow pressurization of the entire tool assembly. Pressurization allows for vacuum generation at the end effector using the 'venturi' effect. In addition to the scraper-and-flap combination, vacuum suction is utilized to pull the salt cake particles up into the tool. Once the sample cup is full, a flag indicating a complete fill moves into the camera's view. The operator then simply removes the cup (after withdrawing the assembly from the tank annulus) and sends the cartridge to the laboratory for testing. A brief operational overview is given with photos in Section 3.2. Additional pictures are shown in Section 4.2.

1.4 Summary

The total value of the contract initiated to produce RTIEE was approximately \$2.4 million. This contract resulted in the technological development and delivery of both an ACFM end effector and a vacuum scarifying sampling tool specifically tailored to completing salt cake analysis in any DoE tank farm. To date, two successful hot tank deployments have been completed, one for RTIEE and one for VSSTA. Also, as a spin-off of the RTIEE, a potential implementation for pulsed eddy current wall coating and thickness technology was investigated for the application of inspecting 55-gallon steel drums.

Throughout the contract duration, the scope of the RTIEE was redefined slightly, however the technology remained unchanged. The two subtasks were of lower profile, however, the VSSTA was produced and delivered, thus both the VSSTA and the RTIEE will be discussed in the following sections. As the contract was primarily concerned with RTIEE, the discussion of the

VSSTA is brief. Due to the complexity of the RTIEE, the end effector discussion will be limited to its current configuration and functionality.

2.0 Objective

As mentioned in the Introduction, the objective of this project was to employ a single end effector on the DoE's Light Duty Utility Arm (LDUA) to perform both electromagnetic and visual inspection simultaneously. The result was an end effector, which employs both Alternating Current Field Measurement (ACFM) and a commercial color video camera. The end effector is accompanied by "user-friendly" software written at OSS to collect and analyze the inspection data. The software was originally written to analyze inspection data automatically, however, the software became more user-interactive at the customer's request. Once again, refer to Appendix A for a detailed explanation of ACFM, the electromagnetic inspection technology utilized by the RTIEE.

The VSSTA's objective was to develop and deploy a sample retrieval system. The objective of the Wall Coating Thickness Sensor was to inspect 55-gallon steel storage drum walls.

3.0 Operational Overview

3.1 RTIEE

There are two modes of operation for the RTIEE: flyby and stationary scan modes. Flyby mode is the coarser, more general mode of inspection. In flyby mode, the end effector is "flown" over the tank walls approximately one inch away from the surface. In flyby mode, defects can be detected and flagged for later observation or study, while simultaneously covering the inspection surface in real-time.

Once RTIEE has been used to flag potential defects in flyby mode, the end effector can be redirected to return to the site of a potential flaw and perform a more detailed scan. This more detailed scan is referred to as a stationary scan because the end effector is "landed" on the surface to be inspected. The scanner frame has a 3"X6" window for detecting and sizing flaws. If a defect is larger than this window, it is visible in the data, but not quantifiable. Stationary scans may be performed at various resolutions. Higher resolution is better for sizing smaller defects, but higher resolution scans create larger files and take longer to complete. The operator's manual which accompanies the RTIEE system offers guidelines on selecting scan options. Stationary scans along with the digitized image from the color camera may be saved and stored in a database corresponding to the tank in which it is created. Tank wall "maps" are created using flyby mode, and defects may be studied and cataloged using stationary scan mode.

In flyby mode, the standoff sensors integrated in the end effector allow the operator to maintain a constant distance from tank walls. In general, 1/2" to 3/4" is ideal for accurate readings from the standoff sensors. There are three standoff sensors which use the same principle of operation as the ACFM inspection hardware, however, they are not necessary for stationary scans, and are therefore only operational in flyby mode. In stationary scan mode, landing status indicators inform the operator when the end effector is in a suitable proximity to the tank wall surface.

Figure 3.1.1 shows the screen image as it appears upon startup of the system. Figure 3.1.2 is a screen image of a stationary scan performed on a stainless steel plate. The flaw is shown in the green/black window as a light and dark spot. This defect is easily sized by analysis with the software written for the RTIEE. The interface is user friendly and accompanied by a user's manual which outlines the procedures for scanning in both flyby and stationary scan modes. The software can also be used to catalog data and produce a database on any given tank so that any examined flaw can be easily accessed for future reference. Figure 3.1.3 shows the screen as it appears for flyby mode. Note the tank wall map region of the screen and the key, which describes the annotations available for indicating potential and confirmed flaws. This region of the screen toggles between ACFM signal data and the real-time camera view during flyby. Figure 3.1.4 shows the screen as it appears in analysis mode, where the flaw is selected within the rectangle.



Figure 3.1.1: Software As It Appears Upon Startup of the System

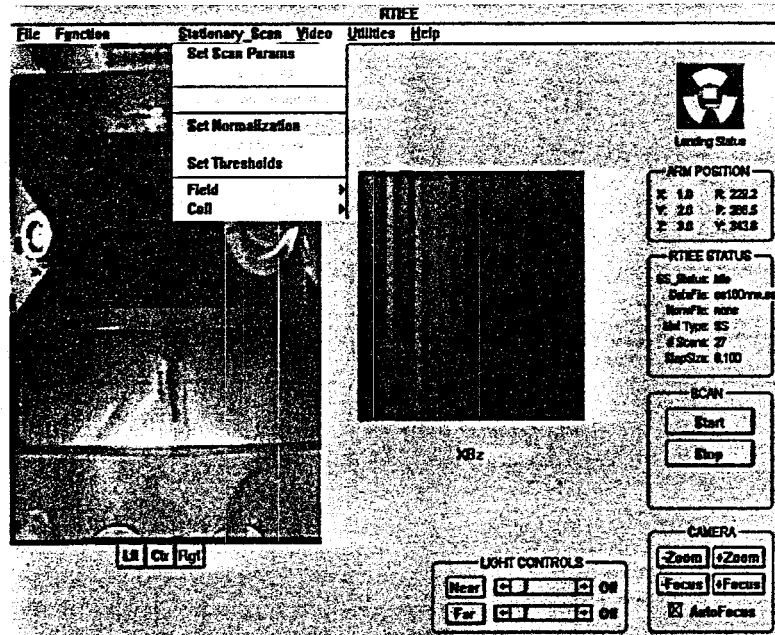


Figure 3.1.2 (a):

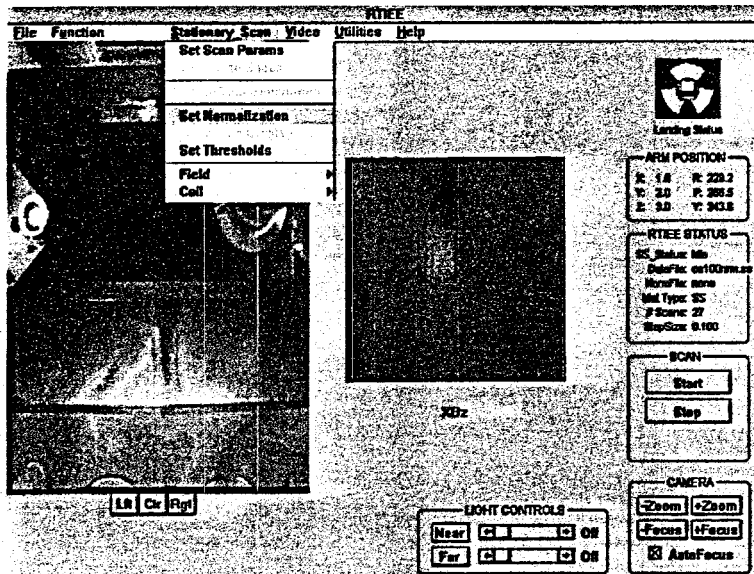


Figure 3.1.2 (b)

Figure 3.1.2: Stationary scan screen images. (a) The first image is that of a scan taken over a clean (known to be free of defects) area of stainless steel plate, showing only the variances among coil readings. This data is used to normalize other scans on the same material alloy, using the same scanning resolution. The value of the signal intensity in a normalization scan is essentially subtracted from subsequent scans to eliminate background variability and establish a consistent background value. (b) This scan shows a defect in the same stainless steel plate. It should be noted that using this technique, welds with good integrity are essentially invisible.

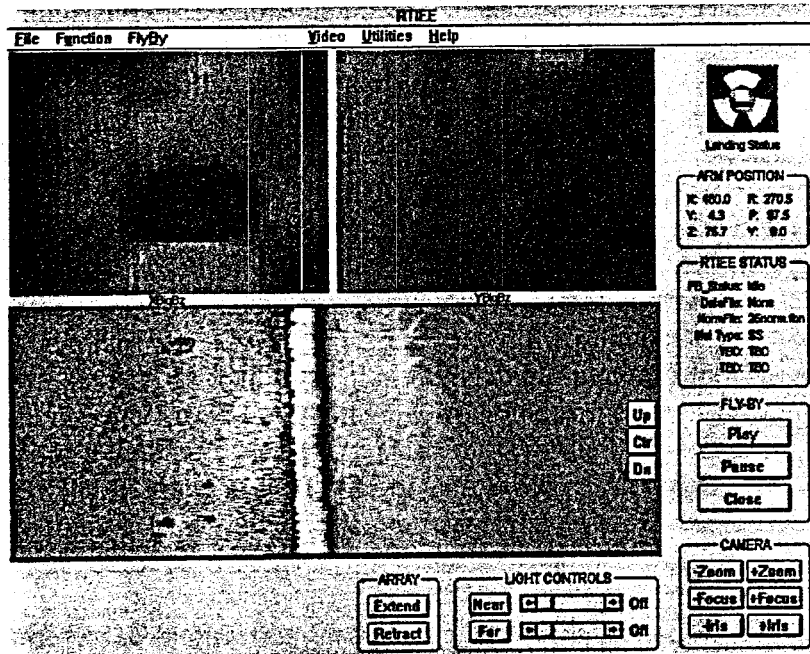


Figure 3.1.3 (a)

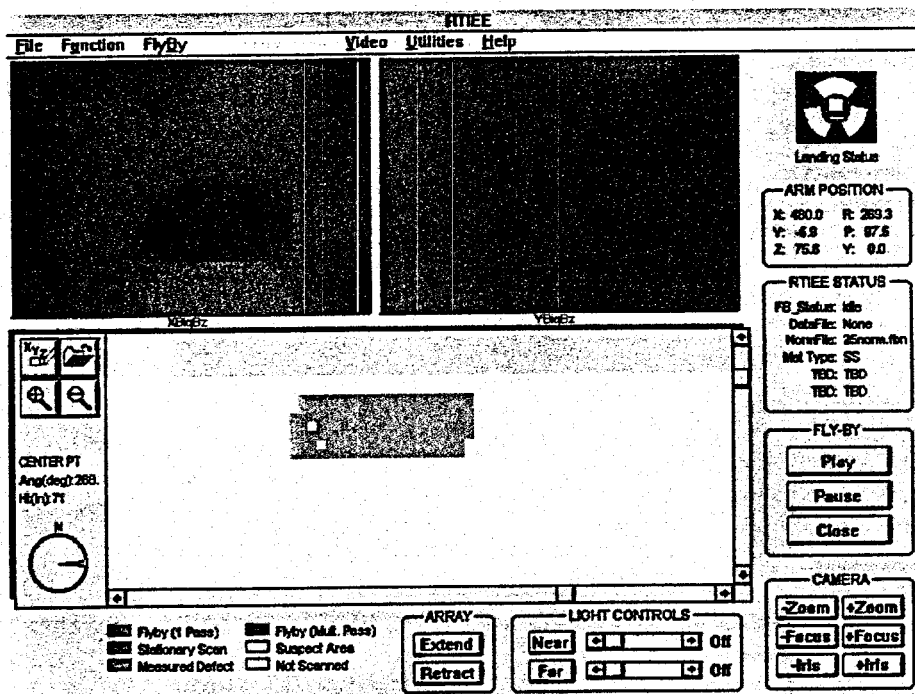


Figure 3.1.3 (b)

Figure 3.1.3: The user interface screen during flyby mode. The upper green/black windows display the ACFM signal intensities, with peak-trough pairs indicating defects in the sample. Note that the lower window can be toggled between the camera view and a tank wall map on which inspection progress status and potential/confirmed flaws can be seen.

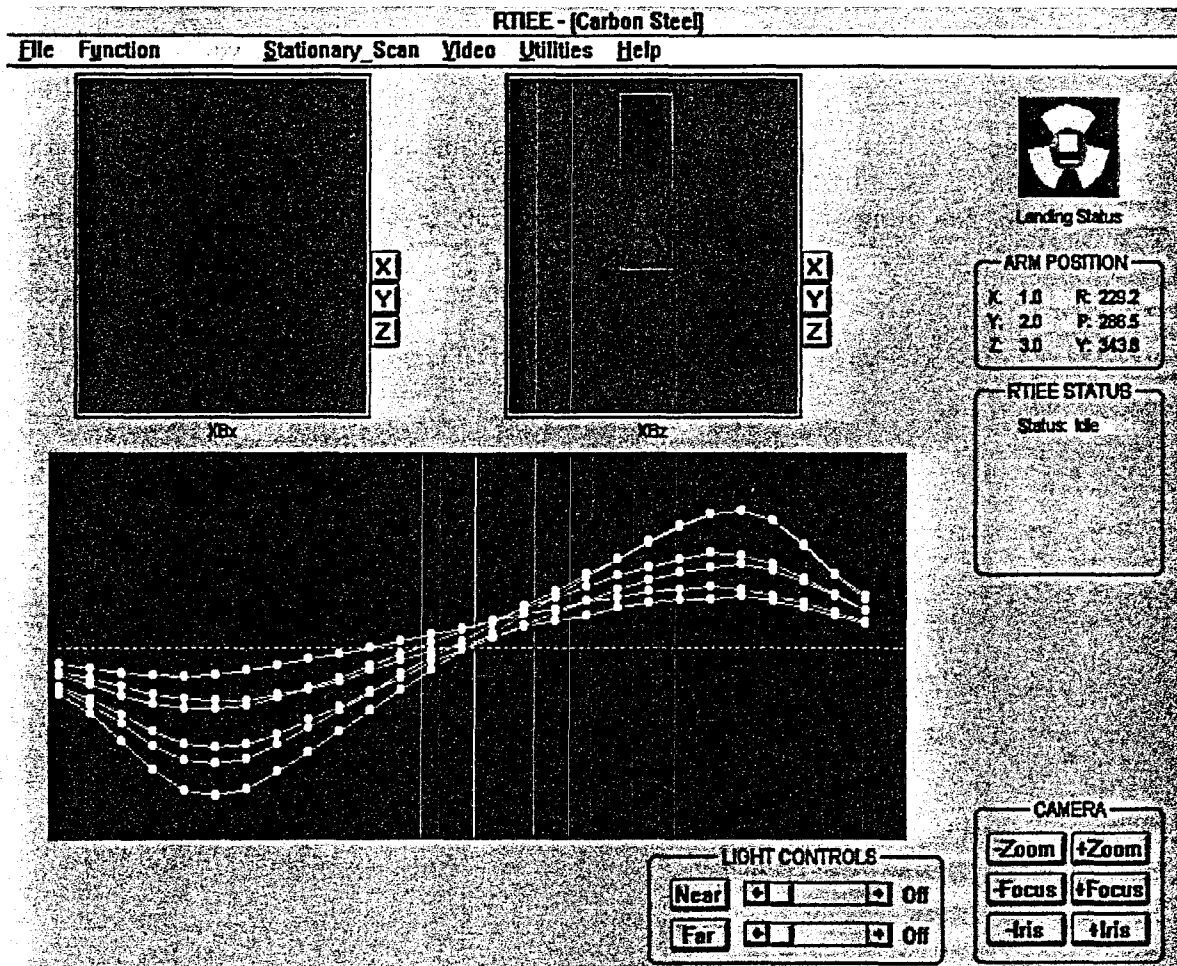


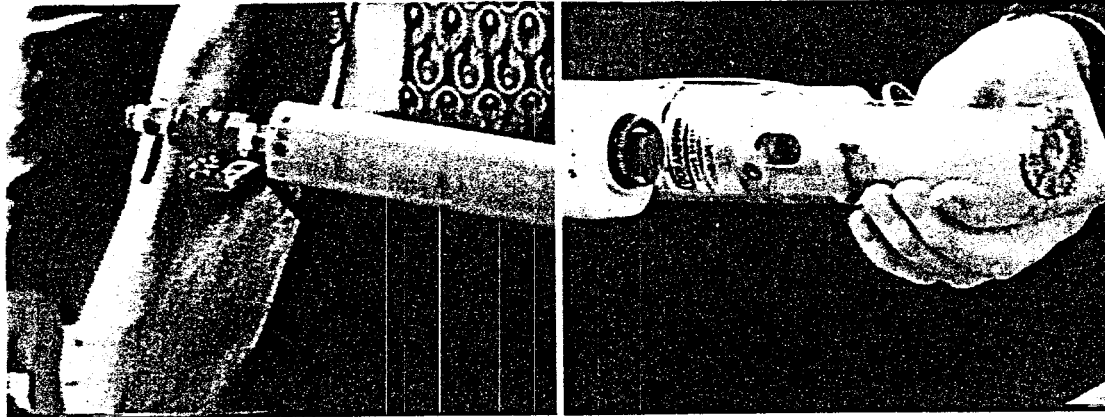
Figure 3.1.4:

Figure 3.1.4: Analysis screen as it appears in sizing flaws, which were inspected by completing a stationary scan. The upper green/black plots show the trough-peak pair in the XBz coil-field combination of the ACFM signal, while the peak-trough-peak signature of a flaw in the YBz coil-field combination is shown on the left. The flaw is selected within the rectangle in the right-hand. The graph underneath the intensity contours shows the intensity profile. Thus, the user gets both an “overhead” and a “side” view of the overall magnetic field surrounding a flaw in the green/black plots, and a corresponding intensity profile of the selected area (the area within the rectangle).

Both test operators and actual INEEL personnel have used the software and found it to be easy to use and effective for tank wall defect detection, characterization, and archival. Also, the color camera and integrated lighting proved helpful during actual tank deployment in verifying scanned data and in navigation to some degree (when combined with other cameras inside the tank).

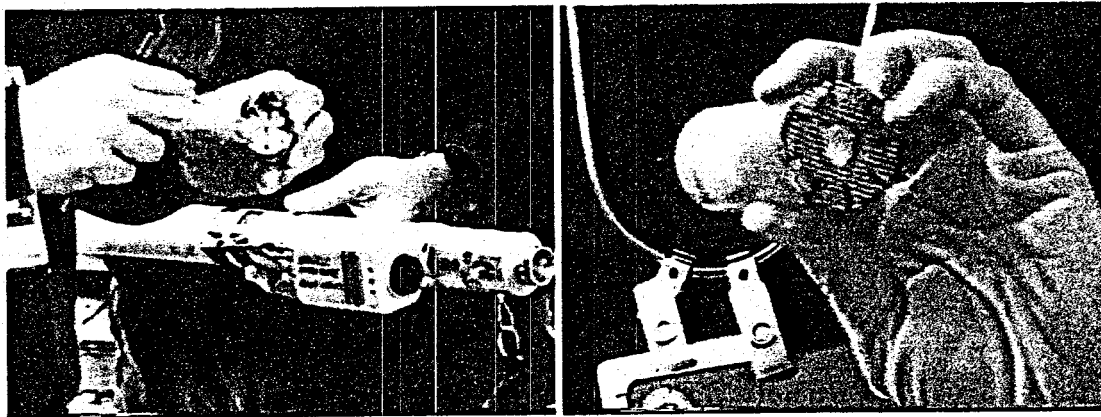
3.2 VSSTA

The Vacuum Scarifying Sampling Tool Assembly is a vacuum-powered tool that collects salt cake samples. An effective way to give an operational overview of this tool is to show its components and the final assembly in use. The following photos are excerpts taken from a documentation video of a cold test demonstration at the Savannah River Site.



(a)

(b)



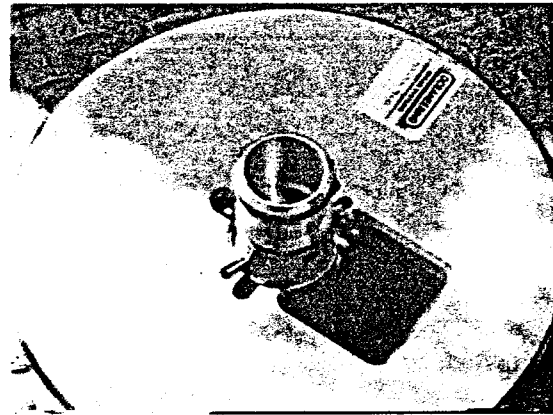
(c)

(d)

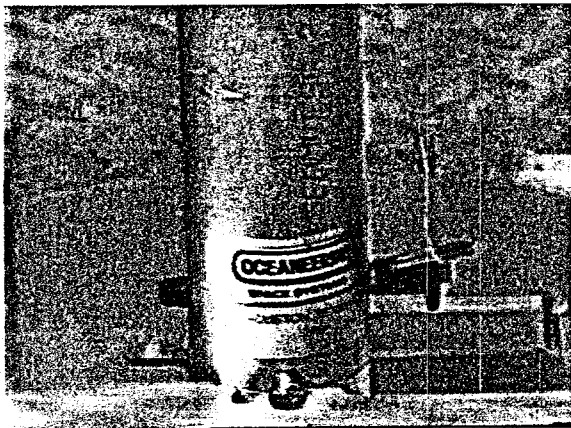
Figures 3.2.1 (a-d)



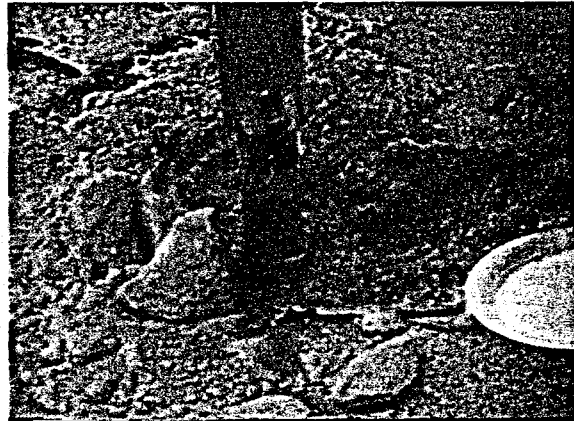
(e)



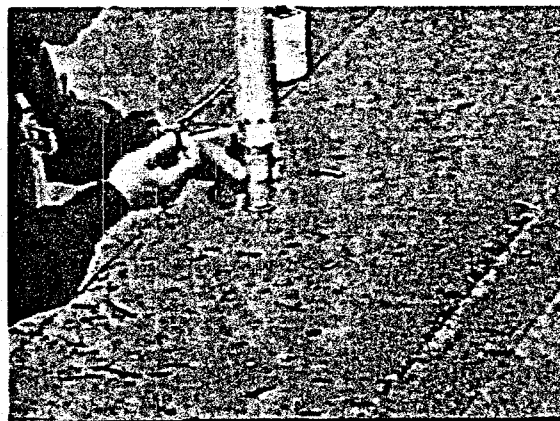
(f)



(g)



(h)



(i)

Figure 3.2.1 (e-i)

Figure 3.2.1 (a-i): These are photos of the Vacuum Scarifying Sampling Tool Assembly. The upper part of this tool assembly (a) has a compressed air inlet in order to create a venturi driven vacuum effect inside the tool to excavate small particles of salt cake as they are ground free. As seen in (b), the lower segment of the assembly contains the majority of the features of the tool,

including the retaining flaps (c), cup attachment (d), and the camera. The cup attachment (d) has a feature similar to a wire brush, which grinds up particles of the salt cake built up inside the annulus region of the underground storage tank. The particles are then pulled up into the tube by means of the vacuum and deposited into the sample cup. There are also radial metal flaps (not shown) inside the tip of this segment to keep the particles somewhat confined to the cup. The cup is removable so that the operator can send the sample to the laboratory for analysis. The color video camera serves as both a navigational and a visual aid while deploying the tool assembly. The tool assembly is composed of eight pressurized aluminum pipes, each approximately 5 feet in length. Figure 3.2.1 (e) shows the complete lower segment, as it would be placed through its retaining plate at the top of a tank platform riser. One of the segments is lowered through and the joint link is shown close up as it fits through the retaining plate (f) into the tank annulus. Each individual segment is sealed at its joint with an O-ring and some lubricant for pressurization, and the segments are linked together with quick release pass through retaining pins (g). The sampling tool was deployed (h) at the Savannah River site, where salt cake was broken up and the particulate captured into a cup. Photo (i) demonstrates the ease of which the sample cup may be removed for examination of its contents.

The VSSTA was deployed into the annulus of Tank 16 at Savannah River on June 3rd, 1998. It was very effective, and allowed sample characterization in support of tank closure. OSS hopes the tool can find use at other DoE sites as well.

4.0 Contract Milestones/Accomplishments

4.1 RTIEE

The RTIEE was successfully demonstrated in Hanford, Washington in 1996 on the LDUA. The next step was to convert the sensitive components of the end effector to radiation hardened components. This was completed during the following few months and more testing was performed to characterize the RTIEE's performance. Figures 4.1.1 and 4.1.2 (a, b) show photographs taken during the cold test deployment at Hanford.

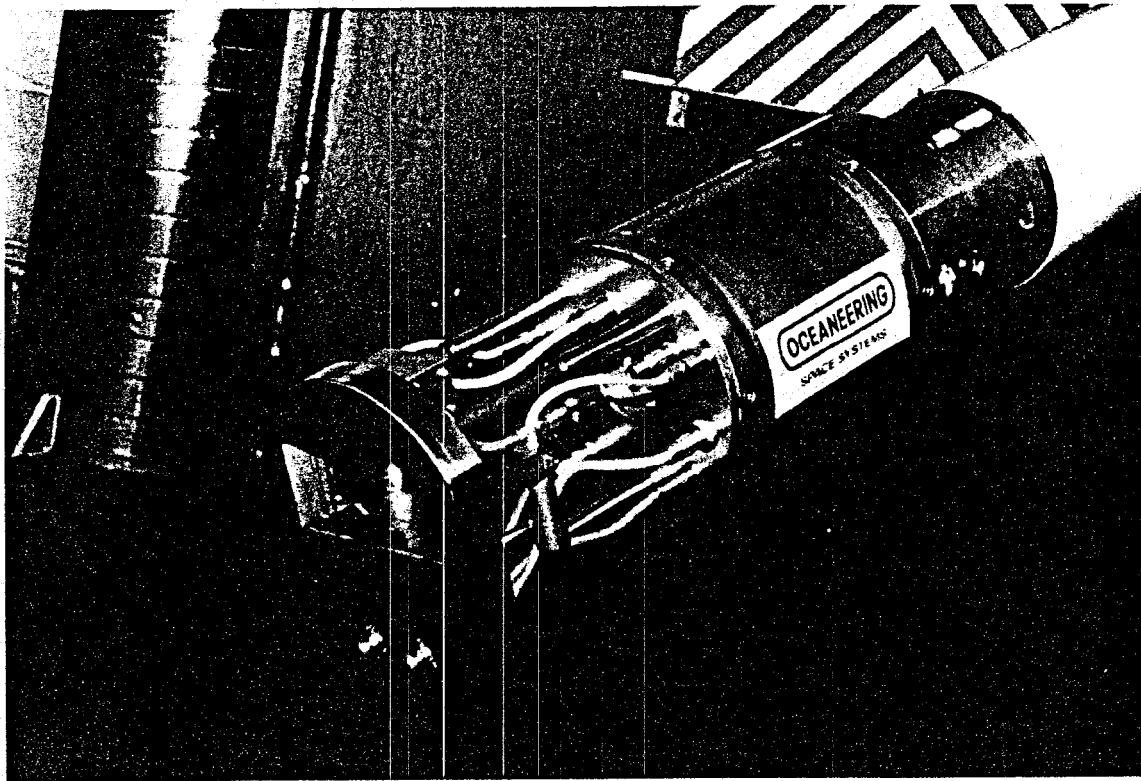


Figure 4.1.1: Robotic End Effector Powered Up on LDUA at Hanford

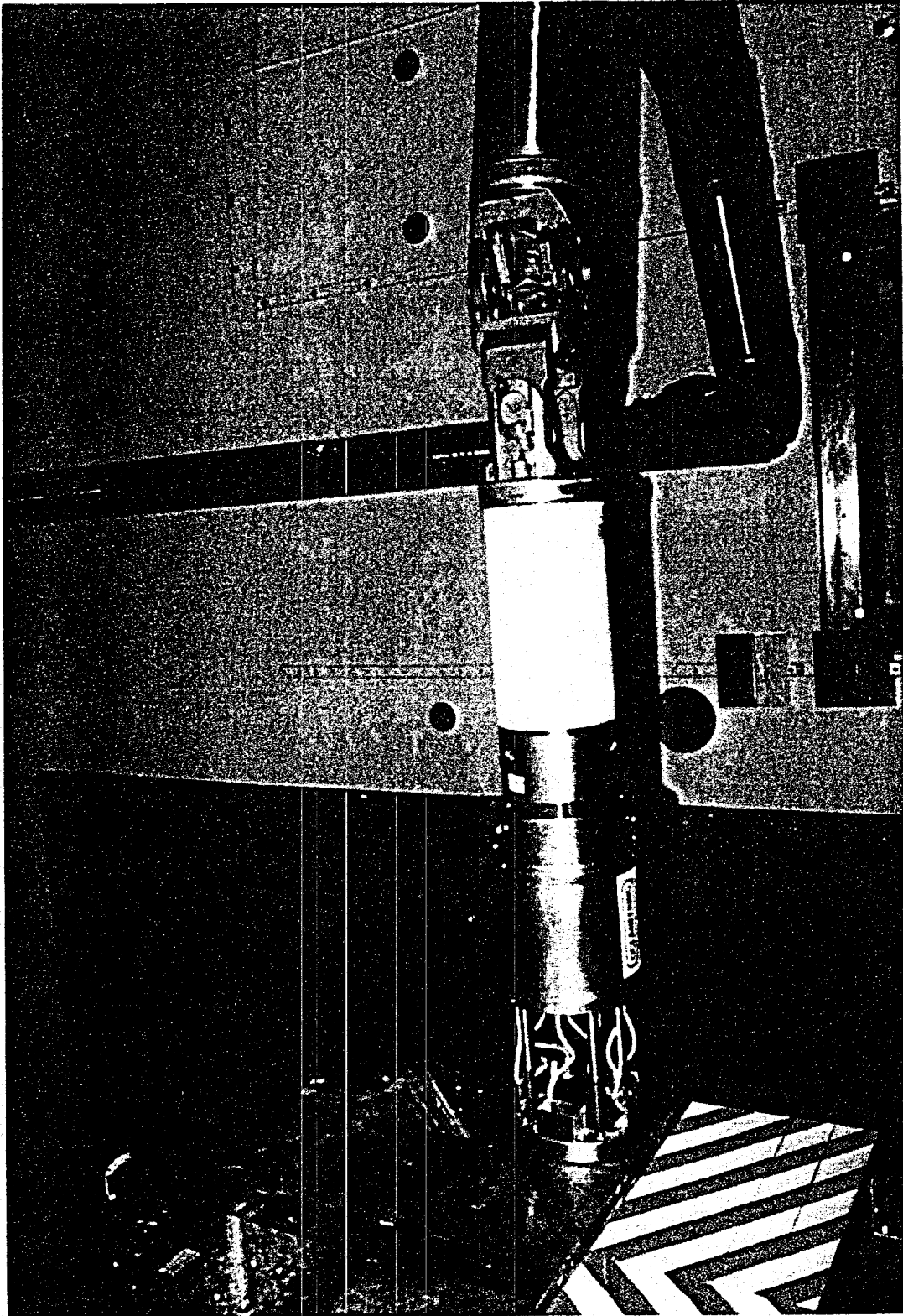
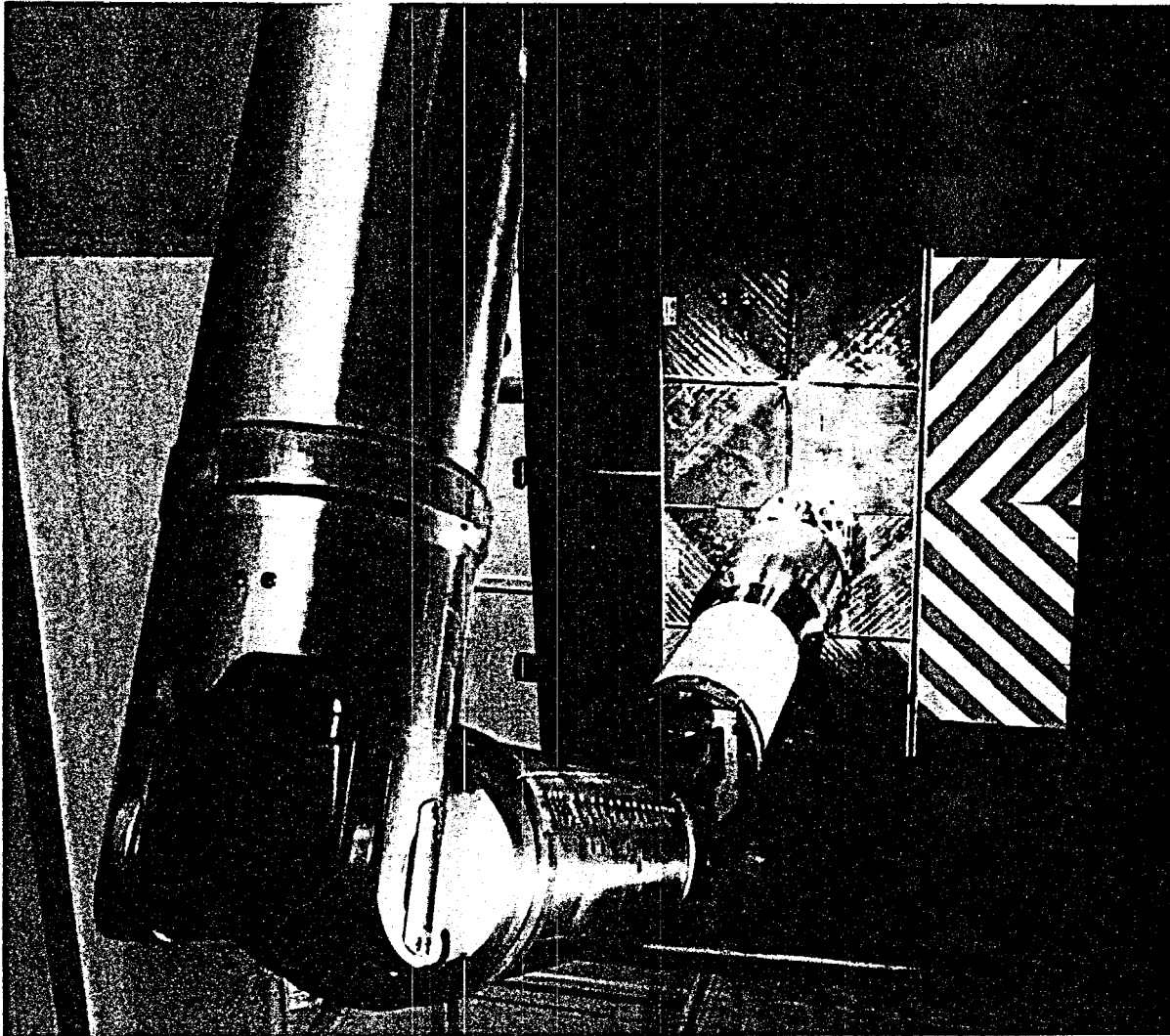


Figure 4.1.2 (a)



Figures 4.1.2 (b)

Figures 4.1.2 (a) & (b): RTIEE deployed in a cold test at the end of the Light Duty Utility Arm (LDUA) at Hanford, Washington. The end effector is positioned over sample plates containing various pits and cracks.

The RTIEE was integrated with another LDUA at INEEL in Idaho Falls, Idaho in May 1998 to ensure that both systems would be operational. In August 1998, the RTIEE was scheduled for a hot tank deployment into a tank containing liquid waste. The scope of the project was then modified to include submerging the end effector beneath the surface of the liquid waste in the tank. For this reason, the end effector (no computer hardware) was shipped back to OSS for retrofitting with leakproof Swagelock fasteners. O-rings were checked and in some cases replaced, and RTV was added to some areas of the inside of the frame to prevent leakage in areas of the end effector that would cause problems with electrical components. The end effector was pressurized and leak tested to ensure that water wouldn't fill its internal cavities. In operation the end effector maintains a constant negative pressure to make it explosion proof in the event of sparking.

In February 1999, the RTIEE was deployed into a hot tank. Although tank WM 188 is radioactive, it was selected for this initial inspection because it was thought to be less radioactive than most at the sight and was expected to have relatively little corrosion. This was favorable for our initial hot tank deployment for safety reasons. Tank WM 188 is among the newer tanks at INEEL and much of its waste had been removed previously. RTIEE was deployed several times into this tank and verified that the tank indeed had little corrosion. The scans and visual inspection revealed some as yet unknown black material on the tank walls, however no significant corrosion or cracks were detected. During the deployment, the camera view clearly indicated radiation in the form of "snow" which was due to the bombardment of the CCD camera by the radioactive particles (some video was recorded). Interestingly, the "snow" got worse when the end effector was facing the liquid waste. When the camera was facing the tank walls, there was much less noise, indicating that the walls did not radiate as much energy as the actual waste in the bottom of the tank. Video was taken of the inspection and several scans were performed during deployment. After this time, the INEEL operators re-deployed the end effector several times on their own and performed scans. The conclusion reached was that the tank appears to be in good condition. Upon removal from the tank, the end effector was "wiped" and found to be clean. In the initial deployment, the end effector only came into contact with the inner tank walls above the liquid waste. The depth of the waste level was very low, less than three feet.

The following pictures are excerpts from video taken at INEEL during the hot tank deployment. Figures 4.1.3 (a-e) show the RTIEE on the end of the LDUA as it is maneuvered to inspect the inside of the waste storage tank. In Figure 4.1.3 (f), RTIEE performs a stationary scan of a weld and allows operators to conclude that there are no defects at that location.

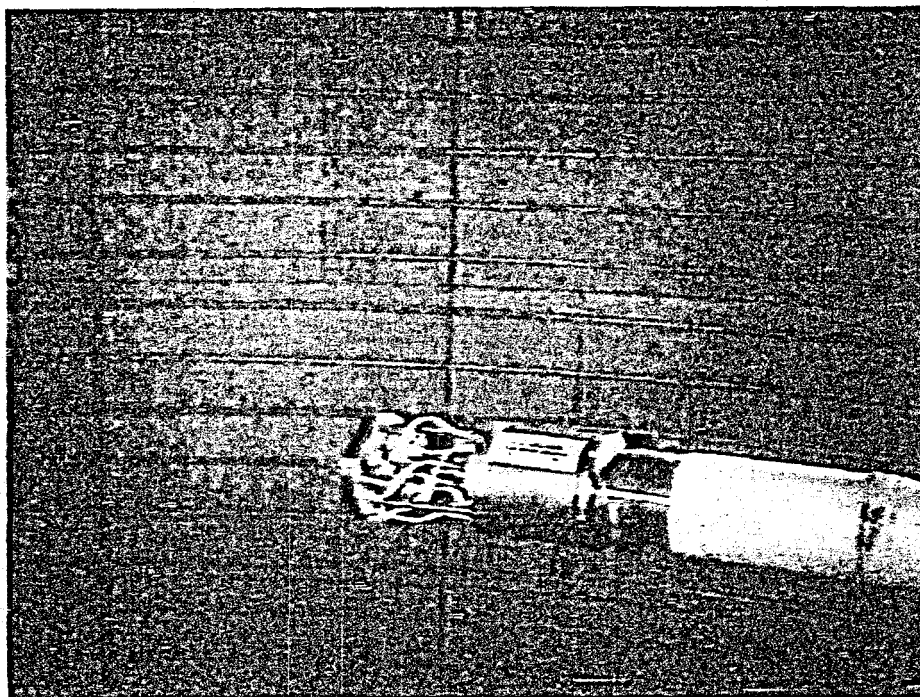


Figure 4.1.3 (a)

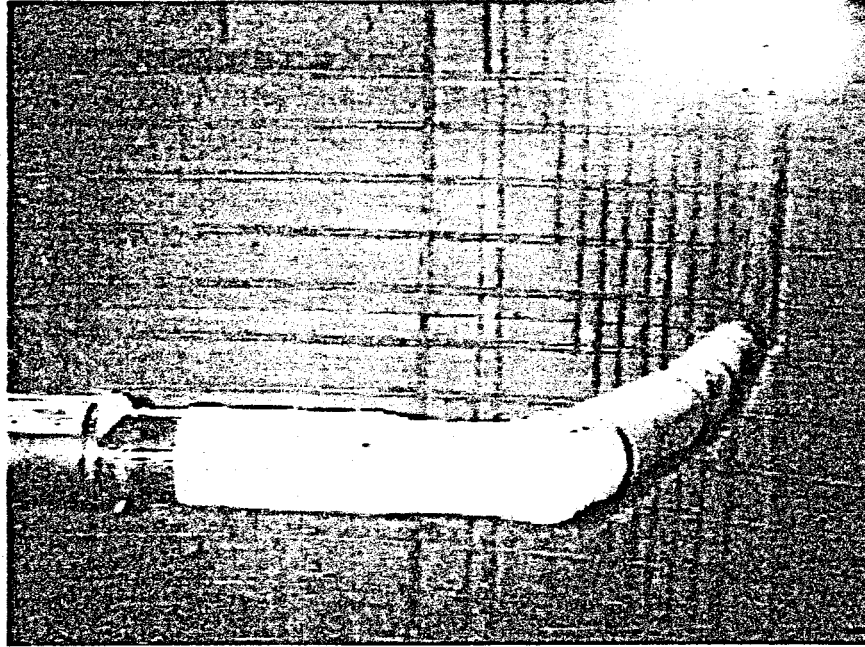


Figure 4.1.3 (b)

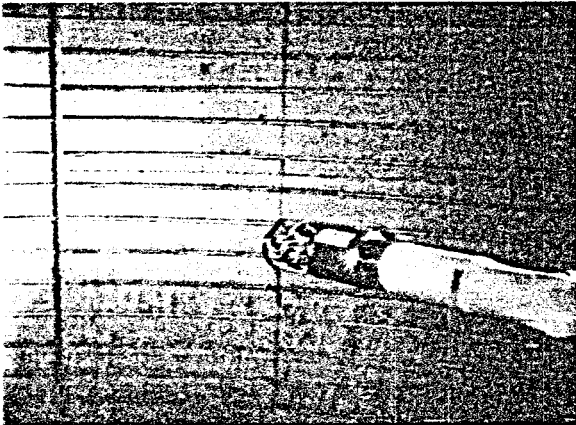


Figure 4.1.3 (c)

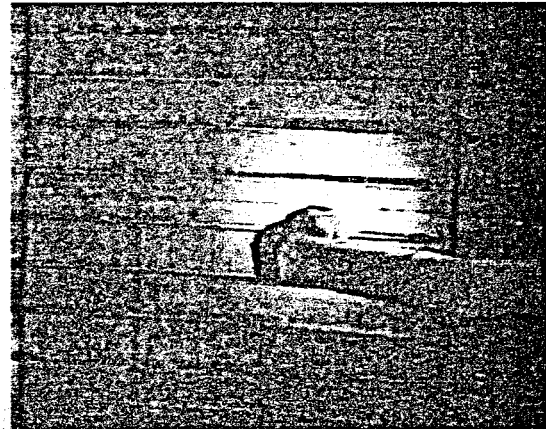


Figure 4.1.3 (d)

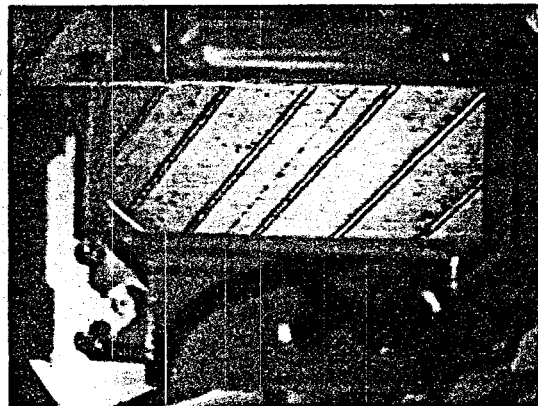


Figure 4.1.3 (e)

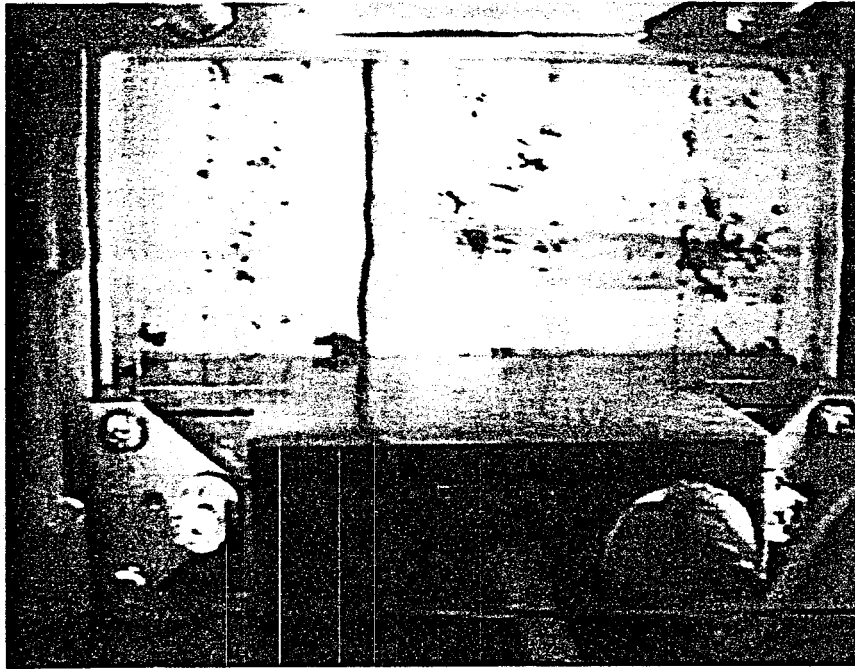


Figure 4.1.3 (f)



Figure 4.1.3 (g)

Figures 4.1.3 (a-g): The photographs presented here are still frames excerpted from video taken during the first hot tank deployment of the RTIEE. The deployment took place in a radioactive underground waste storage tank at INEEL. Frames (a-e) show the RTIEE powered up and operational on the end of the LDUA as it has been lowered through a riser and is maneuvered to take a stationary scan on the inside tank wall of WM188. Frames (e, f) are from video taken by

the camera inside the end effector, where (e) is the view of the cooling coils on the tank wall from a distance. The RTIEE was "landed" between cooling coils (about 3 feet apart) to take several stationary scans (f) on its maiden voyage. Frames (a-d, g) were excerpted from video taken by another camera, which was lowered into the tank through a separate riser to aid in navigating the LDUA about the tank. This particular shot is a close-up of the end effector taking its stationary scan. These pictures give an idea of the scale of the dimensions inside these storage tanks and the large surface areas needing inspection, and benefiting from RTIEE's flyby scanning ability.

After performing several scans in the initial deployment, it was decided that the overall integrity of the tank was good, although a more thorough inspection was to be completed. RTIEE performed flawlessly during its first hot tank implementation.

4.2 VSSTA

The scarifying tool was demonstrated in December 1997 and again with modifications in February 1998. The resulting design changes from this demo were completed and the tool was delivered three weeks later (March 24, 1998) in its final configuration. The Vacuum Scarifying Sampling Tool Assembly (VSSTA) was then deployed in Tank 16 (hot tank deployment) at the Savannah River Site in Aiken, SC for WSRC in December 1997. As mentioned before, pictures of this testing were excerpted from video taken during the final demonstration of the tool and are shown in Section 3.2.

In general, the tool was very well received and praised for its ease of operation and low cost. The tool proved to be effective at scarifying and recovering samples, allowing characterization of the contents of the annulus region in a hot deployment at Tank 16 at the Savannah River Site in June 1998. In fact, the VSSTA enabled the operators to take a higher volume of samples than requested, and in a shorter amount of time than was necessary for other methods. The VSSTA's disposable cartridges allow retrieval of radioactive samples in 60 cc containers that are easily packaged for transportation.

5.0 Future Applications

At present there is a plan to re-deploy the RTIEE system in the summer or fall of 1999 at INEEL. OSS plans on limited attendance for this deployment, as the operators now have experience using the system and have performed inspections several times. If there is interest in producing another RTIEE or VSSTA for the DoE, OSS will maintain the point of contact listed below:

Reg Beer, Robotics & Remote Systems Project Manager.

Phone: 281 228-5414

E-Mail: rbeer@oss.oceaneering.com

Alternatively,

Kent Copeland, Robotics & Remote Systems Program Manager.

Phone: 281 228-5395

E-Mail: kcopelan@oss.oceaneering.com

Document Nº 21100-70004

Revision Date: ~~OCT 01 1999~~

Release Date:

Page A-1

**Appendix A: Previous Final Report Dated 1995 for Robotic End Effector
for Inspection of Storage Tanks**

**Robotic End Effector
for
Inspection of Storage Tanks**

**Contract Number:
DE-AR21-93MC30363**

**Draft Final Report
for period
4 October 1993 - 30 June 1995**

OSS Document Number 21100-70002

For: U.S. Department of Energy

**By: Oceaneering Space Systems
16665 Space Center Boulevard
Houston, Texas 77058**

**Gregory Hughes, Principal Investigator
(713) 488-9080 x3445**

Release Date: 4/28/95

Disclaimer

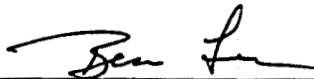
This work was performed for the Morgantown Energy Technology Center (METC) and sponsored by the US Department of Energy, Office of Technology Development.

Referenced herein to any specific commercial product, process, or service by trade name, trademark, manufacturer, or otherwise, does not constitute or imply its endorsement by the United States Government or Oceaneering Space Systems.

**Robotic End Effector
for
Inspection of Storage Tank**

Final Report

Prepared by



**Ben Lee, Oceaneering Space Systems
Engineer**



**William Robertson, Oceaneering Space Systems
Engineer**

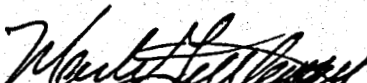


**William Wightman, P.E. Oceaneering Space Systems
Senior Engineer**



**Greg Hughes, Ph.D. Oceaneering Space Systems
Principal Investigator**

Approved by



**Mark Gittleman, P.E., Oceaneering Space Systems
Program Manager**

Change Log

Rev. Ltr. Change N°	ECO (ECP)	Description	Affected Pages	Effectivity (Serial N°)	Release Date	Change Approval (Initial & Date)
IR	N/A	Initial Release	All	N/A	04/28/95	

Abstract

The structural integrity of waste storage tanks is of primary importance to the DOE. Corrosion damage or stress cracking in the inner steel wall liners can allow radioactive liquid or toxic waste to leak from the tank. The nature of the waste stored in some of the tanks precludes access by human inspectors, so teleoperated manipulator arms will be deployed into the tanks, through narrow sealed riser access holes, to perform inspection and remediation work. This project concerns the development of a robotic end effector capable of detecting and sizing corrosion pits in stainless steel and carbon steel tank walls using an advanced electro-magnetic non-destructive evaluation technology, Alternating Current Field Measurement (ACFM). ACFM offers several advantages over more conventional inspection technologies. Specifically, ACFM can detect and size defects without contacting the material to be inspected, works through layers, and does not require the fluid couplant typically required by ultrasonic methods. ACFM is an analytical technique that uses a computer model of the magnetic fields above the wall to size defects; this means that calibration blocks are not needed before conducting an inspection, unlike eddy current techniques. ACFM is also less sensitive to misalignment and standoff than eddy current. In operation, corrosion sites may represent a small proportion of the total inner wall area so, rather than inspect the whole area, a more selective, efficient method of inspection is required. The end effector therefore includes a compact viewing and lighting system that an operator will use to visually discriminate sites of interest prior to conducting a detailed ACFM inspection. The minimum defect of interest is a corrosion pit .030" diameter by .030" deep, which implies very accurate deployment of an NDE inspection device. Typically the large manipulators required to access all areas of an underground storage tank are not designed for such high accuracy. To overcome this constraint an array of sensors is used to scan a 6"x 3" area at one placement, and the whole scanning mechanism is mounted in a compliant frame. The operator will need only to fly the end effector into light contact with the wall to guarantee sufficient alignment for the sensor to inspect. The end effector is suitable for deployment by one of the Department of Energy's (DOE) manipulator systems, such as the Light Duty Utility Arm (LDUA), and is called the Robotic Tank Inspection End Effector or RTIEE.

Acknowledgements

This work is sponsored by the DOE's Morgantown Energy Technology Center (METC). Oceaneering Space Systems would like to thank V.P. Kothari and Cliff Carpenter of the METC for their technical management of this effort. OSS would also like to thank the following personnel at the DOE field centers for their guidance throughout the program: Mike Anderson, Cal Christensen and Brad Griebenow at the Idaho National Engineering Laboratory; and Allan Pardini at Hanford.

Table of Contents

Change Log	i
Abstract	ii
Acknowledgements	iii
Table of Contents	iv
List of Figures	vi
Acronym List	viii
Executive Summary	ix
1.0 Introduction	1
2.0 Project Objectives	2
2.1 Mission	2
2.2 RTIEE Requirements	3
2.2.1 End Effector Contact Frame Requirements	3
2.2.2 Scanner Frame Requirements	3
2.2.3 Structure Requirements	3
2.2.4 NDE Array Requirements	4
2.2.5 GISC Compatibility Requirements	4
2.2.6 CPU and Data Storage Requirements	4
2.2.7 Operator Display and Input Interface Requirements	5
2.2.8 Camera Requirements	5
2.2.9 Lights	5
2.2.10 Cabling Requirements	5
2.3 Assumptions	6
2.3.2 Expected Condition of the Waste Tank Wall	7
2.4 Success Criteria	7
3.0 Background	8
3.1 Department of Energy Waste Storage Tanks	8
3.2 Alternating Current Field Measurement (ACFM) Technology	9
3.2.1 ACFM Overview	9
3.2.2 Comparison of ACFM and other NDE technologies	11
3.2.3 Commercial Utilization of ACFM	13
4.0 RTIEE Design Methodology	15
4.1 System Design and Integration	15
4.1.1 The ACFM Sensor Subsystem	15
4.1.2 The RTIEE Mechanical Subsystem	30
4.1.3 The RTIEE Vision Subsystem	31
4.1.4 The RTIEE Electrical Subsystem	32
4.1.5 The RTIEE Software Subsystem	35
4.2 Safety	44
4.3 Operations	44

4.4	Testing	45
5.0	Results and Discussion	47
5.1	Introduction	47
5.1.1	Performance of the ACFM Sensor Subsystem	47
5.1.3	The Vision Subsystem	69
5.1.4	Electronics Subsystem	70
5.1.5	Software Subsystem	71
6.0	Conclusions	72
Appendix A	RTI End Effector Interface Control Document (ICD)	A-1

List of Figures

Figure E-1: Prototype End Effector Deployed by OI/GE Arm in OSS Robotics Laboratory	xi
Figure 3-1: Resultant Magnetic Fields Due to Uniform Current Flow Around a Pit	10
Figure 4-1: Theoretical Magnetic Field Components for a Point Like Coil Over a Pit . . .	17
Figure 4-2: Theoretical Magnetic Field Components for a Real Coil Over a Pit	18
Figure 4-3: Current Flow Around Holes	19
Figure 4-4: Predicted Responses vs Pit Size	20
Figure 4-5: Model Results for Bx and Bz Response Over Hemispherical Pits	21
Figure 4-6: RTIEE ACFM Sensor Coil and Induction Coil Arrangements	23
Figure 4-7: Detection schemes	25
Figure 4-8: Detection of Large Pits on Carbon Steel	27
Figure 4-9: ACFM Subsystem Layout	28
Figure 4-10: ACFM Data Acquisition Electronics Layout	29
Figure 4-11: Prototype RTIEE General Arrangement	30
Figure 4-12: Electrical Subsystem Component Layout	32
Figure 4-13: RTIEE Software Design Architecture	36
Figure 4-14: Stainless Steel Detection/Sizing Algorithm	38
Figure 4-15: Carbon Steel Detection/Sizing Algorithm	39
Figure 4-16: Operator Interface Screen	43
Figure 4-17: Prototype End Effector and Tank Wall Mockup	45
Figure 5-1: Stainless Steel Plate: Fields Sensed by Array Coils (no defects present) . . .	48
Figure 5-2: Magnetic Fields Measured over 0.25" Pit	50
Figure 5-3: Breadboard Experimental Results Over a Square Pattern of Pits	51
Figure 5-4: Data Collected by Coils Passing Over a Row of Pits	52
Figure 5-5: Map of Defects on Carbon Steel Sample Plate	53
Figure 5-6: First Derivative of Collected Data	53
Figure 5-7: Second Derivative of Collected Data	54
Figure 5-8: Thresholded Plan View of Second Derivative	55
Figure 5-9A: Comparison of Measured XBx Amplitude with Prediction for Depth of Hemispherical Pits in Carbon Steel at .040" Lift Off	56
Figure 5-9B: Comparison of Measured XBz Peak Trough Spacing with Prediction for Diameter of Hemispherical Pits in Carbon Steel at .040" Lift Off	56
Figure 5-10: XBx Amplitudes vs Pit Depth for Hemispherical Pits in Stainless Steel . . .	57
Figure 5-11: Measured XBz Width vs Pit Width for Stainless Steel	58
Figure 5-12: Corrected Width Estimation on Stainless Steel	58
Figure 5-13: Parametric Fits to XBx Data Used for Pit Depth Sizing in Stainless Steel .	59
Figure 5-14: Screen Shot of Stainless Steel Inspection -XBx	61
Figure 5-15: Screen Shot of Stainless Steel Inspection - XBz	62
Figure 5-16: Screen Shot of Detection and Sizing Display	63

Figure 5-17: Screen Shot of Detection and Sizing Display	64
Figure 5-18: Stainless Steel Pit Diameter Estimation (average over multiple depths) . . .	65
Figure 5-19: Stainless Steel Pit Depth Estimate (.25" diameter)	66
Figure 5-20: Screen Shot of Carbon Steel Inspection -ZBz	67
Figure 5-21: Carbon Steel Pit Diameter Estimation (average over multiple depths)	68
Figure 5-22: Carbon Steel Pit Depth Estimate (.5" diameter)	68
Figure 6-1: RTIEE Crack Detection in a Stainless Steel Weld	76

Acronym List

AC	Alternating Current
ACFM	Alternating Current Field Measurement
ACPD	Alternating Current Potential Drop
CCD	Charge Coupled Device
CPU	Central Processing Unit
DC	Direct Current
DNV	Det Norske Veritas
DOE	Department of Energy
GE	General Electric
GISC	Generic Intelligent System Control
GUI	Graphical User Interface
Hz	Hertz
ICD	Interface Control Document
INEL	Idaho National Engineering Laboratory
LDUA	Light Duty Utility Arm
METC	Morgantown Energy Technology Center
NDE	Non-Destructive Evaluation
NEPA	National Environmental Policy Act
OI	Oceaneering International
OSS	Oceaneering Space Systems
POD	Probability of Detection
ROV	Remotely Operated Vehicle
RAIL	Robotic Test and Integration Lab
RTIEE	Robotic Tank Inspection End Effector
TIP	Tool Interface Plate
TSC	Technical Software Consultants, Ltd
UCL	University College London
VCR	Video Cassette Recorder

Executive Summary

In October 1993 the Department of Energy (DOE) contracted with Oceaneering Space Systems (OSS), a division of Oceaneering International, Inc., to develop a robotic end effector capable of detailed non-destructive evaluation (NDE) and visual inspection of its underground waste storage tanks. The award followed a proposal written by OSS to the 1993 Research Opportunity Announcement (ROA) administered by Morgantown Energy Technology Center (METC).

The objectives of this project were to prove that a single end effector could perform both electromagnetic NDE and a visual inspection of the tank walls and to produce a proof of concept prototype system for demonstration at a DOE facility. End effector development was targeted at light duty manipulators ranging from Schilling Titan models to the DOE's to the Light Duty Utility Arm (LDUA). The LDUA program represents the maturing of robotic technologies that will remediate underground waste storage tanks used by the DOE for storing hazardous waste. One of the primary challenges faced by the DOE in this remediation task is characterizing the condition of the inner steel tank wall liners. Corrosion damage, cracking, or weld defects could cause leakage of the tanks' contents. However access to the inside of the tanks is restricted to the LDUA or similar manipulators that, because of their large size, are unsuitable for the accurate deployment normally required by NDE techniques.

Therefore to assist in the remediation of the waste tanks, OSS has developed an inspection system based on the advanced electromagnetic NDE technique Alternating Current Field Measurement (ACFM). This system consists of a robust end effector design that deploys an ACFM scanner in a compliant frame, and combines the NDE function with a powerful viewing and lighting system. The ACFM scanner can detect and size corrosion pitting in carbon and stainless steels. The end effector is controlled by an IBM PC compatible computer and software, developed as part of this project, that features an intuitive operator interface control screen and provides the capability to record all visual and NDE data to VHS tape or computer disk.

The RTIEE was a two phase project. Phase I included the design, fabrication, and testing of both a breadboard and prototype end effector system. Phase II involved testing the prototype end effector system at the Idaho National Engineering Laboratory (INEL). Phase I had four major milestones. The first two were design review meetings, the third and fourth were the delivery of the draft topical report and the final topical report, respectively. During Phase I OSS received a contract modification from METC. This additional work included changes to the prototype design to make it more compatible with the developing LDUA program. To accommodate the additional work the Phase I schedule was extended two months.

The robotic tank inspection end effector (RTIEE) project began with the definition of design requirements. Few DOE requirements existed for the RTIEE because little was or is known of the condition of the tank walls. In addition, one of the manipulators that could deploy the

RTIEE was itself in its design phase. INEL had previously defined pitting corrosion in stainless steel tanks as a major cause of concern and so characterizing pits was made the driving inspection requirement for the RTIEE. End effector size and weight requirements were derived from LDUA performance estimates. The control system design was based on a distributed system with the control console separated from the end effector by several hundred feet. The control system requirements also included compatibility with the DOE's Generic Intelligent System Control (GISC).

OSS produced a breadboard system design and presented it to the DOE at the first design review meeting in January 1994. A mockup of the end effector camera, lighting system, and the scanner drive arrangement was produced to assist in the design effort. When the design was finalized, production of the breadboard system was initiated. The ACFM sensor subsystem was developed in the UK by OSS's subcontractor, Technical Software Consultants, Ltd (TSC). After production, all subsystems were bench tested and then integrated at OSS. Testing of the breadboard system included deployment of the end effector by the OI/GE manipulator in a representative worksite environment in OSS's robotics lab. The breadboard performed well. It allowed inexperienced operators to visually detect large pits on a tank wall, land the end effector scanner over the site, and perform an ACFM inspection. The breadboard system software included specific pit detection and sizing algorithms, which worked particularly well on carbon steel. The breadboard system was exhibited at the Hanford LDUA Cold Test Facility in June 1994.

A second design review meeting was held at OSS and attended by the DOE in July 1994. At this meeting, the prototype design was presented and the breadboard results discussed. The prototype system was then fabricated and integrated at OSS. TSC once again produced the array subsystem and upgraded the detection and sizing algorithms based on OSS's breadboard test results. OSS added several performance enhancements to the prototype end effector, including a more sensitive array and faster multiplexing and data transfer electronics. Although not radiation hardened or explosion proofed as a "field deployable" end effector would need to be, the prototype was designed with deployment on the LDUA or similar manipulator in mind and featured a cylindrical body, increased modularity, and a generic interface plate that could be easily replaced by the LDUA Tool Interface Plate (TIP).

OSS subjected the prototype system, shown in Figure E-1, to extensive testing and evaluation in the OSS robotic laboratory, as well as a system test review attended by representatives of INEL and METC. The RTIEE satisfied all of its defined mission success criteria. The camera and lighting system allow an operator to discriminate small sites of possible corrosion damage from undamaged wall at a distance of up to 45 feet. The compliant scanner frame and status indicators clearly indicate contact with the tank wall and greatly reduce the operator effort required to successfully place the scanner over the inspection site. The scanner consistently moves the ACFM array over the scan window and the array successfully detects and sizes pits on carbon and stainless steel. The software provides a graphical user interface (GUI) that displays all relevant information to the operator and permits the storage of all

visual and NDE information to computer hard disk and VHS tape.

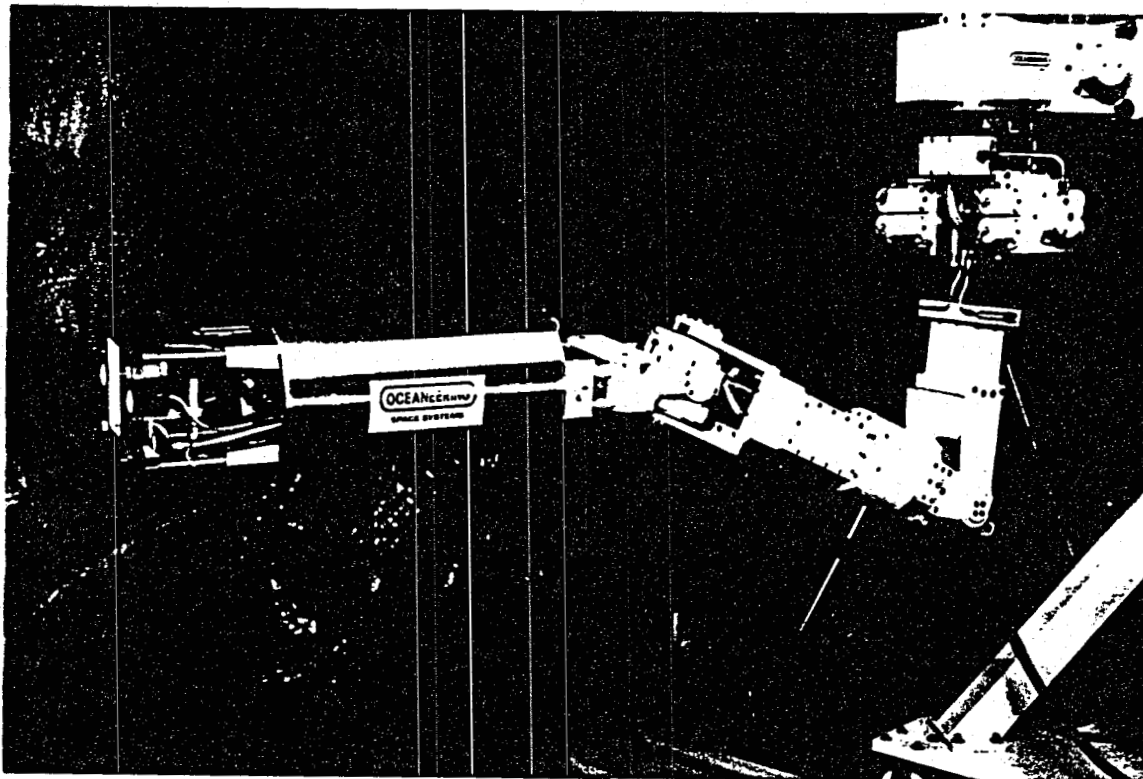


**Figure E-1: Prototype End Effector Deployed by OI/GE Arm in
OSS Robotics Laboratory**

The four broad mission success criteria for the RTIEE are defined and compared with RTIEE design and performance in Table E-1.

Success Criteria (Requirements)	RTIEE Design	Design Margin
1) The system shall allow the operator to view the surface of a storage tank wall when the end effector is deployed by a robotic manipulator in a storage tank.	The end effector camera and lights allow unobstructed viewing of a distant tank wall and close up viewing of the tank wall during an inspection.	The centrally mounted camera not only provides a direct view of the scan area, it also coincides with the likely manipulator control point of resolution thereby reducing operator workload. Two sets of lights are used to provide optimum illumination for both far and near viewing.
2) The end effector shall be able to inspect a minimum 3"x3" area, using an ACFM technique, of a steel tank wall when deployed by a robotic manipulator in a storage tank.	The end effector's compliant scanning frame and strut compression sensing devices allow safe placement of the scanning ACFM array over the target area. The stepper motor driven carriage scans the array over a 6"x3" area of tank wall.	A rotary position encoder reports the position of the scanner carriage to the controller. This allows the selection of multiple scan ranges and step sizes. The ACFM electronics and control firmware allow the collection of multiple data sets during a single scan, greatly increasing the flexibility of the sensor.
3) The end effector system shall use algorithms to size surface corrosion pitting to a resolution not less than 0.75mm diameter by 0.75mm deep. The sizing information shall be displayed on the interpreted inspection data display.	Specifically written detection and sizing algorithms characterize pitting in stainless and carbon steel using theoretical model data and empirically derived relationships. These algorithms can characterize a minimum 0.75mm diameter 0.75mm deep pit.	The detection and sizing algorithms supplement a graphical display of the inspection data. Other defects (non-pit) causing significant disturbances in the inspection fields can also be detected.
4) The end effector system shall display both real time video from the end effector camera and an interpreted inspection data display at the operator control station.	The RTIEE graphical user interface displays real time video and inspection data and results concurrently. Both images can be saved to hard disk or continuously recorded to VHS video tape.	All RTIEE control functions can be accessed from the graphical interface. Functions include: camera zoom, iris, and focus control, near and far lighting intensity, and an extensive selection of file manipulation and data display options.

Table E-1: RTIEE Mission Success Criteria

OSS initiated the Phase II effort by satisfying all relevant NEPA requirements for the prototype

end effector system. Following this, OSS produced an owners manual which outlined set-up and use of the RTIEE system. OSS successfully tested the ACFM inspection end effector at the Idaho National Engineering Laboratory (INEL) in March 1995. Several plates were inspected by INEL personnel demonstrating pit detection and sizing, and crack detection in welds in stainless steel. The system performed as specified despite shipping damage and generated interest within several groups at INEL.

This project has successfully demonstrated that a single robotic end effector can perform both quantifiable electromagnetic NDE and a visual inspection of underground storage tank walls. Through the use of the RTIEE, a highly accurate inspection can be conducted by a teleoperator using a manipulator of only minimal accuracy, and the single RTIEE camera view.

1.0 Introduction

This final report documents the development and testing of the RTIEE prototype. This report is subdivided into the following sections: Objectives (2.0), Background (3.0), Methodology (4.0), Results and Discussion (5.0), Conclusions (6.0).

Section 2.0 - Objectives: describes the project mission and the derived requirements used to guide the engineering development of the RTIEE.

Section 3.0 - Background: provides information on the DOE application needs driving the development of the RTIEE. In addition, this section describes ACFM technology and compares it with other NDE technologies currently available.

Section 4.0 - Methodology: describes the design and functionality of each of the RTIEE subsystems and how they are integrated into a single working system. This section also describes a nominal RTIEE operating scenario.

Section 5.0 - Results and Discussion: evaluates each of the subsystems. Issues that were identified during development are discussed.

Section 6.0 - Conclusions: summarizes the project results and discusses new tasks that would further develop the prototype system and expand its current inspection capabilities.

A description of the Phase II testing and demonstration of the prototype RTIEE at the INEL is appended to this report.

2.0 Project Objectives

2.1 Mission

The focus of this project was to develop a robotic end effector capable of visual and NDE inspection. The mission drivers were the underground tanks at INEL and Hanford. The tanks at INEL are constructed of 304L, ¼ inch thick stainless steel, and those at Hanford of ¼ inch thick carbon steel. It was understood at the beginning of the project that first deployment of an inspection end effector would occur at INEL where tank video images had revealed surface discolorization of the inner wall. Since this discolorization might be evidence of corrosion damage, a system was required that could discriminate between simple discolorization and pitting of the steel. The robotic system to be used for this inspection required an end effector with an NDE device and vision system that could locate areas of possible corrosion attack, discriminate between discolorization and corrosion damage, and characterize any pitting damage it detected.

The following were the inspection system design goals. They were intended to facilitate mission success and are based on OSS's extensive robotic operations and remote inspection experience:

- The inspection system should be simple to operate.
- The sensor should be self-aligning (passively compliant) to reduce positional accuracy requirements levied on the manipulator (such as the LDUA).
- The sensor should use an advanced NDE technology that can detect and size pits, without requiring cleaning of the wall or the use of a couplant.
- The inspection system should feature an easy to interpret inspection data display (GUI).
- The inspection system should provide a vision system that clearly shows the inspected area while also providing the primary manipulator control view.

Pitting corrosion was a primary concern in the newer stainless steel tanks at the INEL complex. This led to the derived requirement for an inspection end effector to perform a very detailed inspection of at least a 3" x 3" area of a tank wall, detecting and sizing pits as small as 0.030" diameter.

2.2 RTIEE Requirements

To meet the mission challenge, OSS developed the Robotic Tank Inspection End Effector (RTIEE) system. The system consists of two major subsystems: the end effector with data collecting sensors, and the operator workstation which archives the data and performs data analysis. The following subsections detail the RTIEE system requirements. These requirements were derived from mission goals, environmental constraints, and extensive customer input.

2.2.1 End Effector Contact Frame Requirements

The contact frame must be stiff enough to allow the scanner frame to operate under worst case wall collision and static loading conditions. An exception to this is unexpected protrusions into the scanning envelope. The contact frame shall provide RTIEE misalignment accommodation up to 15 degrees during wall contact and be constrained against rotation about the RTIEE central axis. The contact frame attachment method must provide impact damping and indication of 4 point contact with the tank wall.

2.2.1.1 End Effector Status Indicators

Contact with the tank wall must be indicated by mechanical and/or electrical status indicators and be provided to the operator in the RTIEE camera view. The status indicators shall show the degree to which the scanner corner is compressed onto the tank wall. The status indicators shall provide the operator with sufficient information to allow the operator to re-align the end effector to within the accuracy required by the ACFM array. The ACFM array will be aligned with the wall to within .060" across the whole of its front surface.

2.2.2 Scanner Frame Requirements

The scanner frame's primary function is array translation. The scanner frame must allow uniform motion of the coil array under remote control. In addition, the frame shall preclude stick/start conditions and damp out any oscillations that may be present during drive operation.

2.2.3 Structure Requirements

2.2.3.1 Weight

Weight of the entire end effector shall not exceed 40 lb.

2.2.3.2 Moment

Moment shall not exceed 600 in-lbs at the interface plate.

2.2.3.3 Envelope

The end effector shall have a maximum exterior-envelope of 10.5" diameter by 30" long. The RTIEE should have provision for insertion and removal guides over catch points where practical. These requirements are derived from the interior tank environment at INEL. Access to the inside of the waste tank is through risers on top of the tank cover. Each riser is approximately 6 feet high and 12 inches in diameter. Inside the tank, some areas of the tank walls are obstructed by cooling coils and possibly debris.

2.2.4 NDE Array Requirements

2.2.4.1 Power

± 15 VDC power from the RTIEE power supply shall be converted to 5kHz AC required to run the NDE array field injection. ± 15 VDC will also be used to power coil and data transfer electronics.

2.2.4.2 Performance

The goal of the array is to detect and size corrosion pits in stainless and carbon steel to a resolution of .030" dia. x .030" deep. The array shall be capable of detecting other types of defects in stainless steel and carbon steel though not necessarily of sizing these other defects. The ability of the array to detect and size "other" defects will be determined by experiment if suitable samples are provided to the project by the DOE.

2.2.4.3 Connector Style

A single shield connector shall be used to connect the array to the support electronics in the end effector.

2.2.4.4 Cabling and shielding

The array shall be mounted inside a carbon steel housing to minimize effects of stray fields.

2.2.5 GISC Compatibility Requirements

The RTIEE must be compatible with the GISC standard. This is interpreted as meaning that all primary control functions, including inspection data transfer, must be controllable from a supervisory computer communicating via an RS-232 serial line.

2.2.6 CPU and Data Storage Requirements

The local CPU shall be a 66 MHZ 80486 DX processor. The primary temporary storage

media shall be a 14 ms, 207 MB fixed hard drive. A means of fixed disk data removal and back-up shall be considered. The system shall allow the transfer and storage of video and display screen graphics to VHS tape (a VHS video recorder/player is not a deliverable of this contract).

2.2.7 Operator Display and Input Interface Requirements

2.2.7.1 Display

The visual display of all data shall be within a GUI environment on a single 17" diagonal SVGA, 256 color monitor, including camera data and the results of any ACFM inspection. Single frame video capture to file shall occur for each scan with real-time recall of multiple scans. Near full screen display of the camera view shall be available for driving the manipulator.

2.2.7.2 Input Interface

The operator input interface shall consist a standard 101 Keytronics style keyboard and mouse. The keyboard and mouse will be used for screen manipulation, file naming, and other display control functions. Camera and lighting functions shall be controllable from the interface screen.

2.2.8 Camera Requirements

The camera shall be centrally mounted in the end effector body. The camera lens must have the ability for remote focus, zoom, and iris control. The preliminary performance specification for the camera requires clear viewing of the scanner frame 6" away and clear viewing of a 3"x3" area of a tank wall 37.5" feet away (half of the single shell storage tank diameter). The camera iris must also accommodate the lighting changes in the system.

2.2.9 Lights

Tank interiors are unlit, therefore, the RTIEE shall be configured with far and near lighting capability. During gross RTIEE movement the general tank wall far lights will be turned on. As the RTIEE approaches the wall, the two far lights can be turned off and near lighting turned on depending on lighting conditions. These lights shall be controlled from the operator interface. The intensity of each set of lights shall also be controllable.

2.2.10 Cabling Requirements

The end effector system shall be capable of being supplied and controlled over a maximum cable length of 150'.

2.3 Assumptions

The development of the RTIEE required several assumptions about the work system on which the RTIEE will be deployed (LDUA or similar DOE manipulator) and the environment of the tank. Below are assumptions about the manipulator and project expectations.

Tank environments vary from relatively benign, not requiring radiation and other protection of the end effector, to extremely radioactive and chemically hazardous. The systems developed for this project were intended as proof of concepts and were not to be radiation hardened or otherwise protected against the actual waste tank environment.

For testing and development purposes, the DoE was required to supply OSS with suitable samples of tank wall corrosion pitting (and any other defects of interest). Sections 2.3.1 through 2.3.2 outline the related assumptions made by OSS in designing the RTIEE system.

2.3.1 Services and Performance Required of the Manipulator to the RTIEE System

Note: The following requirements are based on the completed RTIEE prototype. Modifications to the prototype for field deployment on a new manipulator can be evaluated on a case by case basis.

2.3.1.1 Manipulator Power/Data Requirements

The manipulator is required to provide suitable utility cables for the power lines in the RTIEE umbilical. This includes a minimum of eight 16 AWG or larger lines available to the end effector. The manipulator also must provide a cable and connectors capable of supporting an RS485 serial line. Additionally, this cable and connectors should include a count of 20 x 24 AWG or larger signal lines and a minimum of one 75 ohm coax cable. This cable and its connectors should terminate at one extreme at the manipulator end effector interface and at the other extreme a safe distance from the manipulator base. These requirements fall within the current design specifications for the LDUA manipulator.

2.3.1.2 Manipulator Performance Requirements

The following performance specifications, which reflect the current LDUA design, are assumed regarding the manipulator deploying the RTIEE system.

Accuracy	$\pm \frac{1}{2}$ "
Repeatability	$\pm .2$ "
Resolution	.01"
Maximum speed	6 in/sec at collision

2.3.2 Expected Condition of the Waste Tank Wall

The waste tank wall is expected to exhibit a uniform flatness, not exceeding .030" variation over a 10.5 inch square area of the wall.

2.4 Success Criteria

The success criteria for the RTIEE was defined by the mission for which the end effector system is designed. The four broad mission success criteria defined for this project are listed below:

- 1) The system shall allow the operator to view the surface of a storage tank wall when the end effector is deployed by a robotic manipulator in a storage tank.
- 2) The end effector shall be able to inspect a minimum 3"x3" area, using an ACFM technique, of a steel tank wall when deployed by a robotic manipulator in a storage tank.
- 3) The end effector system shall use algorithms to size surface corrosion pitting to a resolution not less than 0.30" (0.75mm) diameter by 0.30" (0.75mm) deep. The sizing information shall be displayed on the interpreted inspection data display.
- 4) The end effector system shall display both real time video from the end effector camera and an interpreted inspection data display at the operator control station.

3.0 Background

3.1 Department of Energy Waste Storage Tanks

The DOE maintains 332 underground storage tanks to process and store radioactive and chemical mixed waste generated from weapons material production. The tanks are typically 70-85 feet in diameter and 20-45 feet deep and are located in farms at five DOE sites across the U.S.

Excluding of the gunnite tanks at ORNL the majority are one of two types: the older tanks are single shell wall, the newer tanks tend to be double shell wall. The wall material is either carbon steel or stainless steel usually backed by reinforced concrete. The in-service tanks can be pumped down, i.e. have their waste temporarily removed to another tank, allowing access to the entire tank wall. All the underground storage tanks at the INEL are in-service and therefore would use an inspection end effector to quantify corrosion damage in all areas of tank wall, floor, and ceiling. At Hanford this is no longer possible in many of the oldest and most critical single shell tanks. Remediation attempts in the 1960s added absorbent materials to the liquid waste to stabilize it and now effectively prevents the pumped removal of the waste mix. In these most critical tanks, access to the interface of the waste with the wall and the wall above the waste level is possible. The condition of the wall at the interface (a primary site for corrosion because of the available oxygen) and the wall above the waste will provide important information on the condition of the wall beneath the waste. In some tanks, the level of waste has fallen as a result of the removal of fluid. This has resulted in bands of scale and salt cake being left on the wall at the old interface. Most current NDE technologies require that any obscuring layers be removed prior to a visual or detailed NDE inspection.

The tank waste is intended to be processed into a safer form and moved to specially designed storage facilities. Until this occurs, the structural integrity of the underground storage tanks is a primary concern. Corrosion damage or stress cracking in the inner steel wall liners could allow radioactive liquid or toxic waste to leak from the tank. Periodic inspection of the inner tank walls is necessary to assess their integrity. Unfortunately, the nature of the waste stored in some of the tanks precludes access by human inspectors, therefore any work performed in the tank must be performed indirectly, e.g., telerobotically.

Performing a detailed inspection of the entire tank wall may be prohibitively time consuming. Therefore, inspections should concentrate on identified corrosion sites which will represent a small proportion of the total inner wall area. The minimum defect of interest at the INEL is a corrosion pit .030" diameter by .030" deep which implies very accurate deployment of an inspection device. Typically the large manipulators required to access all areas of an underground storage tank are not designed for high positional accuracy.

To address the problem of tank inspection and remediation, the DOE has undertaken to produce a family of teleoperated/computer controlled manipulators and end effectors to be

deployed into the tanks, through narrow sealed riser access holes, to perform inspection and remediation work.

3.2 Alternating Current Field Measurement (ACFM) Technology

3.2.1 ACFM Overview

ACFM is an electro-magnetic NDE technique that has been specifically developed to overcome the shortcomings of eddy current techniques. ACFM differs from conventional eddy current mainly in its use of a uniform input field. This gives ACFM several advantages, including increased tolerance to lift-off and material property changes and increased penetration of current down into deep defects; this comes at the expense of some decrease in sensitivity. The main advantage of using a uniform input current, however, is the ability to analytically model the current perturbations caused by a defect. This allows sizing by comparing measured signal amplitudes directly with theoretically predicted values, thus avoiding the need for the use of calibration notches typically used with eddy current techniques. ACFM is widely used for detecting and sizing surface breaking fatigue cracks and other linear defects with or without coatings, and its reliability and accuracy has been demonstrated in a number of blind trials.

ACFM combines the ability of the Alternating Current Potential Drop (ACPD) technique to size defects without prior calibration with the ability of eddy current to work without electrical contact. This is achieved by inducing a uniform AC field in the target material and measuring the magnetic fields above the specimen. The uniform current flow is modelled analytically, which makes the field response predictable and allows the characterizing and sizing of defects without the use of artificial defect samples (calibration notches) to calibrate the system.

The uniform field allows the use of arrays of coils to cover large areas simultaneously. This is possible because the uniform field does not vary significantly in strength under any part of the array. Under these circumstances, the field strength recorded at any position in the array is similar to that recorded by a single coil scanned in that position. Therefore the array reduces the amount of scanning (physically moving a coil or coils over a target area) required to cover a particular area. Arrays can also be manufactured in a variety of shapes to best suit the geometry to be inspected.

Typically in ACFM, solenoids attached to the inspection tool are used to induce the uniform electric field into the target material. This alternating electric field sets up a magnetic field in the free space above the target area, which is recorded by sensor coils in the tool. Figure 3-1 provides a simplified example of the relationship between a uniform current field and its magnetic field. The coordinate axis used in describing attributes of current flow and magnetic field are defined in this figure. The upper half of the figure illustrates a plate with current flowing across it (the arrows); this is the induced AC field, here frozen in one direction for

illustration. As the current encounters the pit (the dark oval) in the center of the plate, current is diverted around each extremity of the pit. Any surface breaking feature will tend to divert the current flow and hence create a change in the magnetic field above the feature. Current seeks the path of least resistance and the majority of the flow therefore will run round the extremes of the feature rather than flow down into the pit. The magnetic field created by the current flow is perpendicular to the current flow and simply defined by the right hand rule. The three components of the magnetic field above the plate are referred to as B_x , B_y and B_z . All three components are perturbed by the clockwise and counterclockwise flow of the current around the extremes of the pit. The magnetic field disturbance in B_x and B_z are shown and illustrate easily recognizable features (a tipped depression for B_x and a peak/trough pair for B_z).

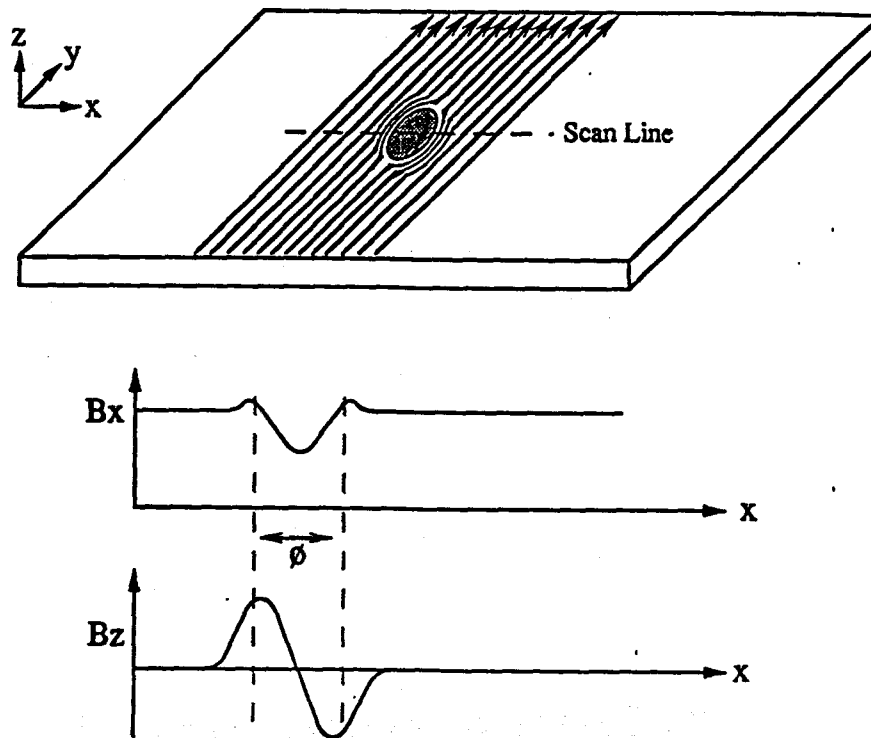


Figure 3-1: Resultant Magnetic Fields Due to Uniform Current Flow Around a Pit

The uniform electric field has a depth (into the target material) that is dependent on the excitation frequency and the permeability of the target material. In ferrous steel this skin depth is so small ($< .005''$) at all practical excitation frequencies that the flow of the field can be considered two dimensional (in Figure 3-1 therefore the flow is constrained to the X and Y direction). If the uniform field is considered to be two dimensional then a mathematical model of the field can be created that predicts the behavior of the current flow at the surface. This same model can then be adapted to model the flow as it encounters a surface breaking flaw or defect. Once the surface flow is known the disturbance in the magnetic field above the surface can also be modelled. It

is the magnetic field above the sample that the ACFM tool measures, allowing model results to be compared to actual results.

Conducting materials other than ferrous steels can have significant skin depth at normal operating frequencies, for example stainless steel has a skin depth of about .25" at 5KHz. The effect of this third dimension to the flow is to make the mathematical modelling of the field very complex. However, the two dimensional model can usually still be used to predict the general current flow in materials of significant skin depth. A practical advantage to increased skin depth is in the sensitivity of the inspection tool to defects beneath the surface of the material.

Designers of tools that use ACFM must consider several aspects of this theory. Initially, the theoretical model is adapted to model the effect of the target defect in a uniform current field (various directions of uniform flow can be tried). Examination of the modelled magnetic fields above the defect will determine which components are perturbed most and therefore have features that are easily recognizable. This allows definition of the optimum uniform current field direction and the most perturbed magnetic field components. Each magnetic field component is best sensed by a coil orientated in its coordinate direction. Similarly the induction of the uniform current field is best achieved by solenoids (large driven coils) oriented in orthogonally to the current field. With the optimum sensor coil and induction solenoid orientations defined the most efficient and practical arrangements of these components can be addressed in the tool design.

3.2.2 Comparison of ACFM and other NDE technologies

3.2.2.1 ACFM vs Eddy Current

The ACFM technique was developed from the Alternating Current Potential Drop (ACPD) technique to combine the ability of ACPD to size defects without prior calibration with the ability of eddy current techniques to work without electrical contact. This is achieved by maintaining a uniform input field (induced or injected) and measuring the magnetic fields above the specimen surface instead of the surface voltages. The main aim of both ACPD and ACFM is to avoid the need for calibration on artificial defects (an eddy current requirement) whenever possible because such calibration is known to be prone to error for a number of reasons:

1. The calibration piece is not representative (e.g., a slot is used to represent a crack)
 - A slot does not behave electrically like a crack
 - The slot is unlikely to be in a material representative of the crack location (i.e. parent plate, heat affected zone, weld)
 - The slot is not generally in a geometry representative of the crack location
2. Calibration can only be valid for the defect length used because crack length influences the signal depth
3. Increased probability for operator error because of an increased number of tasks to perform

A summary of the differences between ACFM and conventional eddy current is given in Table 3-1. The main drawbacks of eddy current arise from the use of a compact circular excitation current. This results in a very sensitive detection capability, but also makes the technique prone to strong lift-off signals and signals due to material property changes. The non-uniform nature of the current also limits its sensitivity to deep defects because the current does not flow to the bottom. The most important consequence, however, is eddy current's inability to model the current flow in a general way, making it necessary to use calibration techniques for sizing.

Property	ACFM	Eddy Currents
Theoretical Defect Depth Interpretation	Yes	No
Calibration Required	No	Yes
Defect Depth Measurement	Yes	Yes
Maximum Depth	30mm (approx.)	5mm (approx.)
Defect Length Measurement	Yes	Yes
Defect Detection and Location	Yes	Yes
Operator Skill Required	Medium-high	High
Easy Deployment in Transition Region (e.g. weld)	Yes	No

Table 3-1 ACFM vs Eddy Current

3.2.2.2 ACFM vs Ultrasonics

Electromagnetic sensors have several advantages over conventional measurement systems that use ultrasonics. Their primary advantage over ultrasonic sensors is not requiring coupling with the wall. Ultrasonic sensors require a coupling medium, such as grease or water, to occupy the space between the sample and the sensor. The coupling allows reasonably efficient transfer of sound energy into the target material and back to the transducer. In addition to the added complexity of incorporating a supply of couplant into the end effector, the couplant itself becomes a form of secondary waste.

ACFM also enjoys another significant benefit over conventional ultrasonic methods with respect to the surface condition of the wall. Any form of surface scale or deposit can offer a high impedance path to the ultrasonic energy and significantly reduce the sensitivity and resolution of the ultrasonic system. In order to effectively use ultrasonic inspection in tanks with saltcake, flaking rust, and similar types of surface deposits, the walls will need to be cleaned, significantly increasing the cost and time of an inspection.

3.2.2.3 ACFM vs X-ray

X-ray techniques can be used to detect pits but are extremely difficult to deploy remotely on manipulators, especially when there is no access to the far side of the wall. X-ray devices imply the handling of a dangerous source and may not be effective in tanks containing ambient radiation.

3.2.3 Commercial Utilization of ACFM

Type of Flaw	Material	Model	Comments
1) Fatigue cracks	Carbon Steel	Yes	Diver hand held unit used in North Sea since 1990 ROV manipulator deployed array, since 1993
2) Corrosion Pits	Carbon Steel	Yes	RTIEE
	Stainless Steel	No	Model under development
3) Weld, lack of penetration	Stainless Steel	No	On Orbit NDE tool, detection only
	Titanium	No	On Orbit NDE tool, detection only
	Carbon Steel	see 1	
	Duplex Steel	see 1	I.o.p. on remote surface detected
4) Weld, lack of fusion	Stainless Steel	No	On Orbit NDE tool, detection only
	Titanium	No	On Orbit NDE tool, detection only
	Carbon Steel	see 1	
5) Weld, porosity	Stainless Steel	No	On Orbit NDE tool, detection only
	Titanium	No	On Orbit NDE tool, detection only
	Carbon Steel	see 1	
6) Stress cracks	Duplex Steel	see 1	Detected and sized transverse weld cracks

Table 3-2 Brief History of ACFM Usage

Table 3-2 summarizes the history of ACFM usage. ACFM has been used extensively for fatigue crack detection on underwater carbon steel structures and on topside structures in such materials as stainless steel and inconel; it has also been used widely on threads of all materials. Development is underway for its use on aluminum.

ACFM technology has been implemented through both single coil probes that are translated across or along suspected defect areas and through coil arrays. The coil arrays have taken two basic forms: those that are moved over the suspected area (as with the RTIEE) and those

that are stationary. The stationary arrays have also taken two basic forms: fixed, as with the On-Orbit NDE tool (OONDE) and flexible, as with the ROV manipulator deployed arrays (approximate size = 6" x 4"). The flexible systems place each coil on its own spring, allowing the array to be pushed into place in contact with the inspection area, in most cases large structural welds. The ROV flexible array recently successfully completed underwater and Probability of Detection (POD) trials witnessed by Det Norske Veritas (DNV). Special probes have also been designed for use at temperatures up to 500 degrees C and an experimental (in-house) probe was built for temperatures up to 900 degrees C.

In conclusion, ACFM is a flexible electro-magnetic NDE technique suitable for a wide range of applications. The defect type drives the design of the coil array (size, spacing, geometry, etc.) and the development of the analytical models. Hybrid arrays have been developed for specific applications and multiple arrays with different associated math models could be incorporated into the same tool. ACFM has been accepted by Lloyd's of London and Det Norske Veritas as an accurate and acceptable NDE technique for determining the structural integrity of offshore energy production platforms and structures in the North Sea.

4.0 RTIEE Design Methodology

4.1 System Design and Integration

Brief System Overview: The OSS RTIEE design combines a compact vision and lighting system with an advanced electro-magnetic NDE technique, Alternating Current Field Measurement (ACFM). The vision and lighting system allows an operator to distinguish possible sites of corrosion on the tank walls before approaching the wall for a detailed ACFM inspection. ACFM provides the capability to detect and size defects without prior calibration. ACFM sensor coils, mounted in an array, are driven up and down a frame that scans a 3"x6" area in one pass. ACFM does not require any electrical contact with the tank wall to detect and size the corrosion pits nor is it particularly sensitive to standoff or orientation. Therefore, the scanning frame is mounted compliantly to allow the manipulator to push the scanning frame up against the tank wall and thus guarantee sufficiently accurate array alignment with respect to the wall. The video camera is mounted on the centerline of the end effector, providing both a primary view for the operator to drive the manipulator around the tank and a direct view of the inspected area within the scanning frame. The operator is provided with both live video and the results of the ACFM inspection on the same monitor. The ACFM appraisal of the wall may be presented in a variety of ways including a two dimensional false color plot of the magnetic field above the inspected surface and a defect map indicating pit size and position.

The RTIEE system is made up of 5 functional subsystems: the ACFM subsystem, the Mechanical and Structural subsystem, the Vision subsystem, the Electronics subsystem, and the Software subsystem. Each subsystem is integrated with the other subsystems, providing essential services to one another and/or the capabilities necessary to ensure the success of the mission as described in Section 2.4.

4.1.1 The ACFM Sensor Subsystem

The ACFM sensor subsystem provides the ability to detect and size surface pitting (minimum size .030" diameter by .030" deep) in stainless and carbon steel in at least a 3" by 3" area when deployed by a robot manipulator arm (Mission success criteria, Section 2.4).

The subsystem design was influenced by two considerations: definition of the best sensors and fields for characterizing pits and the practical application of these sensors and fields for inspecting a minimum of a 3" by 3" area of tank wall. (Note: The design actually provides inspection of a 3" x 7" area of the tank wall.)

4.1.1.1 Theoretical Basis of the ACFM Sensor Design

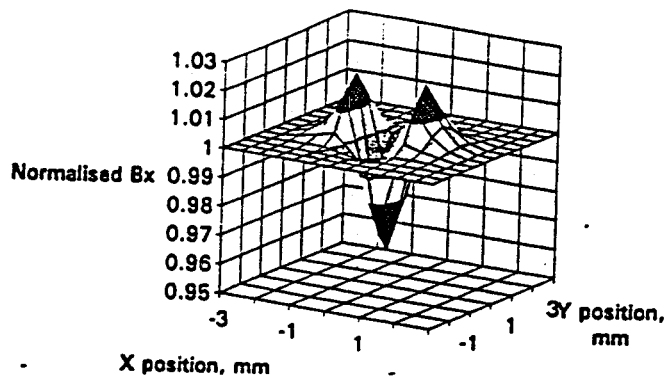
Initial design of the ACFM sensors was driven by work that was performed at the University College London (UCL). UCL modelled the case of a hemispherical pit in a material with thin skin depth (i.e., less than the pit depth). Models exist for this situation for both ferritic and non-ferritic metals. At the frequencies currently available in the ACFM instrumentation (up to 10 kHz), the skin depth in ferritic steel is about 0.005" while that in austenitic stainless steel is about .25". Therefore, for this project the theoretical model for pit sizing applies to hemispherical pits in ferritic steel, however due to the similarities in current flow observed in stainless plate at 5 kHz, empirical relationships to the model can be established that permit accurate sizing of hemispherical and non-hemispherical pits in stainless steel.

Figure 4-1 illustrates the perturbation signals predicted for the three components of a magnetic field produced by a hemispherical pit of .039" (1.0mm) radius in ferritic steel in a uniform input field. The three components are defined as X (parallel to the uniform input B-field), Y (parallel to the uniform input E-field, i.e., the current direction), and Z (normal to the metal surface). The values shown apply to a lift-off of .020" (0.5mm). The values given are all scaled to the value of the uniform input field, i.e., to a background Bx level away from the pit equal to 1. (Lift-off is defined as the distance between the array probe and the surface of the tank wall.)

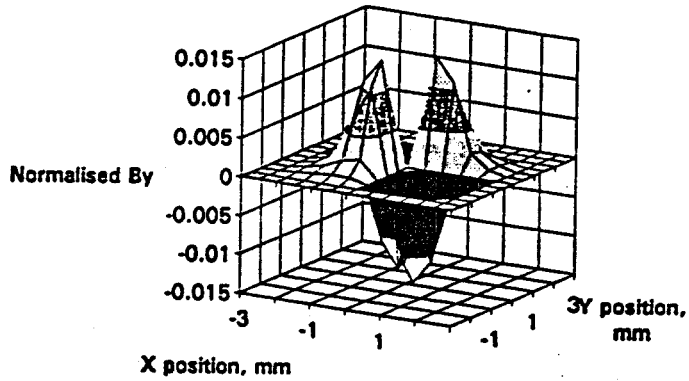
These graphs show the components that would be measured by an ideal point-like coil. In practice, the sensor coils have a finite volume, which means that the coil output is an integral of the input fields over the coil volume. The graphs in Figure 4-2 show the results of numerically integrating the above field distributions in 3 dimensions over the coils (approximated by a rectangular box). Note that the effect of integrating over a finite coil inevitably reduces the signal amplitudes relative to the input field strength, although the actual measured voltages will go up with coil size.

Although all three components of the magnetic field can be measured, in practice two components are sufficient to completely characterize the underlying pit. Since the By signal amplitude is always less than the other two, Bx and Bz are usually measured in ACFM.

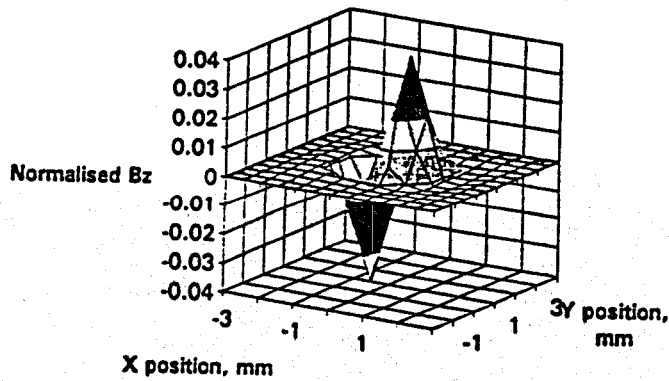
The theoretical model is restricted to hemispherical pits so that a determination of the pit diameter will automatically give the depth (and vice versa). However, the model allows the pit diameter to be determined from either the Bx signal amplitude or the Bz signal spacing (i.e., the distance between the peak and trough). Experience with ACFM on linear defects has shown that in practice the Bz signal spacing is more closely related to, and more sensitive to changes in, the defect length (i.e., diameter), while the Bx signal amplitude is more closely related to, and more sensitive to changes in, the defect depth, at least for large defects.



Theoretical B_x from a 1mm radius pit measured with a point-like coil



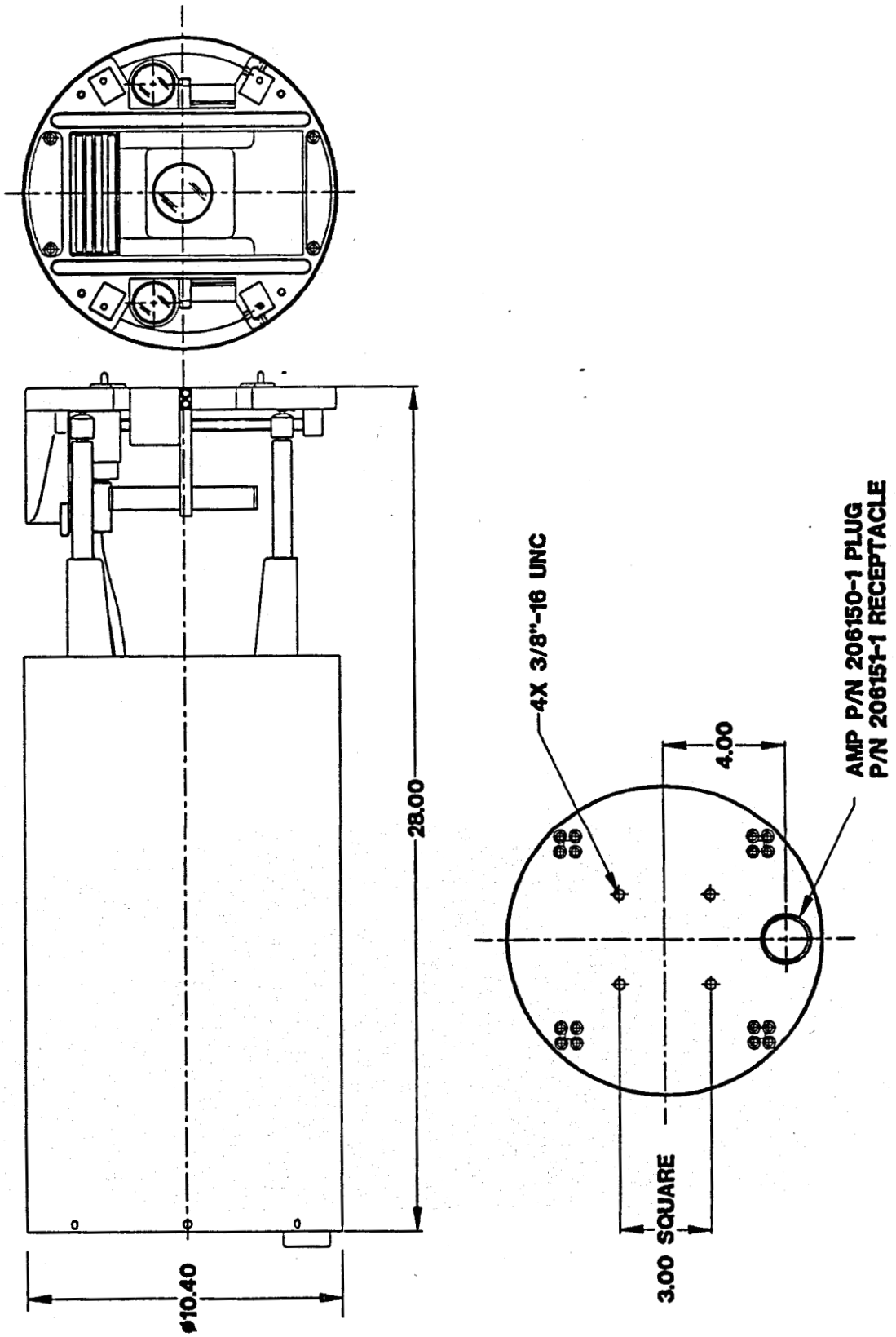
Theoretical B_y from a 1mm radius pit measured with a point-like coil

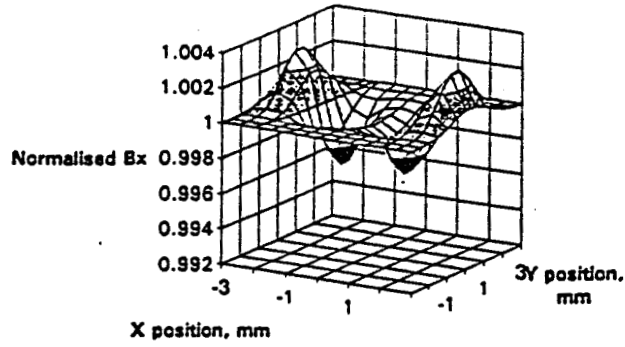


Theoretical B_z from a 1mm radius pit measured with a point-like coil

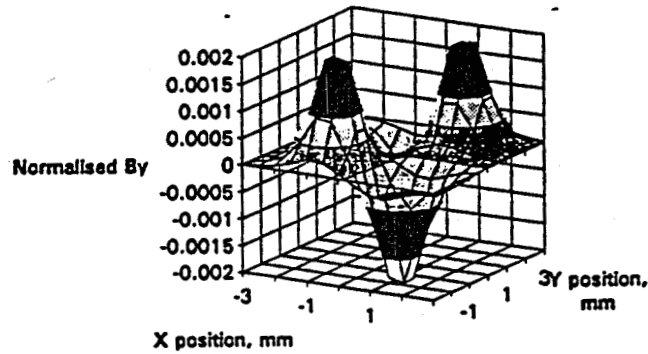
Figure 4-1: Theoretical Magnetic Field Components for a Point Like Coil Over a Pit

RTI Prototype Interface Control Drawing - SK01575

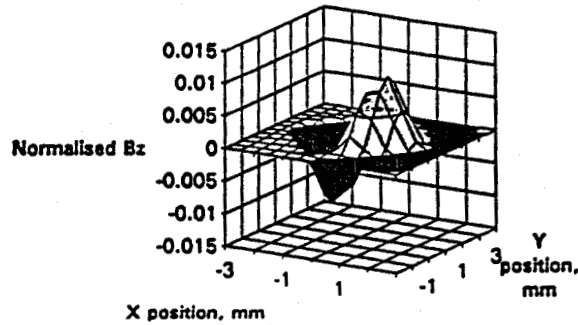




Theoretical B_x from a 1mm radius pit measured with a real coil



Theoretical B_y from a 1mm radius pit measured with a real coil



Theoretical B_z from a 1mm radius pit measured with a real coil

Figure 4-2: Theoretical Magnetic Field Components for a Real Coil Over a Pit

A general approach for sizing spheroidal defects is therefore to estimate the pit diameter from the B_z signal spacing and to estimate the pit depth from the B_x signal amplitude by comparing the amplitude with that predicted for a hemispherical pit and interpolating. This interpolation is straight-forward for pits shallower than hemispherical since the signal from a zero depth pit would be zero. For deeper pits the situation is more complicated because the

nature of all eddy current techniques is such that very little current flows under the pit when the current path around the side is shorter, so that the technique is insensitive to changes in depth for pits deeper than their diameter (Figure 4-3). The insensitivity of ACFM to pits that are substantially deeper than their diameter does not pose a significant problem. This is due to the fact that corrosion on steel does not generally create deep, narrow pits, but usually produces a defect with a much shallower profile.

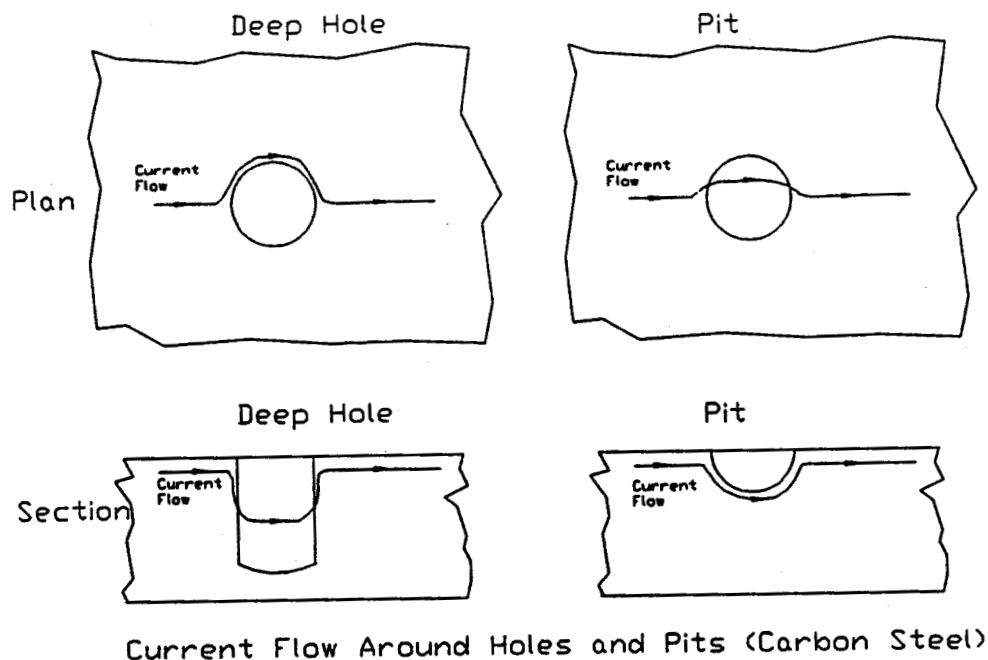


Figure 4-3: Current Flow Around Holes

Figure 4-4 shows predicted curves of B_x and B_z signal amplitudes for a range of pit sizes, derived from the model results for a real coil.

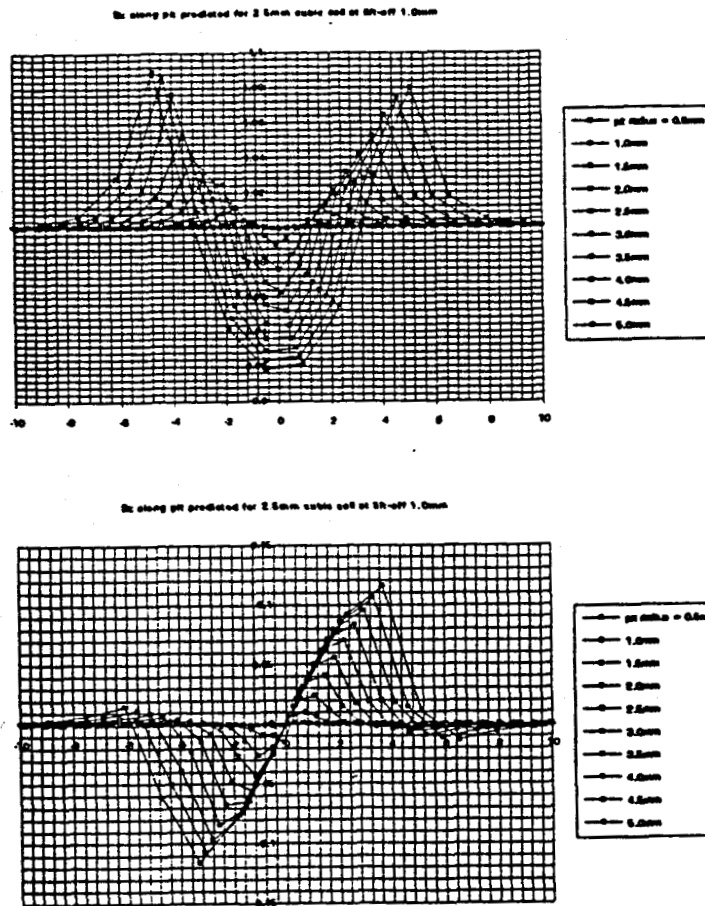


Figure 4-4: Predicted Responses vs Pit Size

Figure 4-5 shows predicted curves of Bx signal amplitudes and Bz signal spacings versus pit size, derived from the ferritic steel model results for a real coil. In previous projects, characterizing features as small as the minimum .030" pit had indicated that the magnetic field disturbances created by these features would be correspondingly small and would decay quickly away from the surface of the material. The signal amplitudes expected from the theory given above are small (1% in XBx for a 1mm deep, 1mm radius pit). A second induced field was therefore incorporated into the design. The second field, a Z field, was not intended to be uniform; instead, when used with the Bz sensor coils, it provides much improved pit detection capability. A Bz sensor in a Z field is a traditional eddy current arrangement and produces a single peak or trough centered over the defect (however eddy current sensors usually use the same coil for both field induction and sensing).

The design of the ACFM inspection system therefore consists of two input fields (X and Z) and two sensor coils (Bx and Bz). Four combinations of field and sensor were possible, two were modelled and two provided supplementary information.

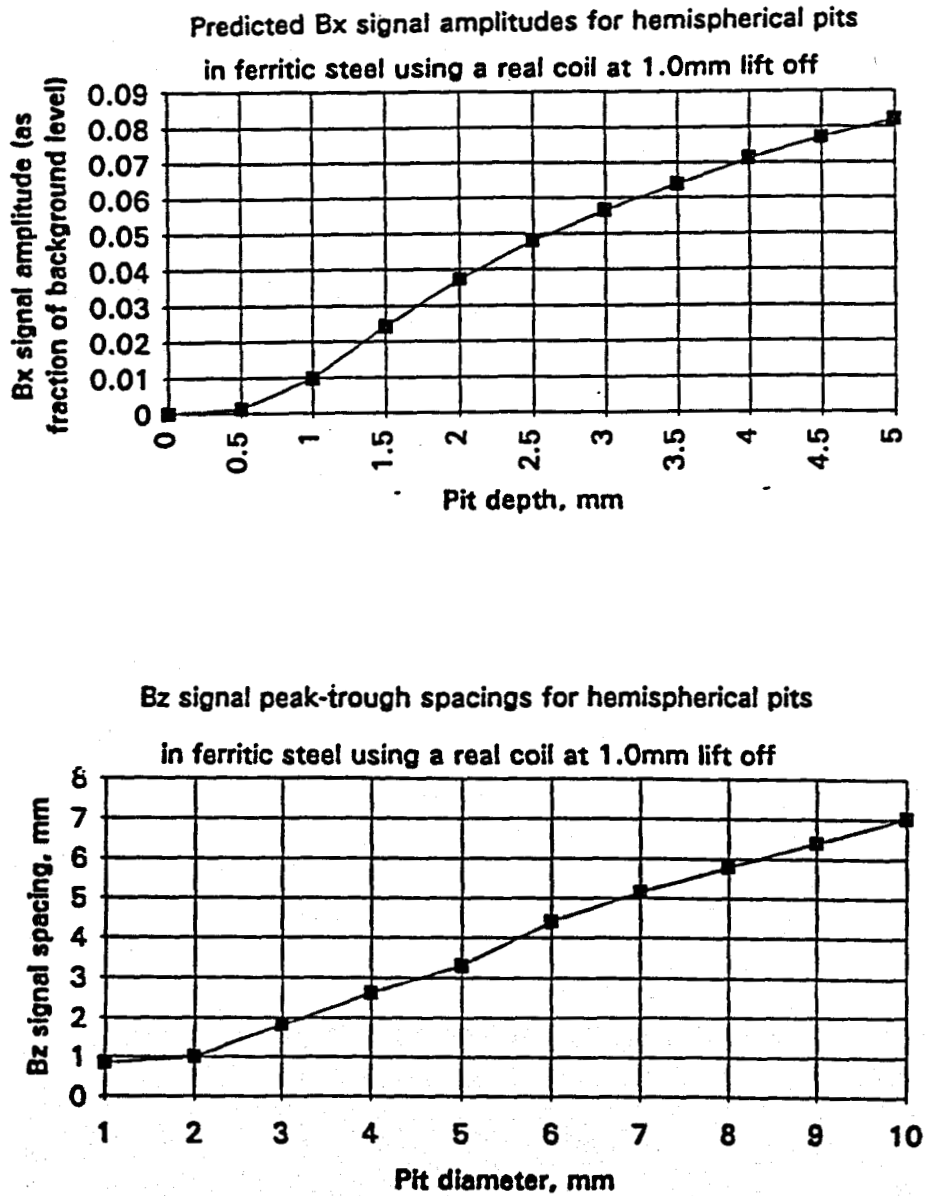


Figure 4-5: Model Results for Bx and Bz Response Over Hemispherical Pits

The X-field usually cannot be made completely uniform because of practical constraints placed on the size and position of the solenoids, and the presence of neighboring metallic components in the field (motors etc.). These non-uniformities are removed by collecting a set of data from a good (i.e., flat, defect free) area of metal and storing this to be subtracted from subsequent data. This normalization process is commonly used in all other ACFM array

applications and helps to emphasize small disturbances in the fields. It is performed by the operator as the first step in an inspection.

4.1.1.2 Hardware Implementation of the ACFM Sensor

Figure 4-6 illustrates the configuration of the ACFM sensor coils. The diameter of the individual sensor coils was the first aspect of the subsystem design to be determined. A coil recording a magnetic field essentially averages the strength of the field over the area of the field it interrogates. A conservative rule of thumb is to estimate that a coil will interrogate an area equivalent to its outside diameter; when deployed close to a surface the coil coverage can be directly superimposed on the surface. This means that a sensor coil much larger than a defect may not sense the defect because the localized perturbation in the magnetic field is averaged with the surrounding field. The minimum defect to be detected is a pit of .030" (0.76mm) diameter. This would indicate that a line of closely spaced coils of about 0.76mm outside diameter would be required to guarantee that no pit was missed during a scan. However the manufacture of such small coils is very difficult and costly. Therefore, an array of staggered lines of sensor coils was designed to provide sufficiently high detection resolution in one dimension, perpendicular to the scan direction as shown in Figure 4-7. The diameter of each coil is 2mm but the centers of the coils in the three Bz rows are 0.75mm apart when the array is moved in the X direction. Only the Bz coils are arranged in this manner because their primary job is detection of the pits. The single row of Bx sensors provides lift off measurement (and hence the depth of larger features) at a lower resolution. The requirement to inspect a minimum of 3" by 3" of tank wall determined the width of the array. Taken together the three rows of Bz sensor coils can inspect a 3" area. The length of the inspected area is determined by the travel of the scanner carriage, which although constrained by the 10.5" diameter of the end effector allows every sensor coil to inspect any location in a 4.4" range. Individual coils can, however, be scanned 6.2", increasing the possible area of defect detection. The resolution in the scanning direction (X) is provided by selecting an appropriate step size and moving the whole array in increments equal to the step size.

With the definition of the sensor coils, arrangements for providing the induced fields were considered. Two types of field were required, a uniform X field and a non-uniform Z field. After considerable experimentation the Z field was implemented by building a channel frame around the array screening box and winding the coil within the channel (see Figure 4-6). The large diameter Z solenoid was wound around the central axis of the array, an axis that was parallel to the 96 Bz sensor coils. The final X field arrangement used two solenoids one on either side of the inspection window wired in series. The individual X solenoids were wound around a 0.25" plastic core and made as long as possible within the diameter constraints of the end effector. This created a field that was as uniform as possible for any position of the sensor array.

RTIEE ACFM Probe

View of the probe footprint as left by the probe when placed on a test sample.

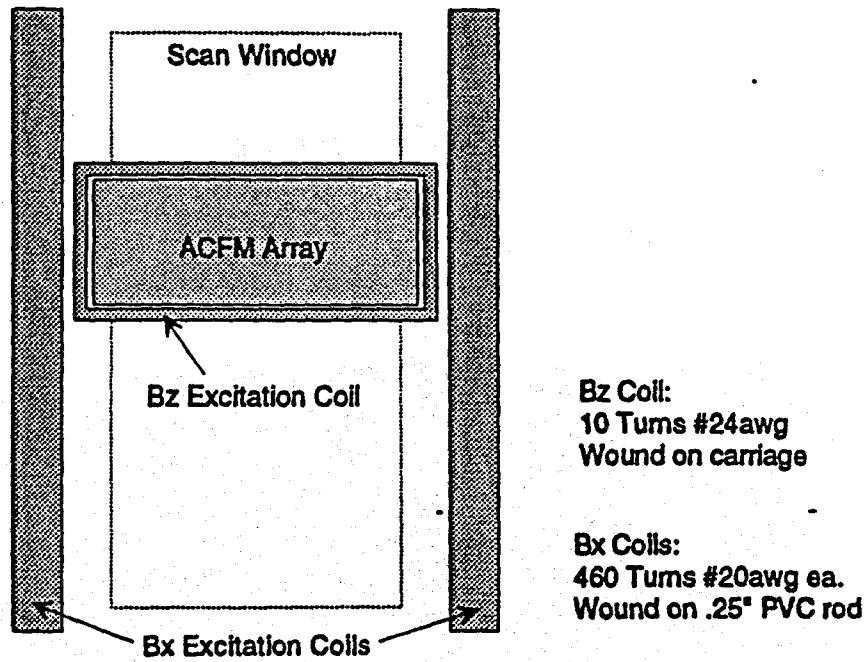
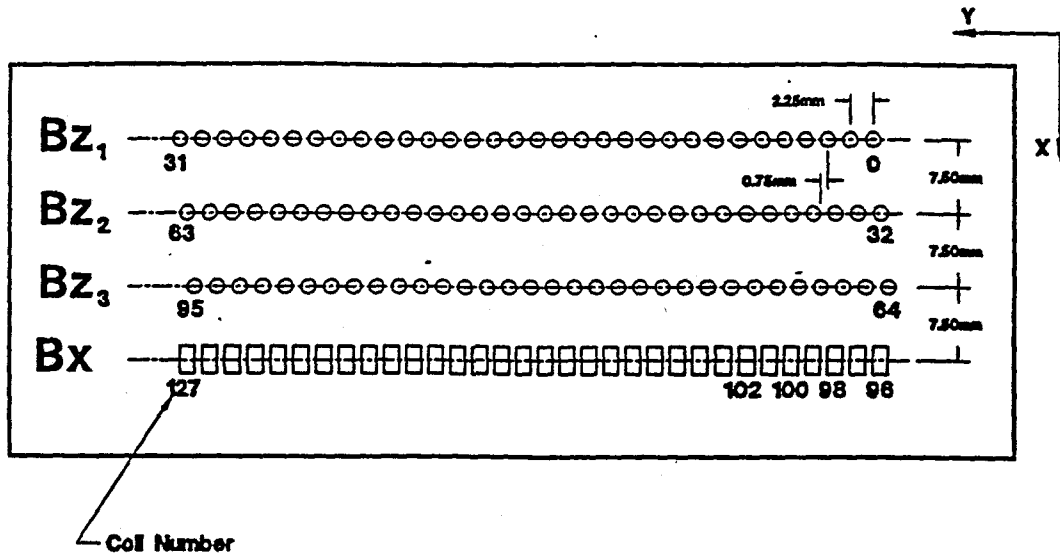


Figure 4-6: RTIEE ACFM Sensor Coil and Induction Coil Arrangements

4.1.1.3 Sensor Signal Phase

The voltage recorded by any one of the 128 ACFM array sensors has two attributes: amplitude (the absolute magnitude of the signal) and phase (how the signal varies in time, relative to the drive signal). Both the phase and amplitude of a sensor signal is affected by the proximity of conducting materials such as the scanner frame and the tank wall. Each sensor therefore experiences a phase shift relative to its neighbors because each sensor is in a slightly different position relative to local conducting surfaces. When these sensor signals are recorded by the data acquisition system, either a full wave rectifier or Phase Sensitive Detector (PSD) can be used. If the precision rectifier is used, the absolute value of the amplitude of the sensor signal is recorded independent of the phase of the signal. If the PSD is used, then the amplitude is recorded with respect to the drive signal reference.

The precision rectifier offers the advantage of being insensitive to phase variation across the scan that is introduced by surrounding structure within the end effector. When the background signal levels are significantly higher than the signal due to a defect, a trough and a peak overall signal is observed which corresponds to the negative and positive components of the defect signal.

In a perfect X field there is no z component except in the presence of a defect and in practice the signal is quite small. When the background signal is quite small compared to the signal due to a defect, then the "trough", which is the negative portion of the defect signal, effectively reduces from the background field below zero to a significantly negative value. Using the precision rectifier, the signal still appears a peak because only absolute value is being recorded. In this case a two peak signature will be recorded instead of the usual peak trough pair.

The variation of phase angle over the scan angle precluded effective use of the phase sensitive detector during the early testing in the breadboard system. During early testing of the prototype system, it was found that the phase change occurring across the scan area over a clean sample plate could be significantly reduced. This was accomplished by electrically isolating the steel plates, which form the array probe case, from one another. When the plates are in contact, a complete current path is formed around the case, which affects the readings taken by the sensor coils. The phase varied as a function of coil location in the array and array location within the scanner frame.

After isolation of the plates in the array shield, the phase variation was minimized and the PSD could be effectively used. By keeping track of the signal phase, the PSD can record both positive and negative signals arising from a defect, thus eliminating the double peak signals and significantly improving the performance of the sensor system. Both options are available in the prototype.

4.1.1.4 Implementation of the ACFM Detection and Sizing Algorithms

Detection and Sizing of Pits in Stainless Steel

The first step in the detection process is normalization of the magnetic field data. This is accomplished by subtracting the values taken during a scan over a defect free sample plate from the values obtained during the inspection of the test plate. This reduces the overall magnitude of the resulting data and highlights the areas which varied from the normalization scan. Next, the XBz signal is differentiated along the path of each sensor coil. This produces a relatively flat result with a peak, or trough, centered on the pit center and the resulting signal is then normalized with the mean raw value of XBx (Figure 4-7). A thresholding function is then applied which flags responses above the user set threshold and are therefore potential defects.

The next step of the procedure uses the previously located suspect sites as a starting point. Beginning with the site with the largest value of $d/dx(XBz)$, a search is performed radially from the center of each site to locate the zero crossing points of the signal, and hence define the boundaries of the site. The process is repeated for each suspect site in the scan.

The diameter of the defect associated with each site is derived by applying the carbon steel model, with correction factors, using the dimension of the suspect site boundaries found above. A final level of checking is performed based on the calculated diameter to reject spurious indications of defects.

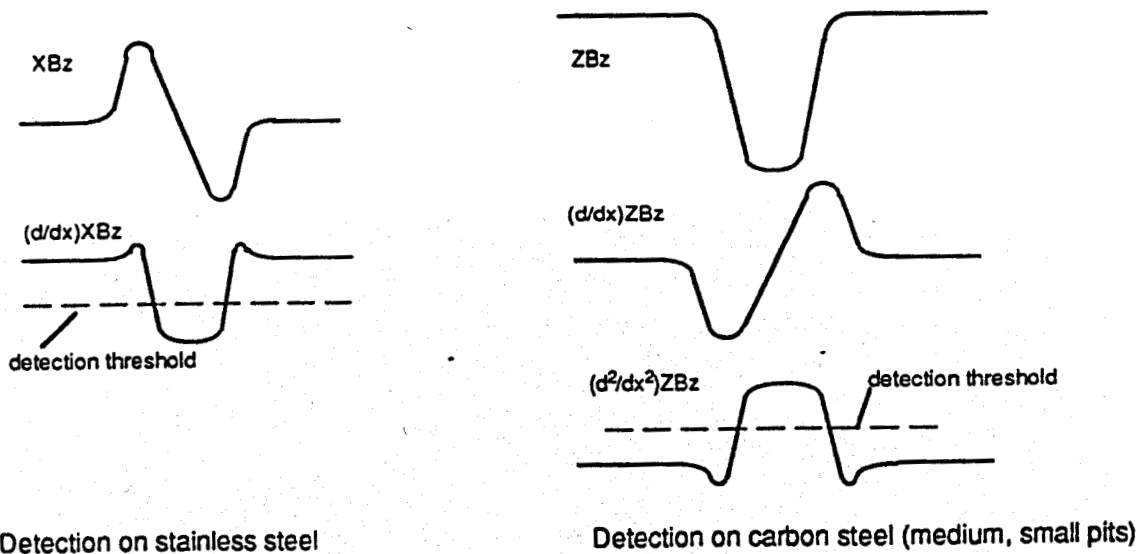


Figure 4-7: Detection schemes

The last step is to determine the depth of each defect and is accomplished by looking to the magnitude of the X_{bx} signal in the area identified as a defect by the previous algorithms. The depth is found by applying the carbon steel model, with correction factors, using the magnitude of the X_{bx} signal and the previously calculated diameter.

Detection and Sizing of Pits in Carbon Steel

The process of identifying and sizing pits in carbon steel is somewhat more complicated than in stainless steel. As with stainless, the first step in the detection process is normalization of the magnetic field data. This is accomplished by subtracting the values taken during a scan over a defect free sample plate of carbon steel from the values obtained during the inspection of the test plate.

Next, the X_{Bz} signal is differentiated along the path of each sensor coil. This produces a relatively flat result with a peak, or trough, centered on the pit center and the resulting signal is then normalized with the mean raw value for X_{bx} . A thresholding function is then applied which flags potential defects which have responses above a preset threshold.

The next step of the procedure uses the previously located suspect sites as a starting point. Beginning with the site with the largest value of $d/dx(X_{Bz})$, a search is performed radially from the center of the site to locate the zero crossing points of the signal, and hence define the boundaries of the potential defect site. The process is repeated for each suspect site.

The diameter of the defect associated with each site is derived by applying the carbon steel model using the dimension of the suspect site boundaries found above. A final level of checking is performed based on the calculated diameter to reject spurious indications of defects.

The depth of each defect is found by looking to the magnitude of the X_{Bx} signal in the area identified as a defect by the previous algorithms. The depth is calculated by applying the carbon steel model using the magnitude of the X_{Bx} signal and the diameter previously calculated.

At this point, unlike the procedure for stainless, a second level of detection is performed to identify smaller potential defects using a more sensitive field combination. For very small pits, which are only seen in B_z , the pit depth causes a second-order variation in the B_z amplitude. The second differential of the Z_{Bz} field is calculated and then normalized with the mean raw X_{Bx} data (Figure 4-8). The resulting data is inspected against a user defined threshold and any sites which exceed the threshold are considered potential defect sites.

Any defects previously identified as defects using the X_{Bz} field are removed from the list of potential sites as they have already been characterized. If not, the larger pits may be

wrongly classified as two or more smaller pits. This arises because a wide pit produces a flat-bottomed ZBz and thus two peaks in the second derivative (or for very large pits as a torroidal ring shape which is interpreted as a ring of small pits). This effect is demonstrated below in Figure 4-8.

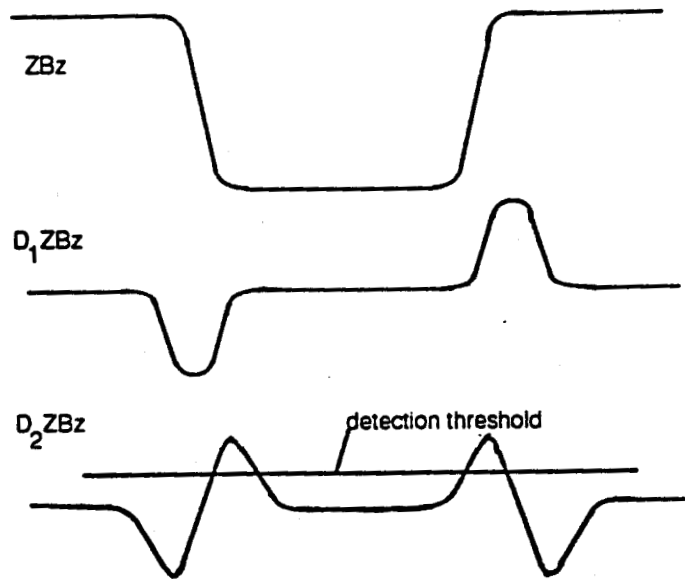


Figure 4-8: Detection of Large Pits on Carbon Steel

Beginning with the site with the largest value of $d^2/dx^2(\text{ZBz})$, a search is performed radially from the center of the site to locate the zero crossing points of the signal, and hence define the boundaries of the suspect location. The process is repeated for each suspect site.

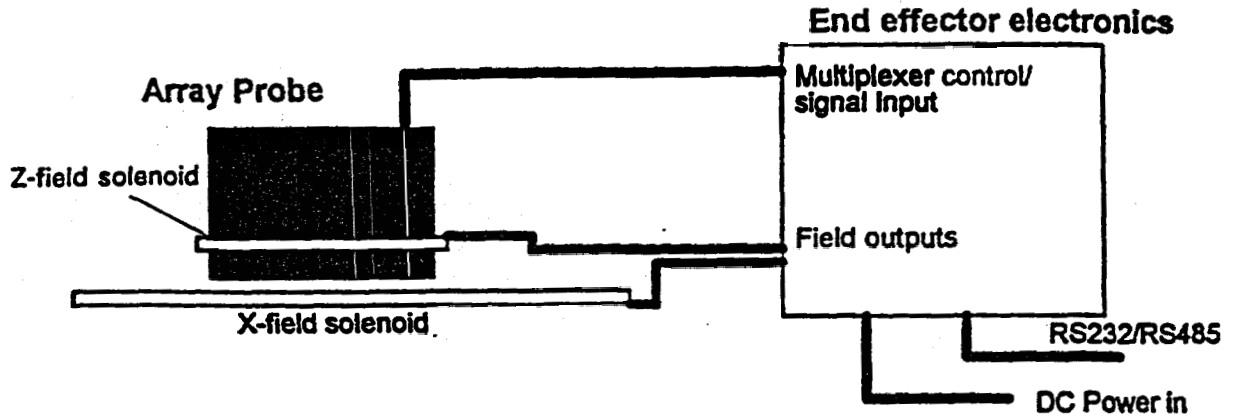
The diameter of the defect associated with each location is found by applying the carbon steel model using the suspect site boundaries found above. If the value of $d^2/dx^2(\text{ZBz})$ is below a preset threshold, then the diameter is calculated as a function of the amplitude of the ZBz signal. This signal is used as it provides the most accurate data for very small pits in carbon steel. A final level of checking is performed based on the calculated diameter to reject spurious indications of defects.

The depth of each defect is found by looking to the magnitude of the ZBz signal in the area identified as a defect by the previous algorithms. The depth is calculated by applying the carbon steel model using the magnitude of the ZBz signal and the diameter found by the previous function.

4.1.1.5 Controlling the ACFM Subsystem

With the sensor array and field induction arrangements defined, the next task was the design

of the control system and signal processing electronics (see Figure 4-9). It was decided to collect and digitize the sensor data locally within the end effector. This had the advantage of allowing data transfer between the end effector and control computer to occur via a serial line, a much more robust method of transfer than trying to transmit the very small voltage signals across large lengths of cabling (150'). It was further decided to multiplex the sensor signals at the array and reduce the number of conductors carried in the array umbilical, which in turn reduced the loading on the scanner carriage.



The components inside the array probe are shown in more detail below:

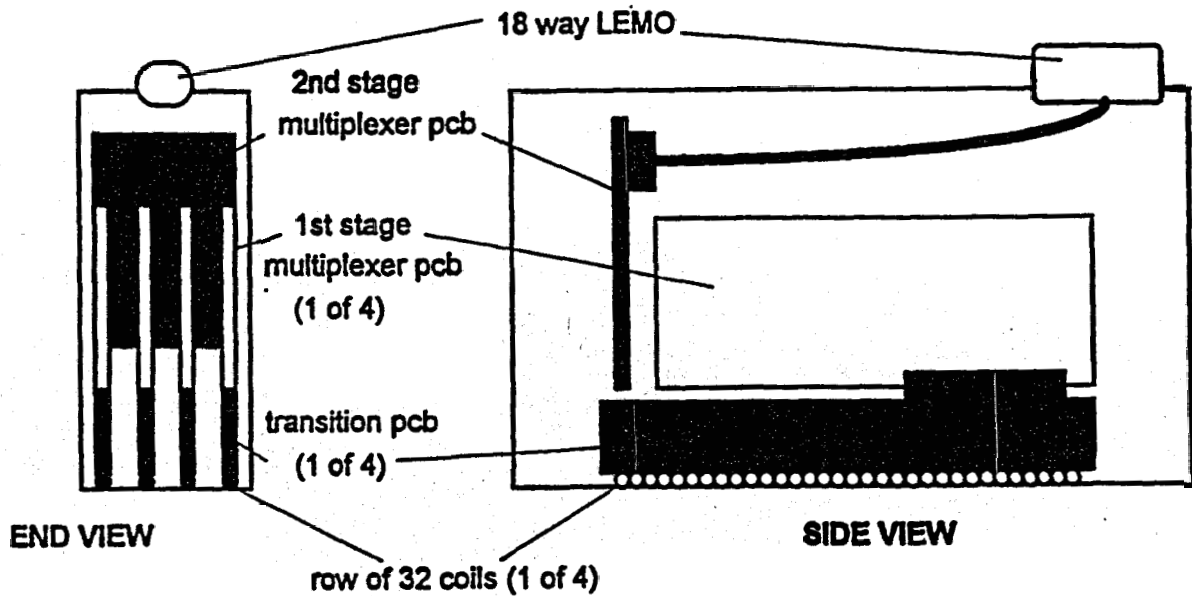


Figure 4-9: ACFM Subsystem Layout

The prototype sensor system is therefore split into two main components, the sensor array and the data acquisition electronics. The sensor array is made up of 96 Bz coils and 32 Bx coils arranged in four rows (convenient numbers for multiplexing). Behind each row is a printed circuit board (pcb) populated with multiplexing and signal processing chips and components. Each pcb is connected via a transition pcb to an umbilical. The umbilical connector and all the boards are mounted inside a carbon steel box, the arrays screening box, which is located in the sensor array carriage. The umbilical connects the array to the data acquisition electronics; the data acquisition electronics are connected to the control computer via a serial line. A dedicated microprocessor card controls the data acquisition and array and the field set-up using specifically written firmware. These firmware commands can be accessed via an RS-232 serial line and a suitable terminal emulator. The data acquisition electronics are mounted on five cards connected to a common backplane in the end effector. The cards and backplane are shown in Figure 4-10.

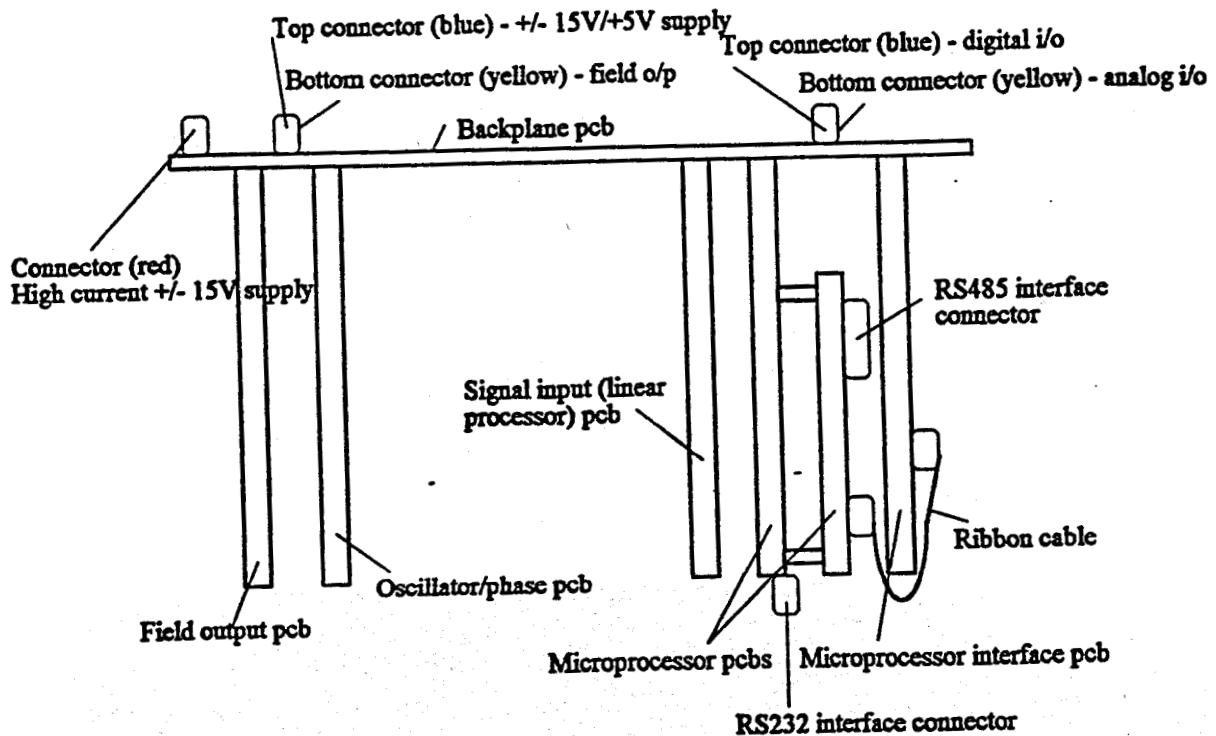


Figure 4-10: ACFM Data Acquisition Electronics Layout

4.1.2 The RTIEE Mechanical Subsystem

The mechanical subsystem is designed to contribute to mission success criteria number 1 and 2 (Section 2.4). Its task is to house and protect the ACFM sensor and the vision subsystems as well as provide an interface for the manipulator system. Details of the relevant mechanical and electrical connectors for the RTIEE to manipulator interface are contained in the RTIEE Interface Control Document (ICD) in Appendix A.

The body of the end effector consists of the structural members, the wall compliance accommodation devices, internal component mounting accommodations, and a scanner frame assembly, as shown in Figure 4-11. The main body attaches to a manipulator through a base plate which includes both the mechanical and electrical interface to the manipulator. Four struts protruding from this plate carry the cylindrical shell and provide a load path into the base. The camera, lens, and sensor electronics are mounted within the main body. The camera, lens, and sensor electronics are mounted within the main body.

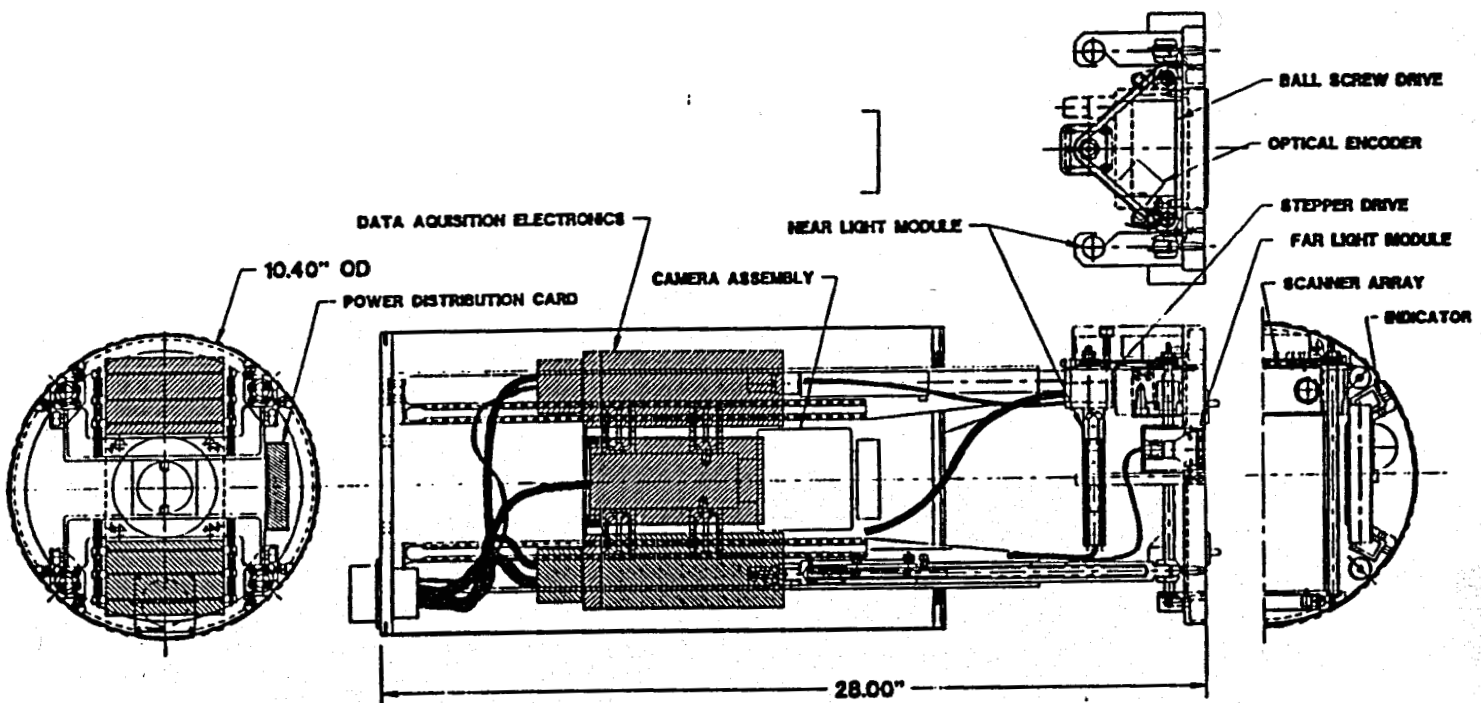


Figure 4-11: Prototype RTIEE General Arrangement

Four stainless steel compression rods are sprung in aluminum-bronze housings and mounted between the end effector shell and the compliant scanner frame. These compression rods allow pitch and yaw movement of the scanner frame relative to the main body and absorb impact loads as the end effector is pushed up against a tank wall. Each compression rod also has a secondary high stiffness compression spring that significantly reduces peak loads due to inadvertent bottoming of compression rods.

The scanner frame carries the ACFM sensor array. The array is driven up and down within the frame on two acme lead screws. The drive shafts are connected to a stepper motor by a timing belt. The position of the head is tracked with an optical encoder engaged to the timing belt. In this way, exact position of the scanner may be known at any time. Additionally, any interference with wall protrusions that interfere with scanner motion is easily detected. Two limit switches are attached to the frame and report the two extreme positions of the sensor array carriage for software stops. Four mechanical status indicators are mounted in the frame and are visible in the operator's camera view. When the protruding push rod of the status indicator is depressed by contact with a wall, a colored strip moves within the indicator window that faces the end effector camera. The combination of the four indicators gives the operator pitch/yaw cues during landing and visual indication of flat contact with the wall. In addition to these indicators, each strut is outfitted with optical sensors to detect and report compression levels of 0.25" and 2.00" of the maximum 3.00" stroke. The indicators are displayed in the upper right hand portion of the control screen and allows the operator to determine when the scanner frame is preloaded against the wall as well as providing indication of excessive contact force with the wall causing the struts to compress past their nominal 2.0" compression.

4.1.3 The RTIEE Vision Subsystem

The camera and lights subsystem contributes to mission success by providing the RTIEE operator with a view of the storage tank wall surface when the end effector is deployed by a robotic manipulator. This subsystem has three primary functions. The first is to allow an operator to locate possible areas of corrosion attack at up to 37.5' from the tank wall. The second is to provide the operator feedback on the condition and compliance of the scanning frame during contact with the wall. The third to record a high resolution video image of the area of tank wall to be inspected.

A CCD camera is mounted on the centerline of the end effector body. A motor driven lens is attached to the camera and a wide angle lens adaptor is attached to the lens. The lens adaptor increases the field of view of the camera from 41.9 degrees to 56.6 degrees and allows the operator to view the back of the scanning frame (useful when seeking contact with the tank wall) and to view a distant object (useful for identifying inspection sites on the tank wall) without any of the scanning frame obstructing the view.

The lighting system consists of two sets of lamps. The near set, mounted on either side of the

scanning frame, illuminate the rear of the scanner frame and the tank wall at close range. The far set, mounted on the front face of the scanner frame, illuminate distant objects. The near lamps each have a power rating of 20 watts per side and the far lamps are rated at 35 watts each. The motor driven iris, zoom, and focus functions and the lighting intensity of all the lamps are controlled from the operator interface screen. Local control logic circuitry mounted in the end effector body supports the lighting control functions and the stepper motor power drive.

4.1.4 The RTIEE Electrical Subsystem

The electrical subsystem contributes to all four mission success criteria. Its task is to provide power, data and control functions for all the active components in the end effector body. Figure 4-12 shows the overall layout of the system components.

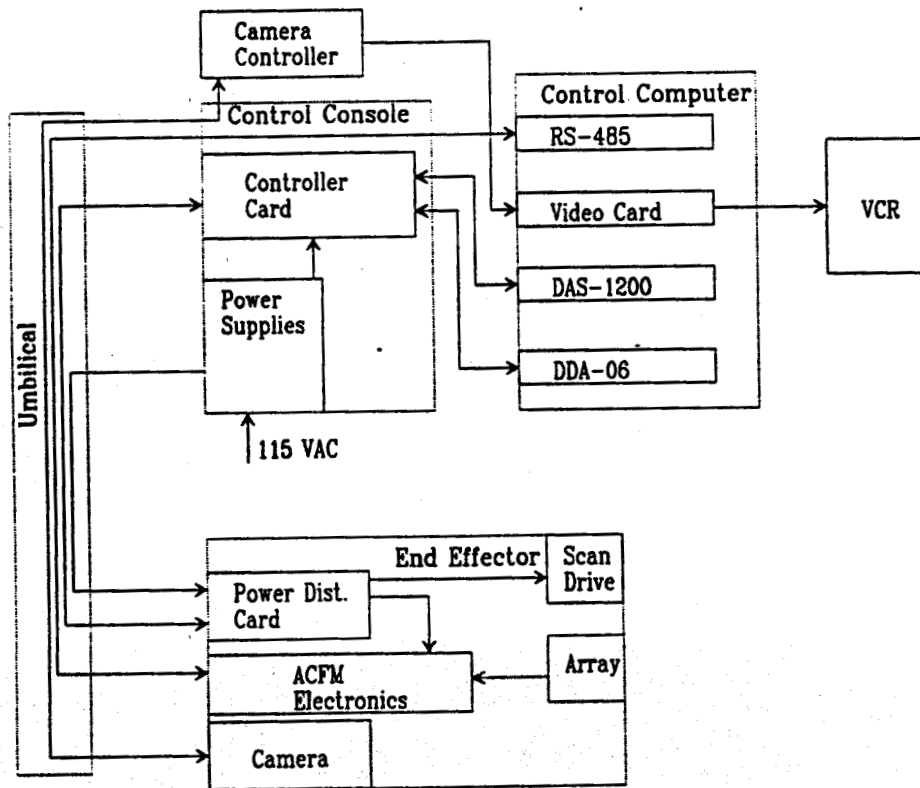


Figure 4-12: Electrical Subsystem Component Layout

This subsystem consists of all of the RTIEE electronic hardware on the end effector as well as the support electronics at the operator workstation, such as the power distribution station and computer workstation and the cabling in between. It is functionally subdivided into power, data, control, and the umbilical linking the end effector with the operator workstation.

4.1.4.1 Power Distribution

The end effector system requires a single power source of 115 VAC at 7A max. The power distribution enclosure at the operator console provides all secondary power requirements from the 115 VAC source, thus eliminating the need for special purpose outside power sources.

In addition to supplying the power required for the controller board at the operator workstation, the system also provides three secondary power sources via the umbilical for use by the end effector systems. They are $\pm 20\text{VDC}$ (5A max unregulated, linear), 12VDC (13A max regulated, switching), and $\pm 5\text{VDC}$ (3A max regulated, linear). The incoming 115VAC line is fuse protected and all power outputs to the end effector are either electronically protected or fused to protect against over-current conditions.

Within the end effector, the +12VDC source is used by the lighting system. The $\pm 20\text{VDC}$ source is regulated and conditioned within the end effector to provide power for the field generation electronics, microprocessor systems, and the analog signal processing system. Each of these systems has its own regulator and filter to minimize noise and crosstalk between systems. The $\pm 5\text{VDC}$ source is used as the power source for the stepper motor used to position the scanner head.

4.1.4.2 Data Transfer

All data exchange between the end effector and the operator workstation is accomplished via a single umbilical and can be grouped into three areas. The first is the video information from the end effector camera to the computer monitor. This is transferred over a single RG-63 coax cable in the umbilical, which both carries power to the camera and returns video to the camera controller. Video supplied from the camera controller is NTSC, 30fps, line-level video. The video is supplied to both the multimedia video card and any other recording device such as a VHS VCR.

The M&M Pro is a single slot multimedia card that overlays video onto a SVGA pass through. The video section uses 24-bits to provide 16.7 million true colors to represent live video onto the computer screen. For live video windowing and frame capture the M&M Pro accepts NTSC, PAL, SECAM and S-Video. An attached daughter board provides video encoding capabilities to record flicker free NTSC, PAL, and S-Video output of VGA video and overlay screen.

The second data group is the RS-485 communication between the end effector microprocessor and the control console. This path serves to transfer system commands to the ACFM system as well as provide a path for all scan data to be returned to the RTIEE computer for display and analysis. The RS-485 protocol is used for its ability to run long lengths at relatively high transmission rates. The communication rate over this link in the prototype end effector is 19.2kbs.

The remaining communication between the end effector and operator console occurs in a parallel format. This includes data used for driving the scanner frame, sensing strut compression limits, and lighting control. All of the digital signals in this parallel link utilize RS-232 drivers/receivers to maintain signal integrity and protect against damage from short circuits.

4.1.4.3 Control Subsystem

The microcontroller in the end effector is responsible for local control of the excitation field and for scanning the appropriate sensor coils in the array. When the software issues a command for a scan of a particular set of sensor coils, each coil is sampled and the data is stored in RAM in the end effector controller until the scan is complete. This minimizes the number of separate transmissions over the serial link and hence minimizes the overall data transmission time.

The control computer for the RTIEE prototype has been fitted with 2 Analog/Digital I/O cards. The first is a DDA-06 Cyber Research analog output card. The card provides 6 channels of analog output along with 24 channels of TTL compatible digital I/O. The second card is a DAS-1200 Cyber Research analog input card. Eight channels of analog input are provided along with 24 channels of digital I/O.

These two cards are connected to the control console via three 37 conductor ribbon cables. Here, they interface with a card which provides suitable buffering for all of the dedicated digital I/O lines which continue on to the end effector. An example of a function using these digital I/O lines are the strut compression indicators. Eight of the I/O lines are used by an 8-bit control/data bus on the controller card which manages the operation of the stepper motor driving the scanner. The RTIEE software loads the next scan step size on the controller buffers, sets a scan direction, and then issues a run command. The computer is then free to perform other operations and will be notified when the motion is complete.

All scan position data is verified by a quadrature encoder mounted to the drive line of the scanner. After each step, the RTIEE software checks that the actual distance traveled by the scan head corresponds to the commanded motion. This check assures an accurate record of the scanner position and allows the system to detect any anomaly which might preclude proper scanner travel.

4.1.4.4 RTIEE Umbilical

Power and data is transferred to and from the end effector through a single umbilical. This umbilical terminates at a 37 pin connector at the rear of the end effector. The umbilical is 50' long to simulate transmission of power and data over a representative length. Provision has been made in the prototype system to drive all supply and signal voltages through 250' of cable if required.

4.1.5 The RTIEE Software Subsystem

The software subsystem contributes to all aspects of mission success. It facilitates (1) operator viewing of the tank wall, (2) control and data acquisition of the ACFM sensor, (3) analysis of the data to detect and size pits, and (4) displaying live video and inspection data on the computer monitor.

The software code is written in C and developed for IBM compatible microcomputers operating in a Microsoft Windows environment. The software architecture is presented in Figure 4-13. It is structured in a top-down, hierarchical fashion and is functionally modular.

The software is designed around an internal RTIEE messaging system encapsulated inside of the Windows messaging system. The internal RTIEE messaging system (the Command Buffer Module) was implemented to facilitate GISC message processing. It was separated from the Windows messaging system to reduce dependency on Windows should the software package be ported over to a different platform, e.g., UNIX. Internal RTIEE messages have two sources. One source is the operator at the workstation performing a windows operation such as selecting an item from the Graphical User Interface (GUI). The other source is from the RS-232 port. This is a design scar for future integration into a GISC environment.

The software subsystem modules shown in Figure 4-13 can be subdivided into three groups. Control modules support control of the RTIEE functions such as camera, lighting, and the ACFM sensor array. The overall RTIEE control module that oversees all internal RTIEE messaging is also included in this group. Data collection and analysis modules control the transfer of data from the end effector to the computer, analysis of the data, and subsequent storage of the data to secondary storage. The GUI modules control the visual interface provided to the operator to control and monitor the RTIEE.

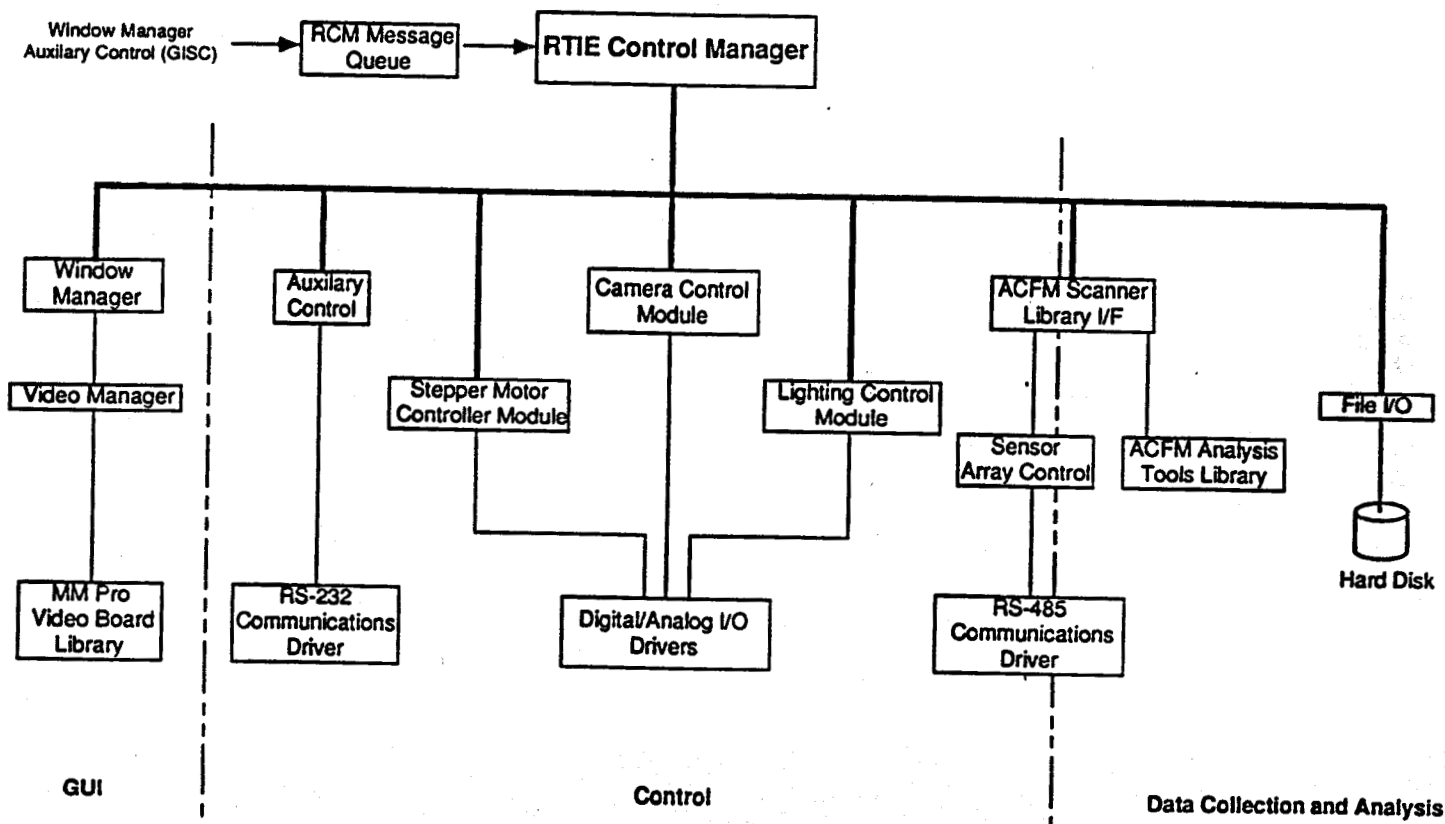


Figure 4-13: RTIEE Software Design Architecture

4.1.5.1 Control Modules

There are three end effector functions that are controlled through software: camera, lighting, and sensor scans. RTIEE camera zoom, focus, and iris controls are controlled through software and the digital to analog boards which generates the electrical control signals to the end effector. Real time video from the RTIEE is simultaneously channelled to the main screen for viewing and out to a separate monitor or Video Cassette Recorder for recording. Lighting is also handled through dedicated D/A channels which control on/off and intensity. Both camera and lighting are controlled open loop.

The stepper motor, which drives the sensor carriage, is also controlled open loop, but has a feedback path via an encoder for the software to monitor the size of each scan step. Any scan steps beyond a specified error tolerance will be considered a scan error and the operation will be aborted.

4.1.5.2 Data Collection

Between each scan step, software routines are executed that activate the magnetic fields and sample the individual coils. Data is sent through the RS-485 serial port to the computer where analysis can be performed. Collected data and video images can be stored onto secondary storage media (e.g., hard disk) and retrieved for data analysis at a later date. The data files are stored in ASCII and binary. The scan data is stored in ASCII, for compatibility with other software packages for analysis, and the sensor coil characteristics are stored in binary. Video Image data can be stored in a variety of file formats: .PCX, .BMP, .TGA.

4.1.5.3 Data Analysis

The analysis routines currently supplied are "Normalize", "Locate Defects", and "Calculate Lift Off". "Normalize" uses a data scan from a clean sample plate and produces a map of nominal values for each scan site which is subtracted from the data. "Locate Pits" determines the location, size, and depth of detected pits. "Calculate Lift Off" produces a low resolution surface map of the surface and produces a low resolution surface map of the surface.

Locating Defects in Stainless Steel

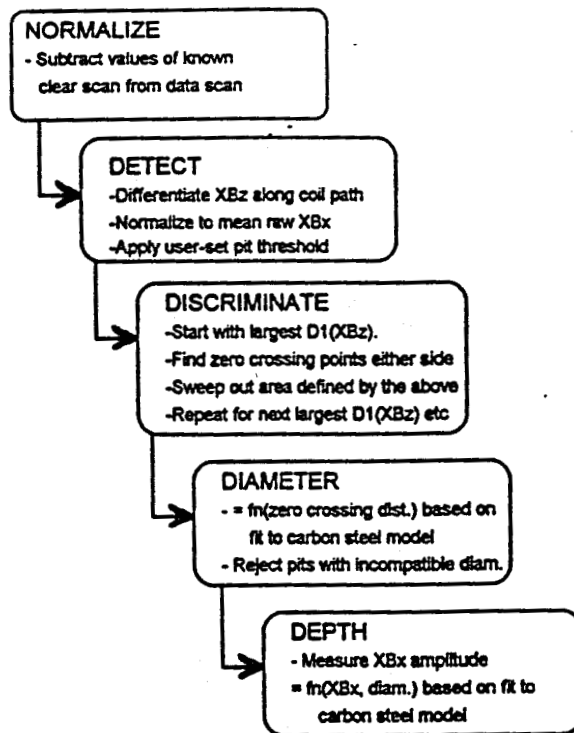


Figure 4-14: Stainless Steel Detection/Sizing Algorithm

The five stages involved in the process are:

Normalization	Designed to subtract the effects of non-uniformities in the background field inputs and coil sensitivity variations.
Detection	The normalized XBz data (the most sensitive data for stainless steel) is filtered (by looking at the derivative along a coil path). All points breaking the user-set threshold are then marked and stored. The threshold should be set close to the "noise" value. Setting a high value will result in no spurious calls giving a rapid response from the routine, but will miss small pits. Setting a low value will detect small pits but will also give rise to spurious calls thus slowing down the routine.
Discrimination	This is designed to amalgamate all points marked by the detection algorithm into a smaller number of discrete pits. The largest signal

$(d/dx)[XBz]$ is tackled first. The associated XBz peak-trough pair separation is found, and an area around the pit center based on this separation is swept out. Any threshold breaking points inside this area are assumed to belong to the same pit. This procedure continues with the largest remaining threshold-breaking XBz derivative until all points are dealt with.

Diameter The diameter is calculated from the XBz peak-trough distance using an algorithm derived from past results compared to carbon steel model predictions (see Section 4.1.1.4).

Depth The depth is calculated by comparing the XBx trough amplitude with results based on previously obtained data (i.e., a parametric fit to carbon steel data - see Section 4.1.1.4). If the defect site was not inspected with the Bx coils, a zero depth is recorded.

Locating Defects in Carbon Steel

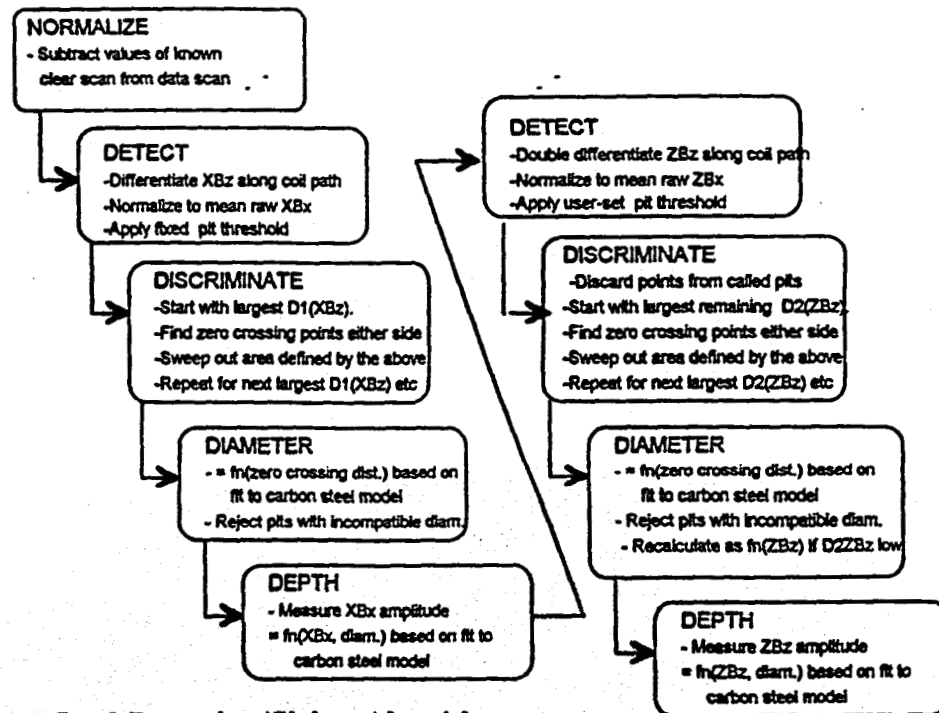


Figure 4-15: Carbon Steel Detection/Sizing Algorithm

Although ZBz is the most sensitive field component for pit detection in carbon steel, XBz data is investigated first because large pits are not discriminated very well in ZBz (i.e., ZBz was found to split large pits into two or more smaller pits as described in Section 4.1.1.4). The procedure is thus to detect larger pits first in a similar manner to that used for stainless

steel (but using a higher threshold), and then to go back over the ZBz data to find smaller pits missed in XBz.

The nine stages involved in the process are:

- Normalization** Designed to subtract the effects of non-uniformities in the background field inputs and coil sensitivity variations.
- Detection of large pits.** The normalized XBz data is filtered (by looking at the derivative along a coil path). All points breaking an internally fixed threshold are then marked and stored. The threshold is set to a value below that arising from a pit where the pit-splitting phenomenon would occur (i.e., about 3mm diameter).
- Discrimination of large pits** This is designed to amalgamate all points marked by the detection algorithm into a smaller number of discrete pits. The largest signal $(d/dx)[XBz]$ is tackled first. The associated XBz peak-trough pair separation is found, and an area around the pit center based on this separation is swept out. Any threshold breaking points inside this area are assumed to belong to the same pit. This procedure continues with the largest remaining threshold-breaking XBz derivative until all points are dealt with.
- Diameter of large pits.** The diameter is calculated from the XBz peak-trough distance using an algorithm derived from past results compared to carbon steel model predictions (see Section 4.1.1.4).
- Depth of large pits.** The depth is calculated by comparing the XBz trough amplitude with results based on previously obtained data (i.e., a parametric fit to carbon steel data - see Section 4.1.1.4).
- Detection of small pits.** The normalized ZBz data is filtered (by looking at the second derivative along a coil path). All points breaking a user-set threshold are then marked and stored. The threshold should be set close to the "noise" value. Setting a high value will result in no spurious calls giving a rapid response from the routine, but will miss small pits. Setting a low value will detect small pits but will also give rise to spurious calls thus slowing down the routine. The set of marked points is then reduced by dropping any points covered by the large pits found earlier.
- Discrimination of small pits** This is designed to amalgamate all points marked by the

detection algorithm into a smaller number of discrete pits. The largest remaining signal $(d^2/dx^2)[ZBz]$ is tackled first. The associated $(d/dx)[ZBz]$ peak-trough pair separation is found, and an area around the pit center based on this separation is swept out. Any threshold breaking points inside this area are assumed to belong to the same pit. This procedure continues with the next largest remaining threshold-breaking ZBz second derivative until all points are dealt with.

Diameter of small pits

The diameter is calculated from the $(d/dx)[ZBz]$ peak-trough distance using an algorithm derived from past results compared to carbon steel model predictions (see Section 4.1.1). The calculated diameter is compared to the value of the XBz peak-trough separation to reject some false calls. (The assumption is that any large diameter but shallow pit should also show up in XBz data). If the $(d^2/dx^2)[ZBz]$ value is below an internally fixed value (below the "noise" level), the diameter is recalculated from the amplitude of the raw ZBz data - the reason being that this is the most sensitive parameter to relate to for very small pits in carbon steel.

Depth of small pits

The depth is calculated by comparing the ZBz amplitude with results based on previously obtained data. If the pit is so small that the ZBz amplitude has been used to calculate the diameter, the depth is set to be equal to half the pit diameter.

Calculating Lift Off

Normalization

Designed to subtract the effects of non-uniformities in the background field inputs and coil sensitivity variations.

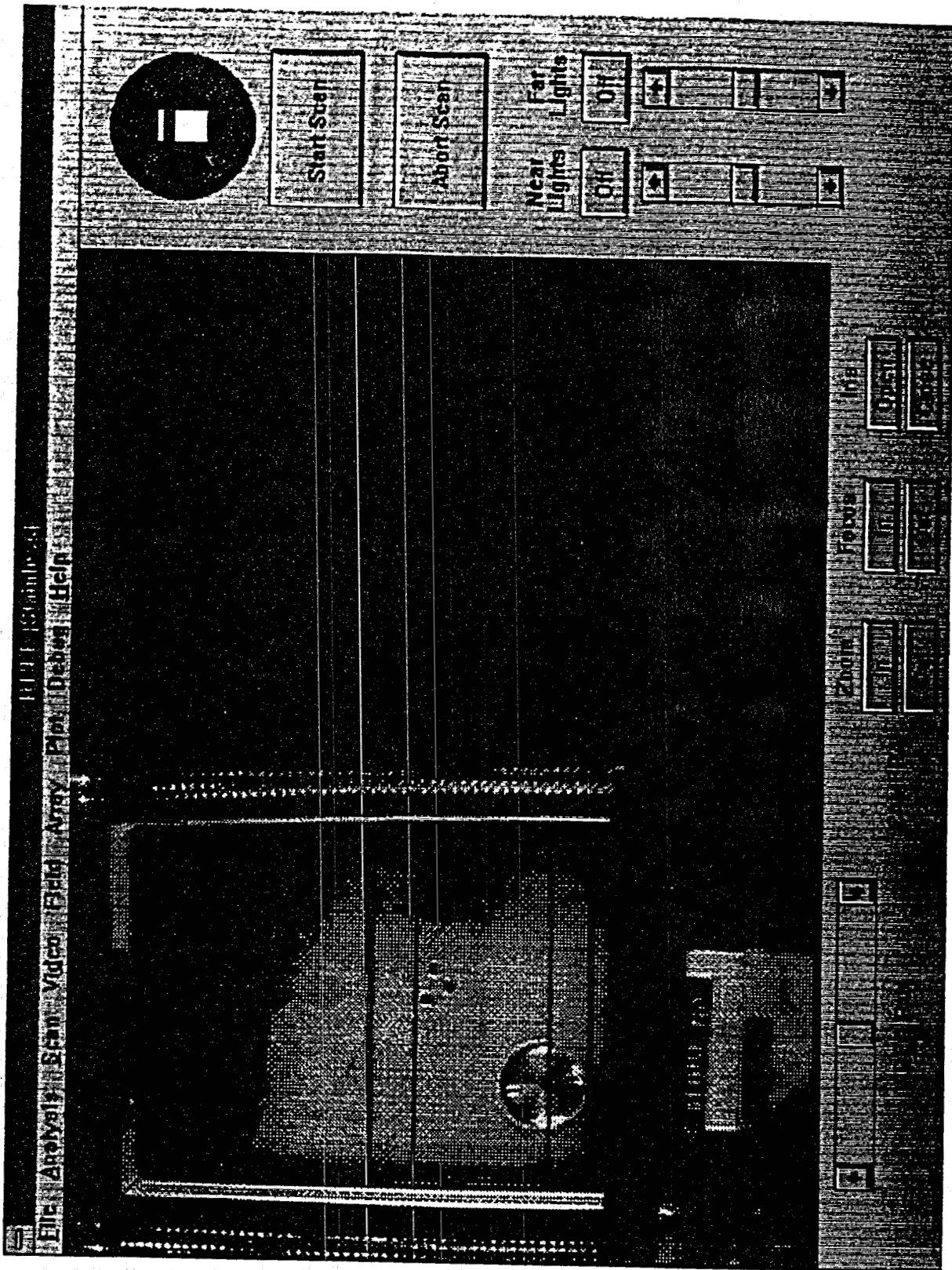
Measure Troughs

Scan XBx for troughs. All peaks are ignored. All deviations below the noise threshold is set to zero. The amplitude of the remaining troughs are then related to lift-off through an empirical factor derived from testing.

4.1.5.4 Graphical User Interface

The operator controls the end effector using a customized graphical user interface (GUI). Figure 4-16 shows the operator interface screen. Surrounding the video image are the mouse activated menus and functions. The movement of the sensor array can be initiated and halted by clicking the buttons marked Start, Scan, and Abort. The Save Scan button and the pull-

down menus allow the video image to be grabbed and saved to hard disk along with the scan data. These menus and additional buttons also control the analysis of the ACFM inspection data and the recording of the visual data to VHS. Several data display and analysis options are available from the menus including the detection and sizing algorithms. One menu option is to show the scan area boundary boxes which overlay the video (as shown in figure 4-16). The green box depicts the area that is scanned by at least one sensor coil and the red box depicts the area that is scanned by all four rows of sensor coils. The near and far light intensity is controlled by the sliders and buttons in the lower right corner of the screen. Controls for the camera lens zoom, focus, and iris are arranged below the inspection windows.



specified area;

- After the scan is complete, the operator is shown a representation of the magnetic fields. The operator may choose to perform analysis on the data to locate any pitting, or may choose to run analysis routines at a later time;
- Once analysis is complete, any pits found can be graphically displayed by selecting Pits under the Plot menu; and

4.4 Testing

Development testing for the Prototype RTIEE was performed at the OSS RTAIL facility. The testing included both bench testing of the complete end effector system as well as evaluation of the prototype system on the OI/GE manipulator. Figure 4-15 shows the RTIEE prototype on the OI/GE manipulator system .

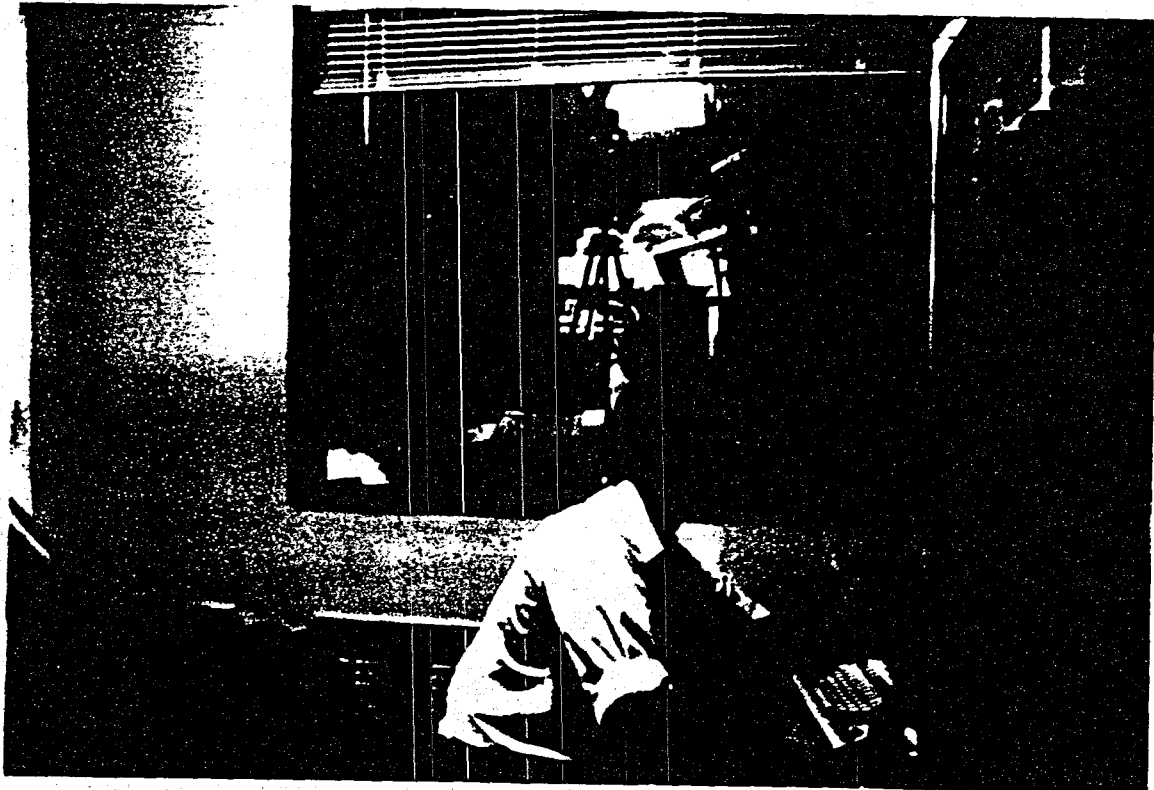


Figure 4-17: Prototype End Effector and Tank Wall Mockup

The RTAIL includes both an electrohydraulic, force reflecting manipulator system and a Puma Model 560 robot. The electrohydraulic system, an OI/GE ARM, was developed by Oceanering and General Electric for use deep underwater. It is, however, capable of

4.2 Safety

On power up, the RTIEE end effector enters a known static condition with the scanner in a disabled state. On software command, the scanning system is initiated, at which time it may be stopped either from software with an abort command or via an emergency stop switch on the console. The end effector does not produce any secondary waste during the inspection process nor does it generate any hazardous fields.

4.3 Operations

A key feature of the RTIEE is the dramatic reduction in the level of operator expertise required for a successful inspection. Inspection using the RTIEE does not require the operator to have any knowledge of ACFM theory, although detailed analysis of the results would require an understanding of both the theory and its implementation.

Nominal RTIEE operating scenario:

The RTIEE is operating on the end of the LDUA. The manipulator and end effector are in the tank searching the tank walls for areas of corrosion. The tank has been emptied.

Then :

- Using the RTIEE camera and lighting system the operator finds a discolored area on the tank wall that requires NDE inspection;
- The operator moves the end effector toward the tank wall using the manipulator and RTIEE camera and lighting system;
- As the RTIEE approaches the tank wall to within a foot, the operator zooms the camera to a wide angle view and switches on the near lights to view the status indicators;
- The operator continues to drive the RTIEE towards the wall until all end effector landing pads have contacted the wall. The operator will be notified by the status indicators on each of the landing pads when contact is made. Each compression strut contains 2 sensors to indicate 0.25" and 2" compression of the maximum 3" stroke. The operator should maneuver the end effector until all four struts indicate 0.25" to ensure a solid landing, but not exceed the 2" operational limit;.
- Once the RTIEE is properly positioned against the wall, the operator, after ensuring that all the scan parameters are set to cover the desired area at the desired resolution, initiates a scan by depressing the SCAN button on the screen using the mouse;
- The RTIEE will reposition the sensor carriage if necessary and proceed to scan the

emulating various telerobots and operating with a variety of master controllers through a modular, reconfigurable digital controller developed by OSS. It is used currently to emulate the LDUA developed by Spar Aerospace Ltd. and the Canadian Space Agency Special Purpose Dexterous Manipulator (SPDM) which is also developed by Spar. Both require the use of two 3 DOF hand controllers operating in Jacobian resolved rate control mode with programmable levels of autonomy.

Testing on the OI/GE manipulator included landing the end effector system on a section of simulated tank wall. The simulated waste tank wall consisted of several segments of an above ground steel tank assembled in the laboratory. Several different sample plates were manufactured at OSS and attached to the tank wall to provide known target defects for the end effector evaluation. During testing, the lab was darkened to simulate the lighting conditions within a waste storage tank and only the end effector lighting system was used to provide illumination for the operator.

5.0 Results and Discussion

5.1 Introduction

The development of the RTIEE system included four phases of testing. Initially, breadboard bench tests were performed on each of the breadboard subsystems. Following integration of the subsystems the complete breadboard end effector was evaluated by performing realistic tank wall inspection in the OSS laboratory. For these tests the end effector was deployed by the OI/GE manipulator. The prototype development also included subsystem bench tests and integrated end effector testing on the OI/GE manipulator. Test plans are included in the management report and the results of this testing are reported next, in sequence.

5.1.1 Performance of the ACFM Sensor Subsystem

The X and Z fields: ACFM relies on the imposition of current fields onto the surface of the material to be inspected. In the RTIEE system, the uniform field is induced in the X direction; the induced currents on the plate surface created by this field oscillate in the Y direction because current fields run perpendicular to magnetic fields. The second induced field is not necessarily uniform; this is the Z field. Currents induced by the Z magnetic field flow in a circular pattern, clockwise then counterclockwise.

Figure 5-1 shows the X and Z field generated by the RTIEE prototype on steel. Note the curvature of the fields. Ideally the X field, here sensed by the Bx coils, would be flat but in this case as long as the field is planer beneath the array it can be considered uniform. The Z field, here sensed by the Bz2 coils, is a much stronger field than the X and has a regular shape. The shapes seen in the fields are caused by the presence of conducting materials in the end effector frame. Although these disturbances can confuse analysis of the fields they are so consistent that normalization effectively removes the majority of their influence before analysis

Normalization: The variation in the magnetic field caused by the smaller pits is very small compared to the general field (generally less than 1%) so a normalization procedure is used to highlight the pit signal. Experimentation indicates that normalization of the whole scan area is the most effective method. This implies that a single complete scan of the 6" by 3" window on a known good plate is subtracted from all subsequent scans of similar material. As stated, this method has the additional advantage of removing all repeatable field variations caused by the presence of end effector structure around the array. A plate suitable for normalization would be made of the same grade of steel as the tank wall and be the same thickness, it would also be of a large enough area to prevent the plate edges disturbing the field produced by the end effector (currently this is about 14"x14"). Normalization can occur any time before an inspection and would probably occur as part of an end effector initial calibration exercise prior to operational use.

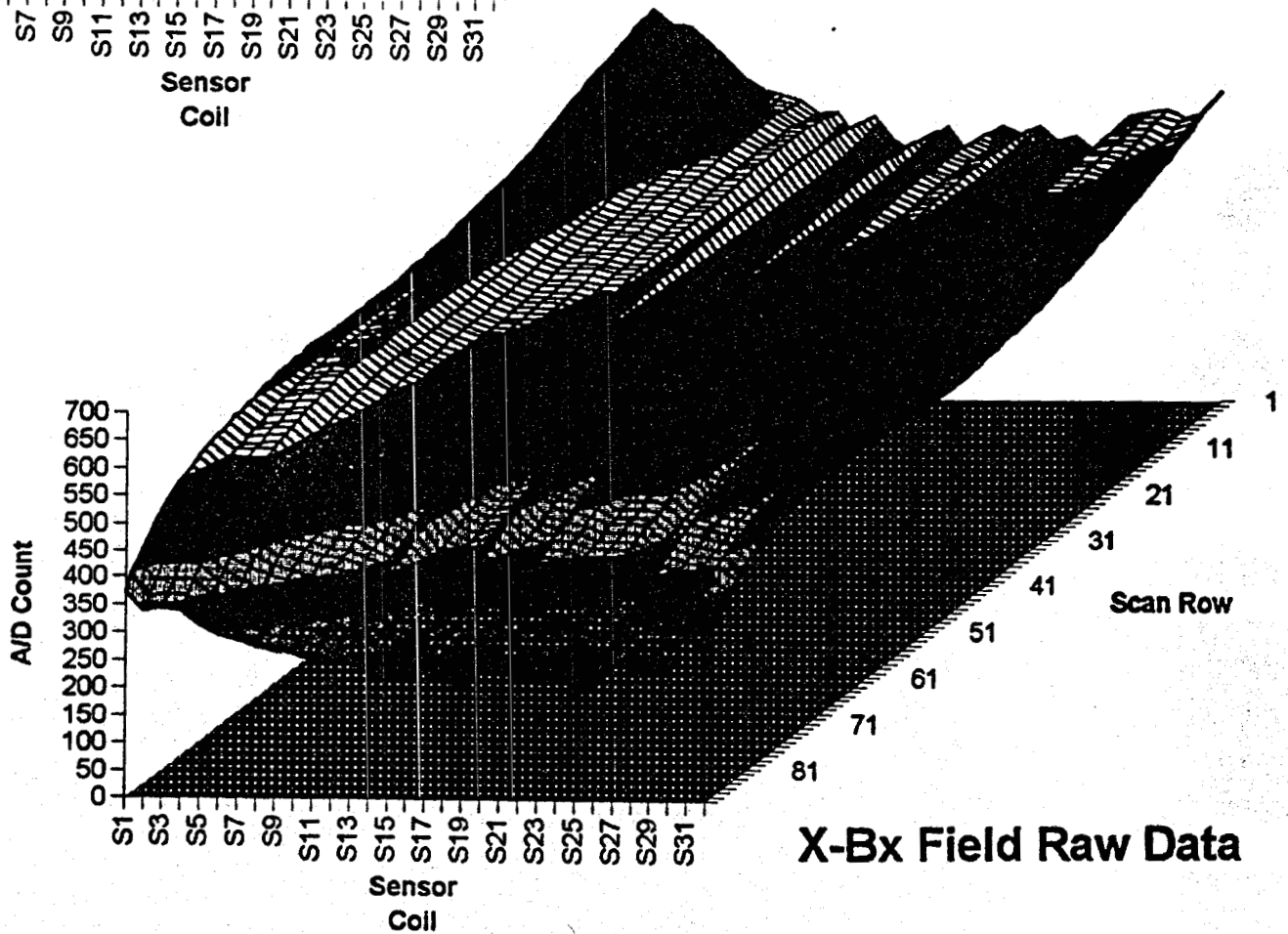
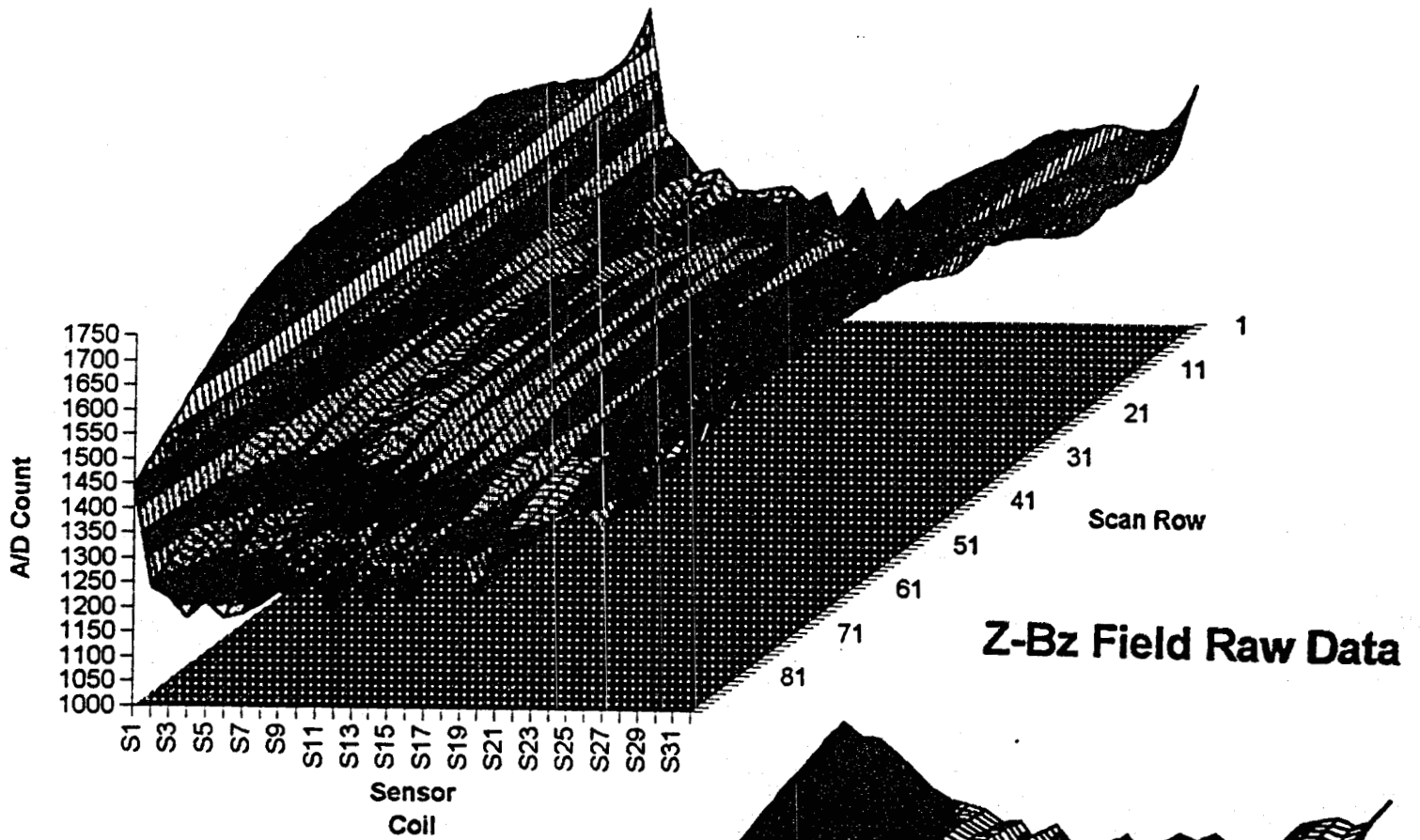


Figure 5-1: Stainless Steel Plate: Fields Sensed by Array Coils (no defects present)

Fields and Sensors: Figure 5-2 illustrates the main fields generated and used by the RTIEE system to detect and size pits in steel. In this figure, the field disturbance recorded by the RTIEE scanner over a .25" diameter, .125" deep hole (representing a pit, after normalization) is illustrated. These results clearly show both the usefulness of the theoretical model in identifying the dominant features of the field disturbance and the relative strength of the disturbances between the field/sensor combinations. For instance, even though the ZBz disturbance is not modelled (and hence not truly a theoretically predictable response) it is such a strong response that the RTIEE uses it to detect smaller pits in carbon steel. This is the classic eddy current response consisting of a peak (or trough) centered over the defect. Having detected a peak (using derivatives of ZBz or XBz) and established its location, the X field/sensor combinations can be examined in the same area to locate their dominant features. If the right features are located (peak/trough pair for XBz and a tipped depression for XBx) then confidence in the presence of a defect increases and the size and position of the dominant features can be used to size the defect. Sizing is based on the analytical model for a hemispherical pit in carbon steel. Although a hemispherical aspect (i.e. having a depth of about the same size as the diameter) is a good assumption for real corrosion pitting, none of the pits sized by the RTIEE algorithms are assumed to be hemispherical. The hemispherical model is used as the basis of the sizing with specific empirical relationships developed from it, where needed, for the sizing of pits in stainless and carbon steel. The model greatly reduces the cost of developing an inspection tool by reducing the number of test plates required to calibrate the system prior to its operational use.

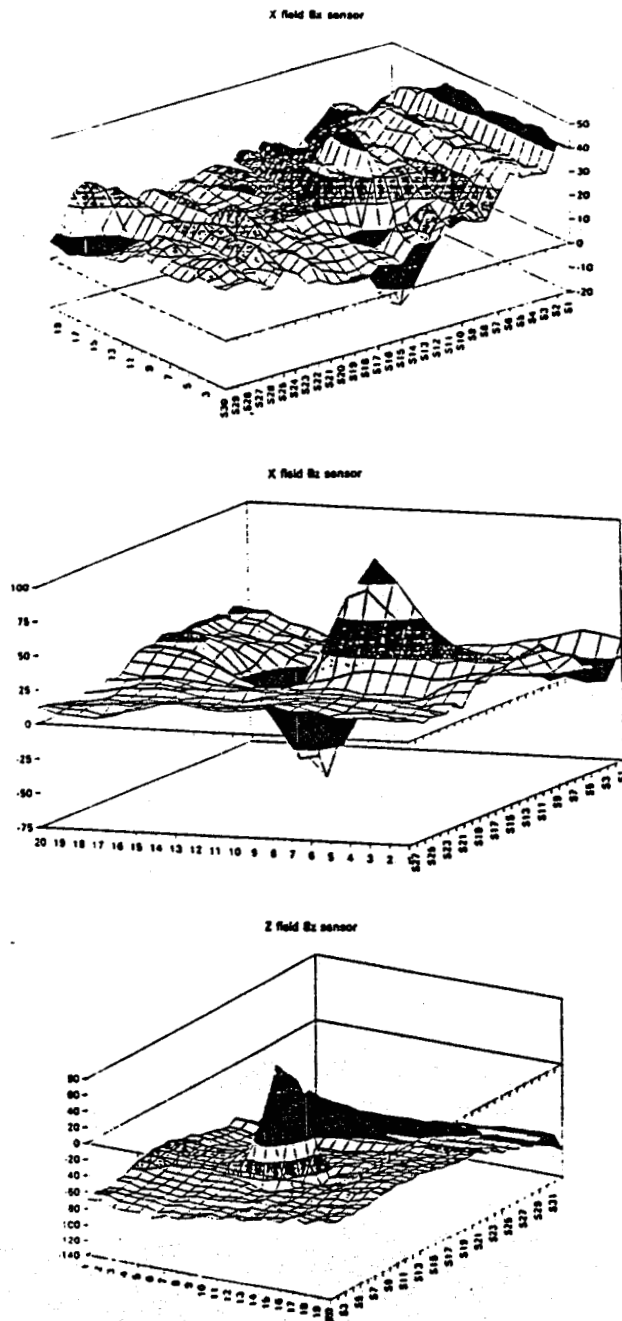


Figure 5-2: Magnetic Fields Measured over 0.25" Pit

5.1.1.1 Pit Detection

The first priority in characterizing a defect is to detect and locate it within the inspected area. The detection algorithms have the difficult task of efficiently identifying the very small disturbance caused by the smallest pits in a background magnetic field with large variation. Figure 5-3 illustrates early experimental data recorded by the breadboard system over a

Figure 5-4 shows the perturbation of the magnetic field sensed by seven Bz3 coils in the same field shown in figure 5-3. The array has performed 200 scans over a 4" length to cover the grid. A pit will produce a single trough in this particular field/sensor combination. The variation of the background field strength, even after normalization (i.e., the subtraction of a field recorded over a clear plate), is clearly evident. The pattern and actual pit sizes are shown in figure 5-5. A single differentiation of the data produces figure 5-6 ; suddenly the larger pits are clearly visible (the troughs become peak/trough pairs after differentiation). A second differentiation indicates the presence of the smallest pit, which is better shown in the plan view of the second differential data figure 5-8. The second differentiation turns the peak/troughs into double trough-peaks (figure 5.9). Figure 5-8 fuses and thresholds the data from each row to produce an image that can be simply thresholded again to detect and locate 100% of the pits. This image also indicates that at this particular detection threshold there are some false indications, confusing the result. Ideally, detection thresholds are selected that detect the minimum pit without any spurious indications. A slightly larger minimum target pit would also reduce spurious indications.

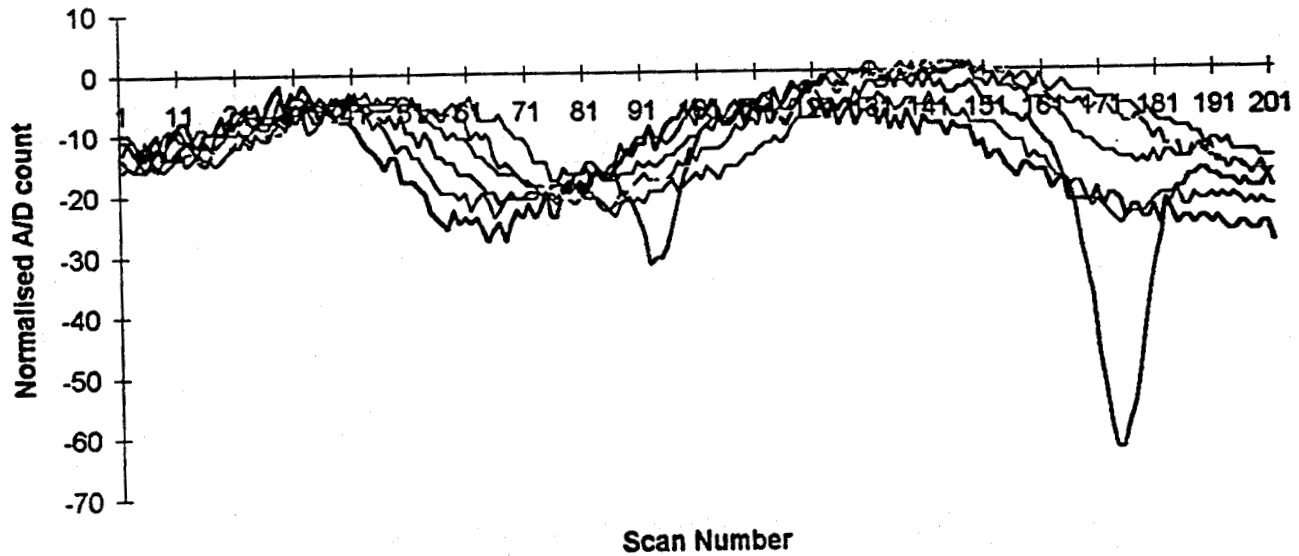


Figure 5-4: Data Collected by Coils Passing Over a Row of Pits

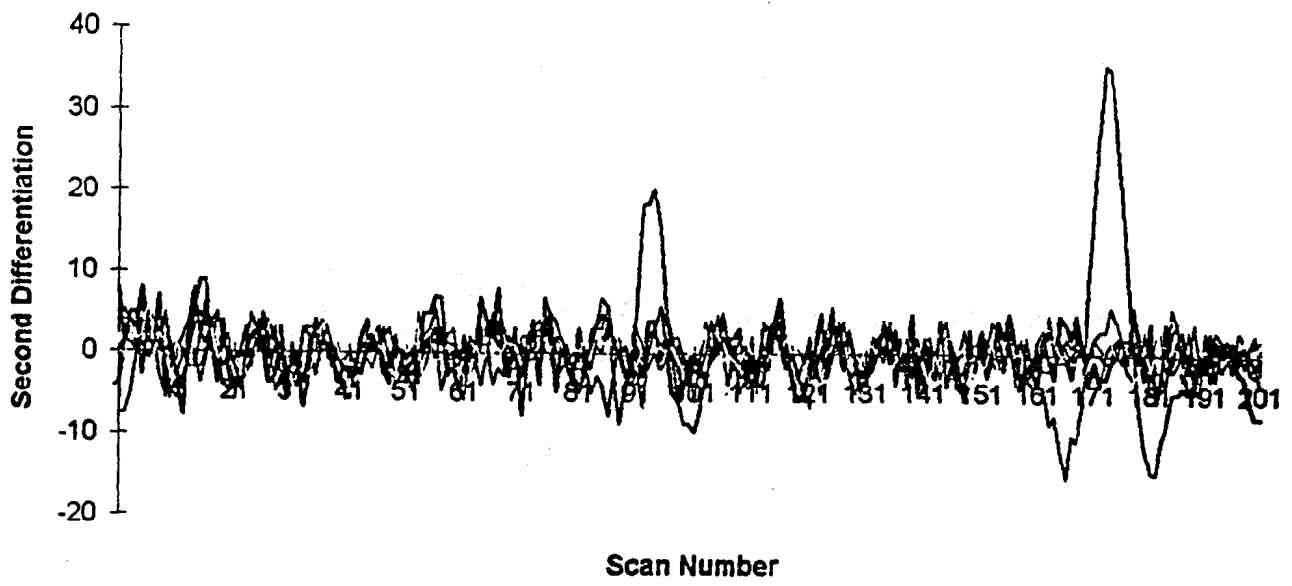


Figure 5-7: Second Derivative of Collected Data

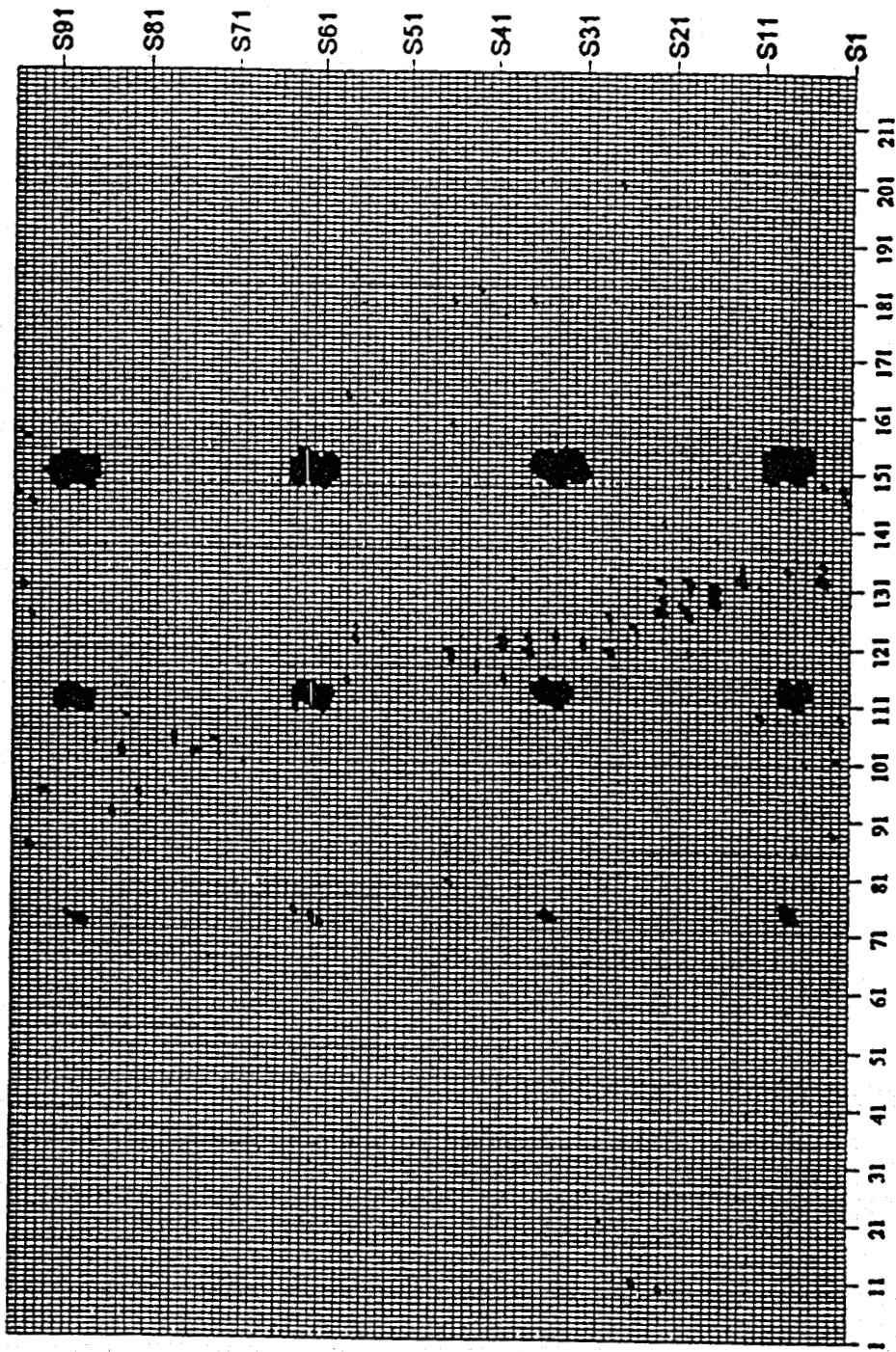


Figure 5-8: Thresholded Plan View of Second Derivative

5.1.1.2 Pit Sizing (Hemispherical Pits)

The following graphs (Figure 5-9) show experimental results for hemispherical pits in carbon steel, compared to the model predictions shown in Section 4. As can be seen the agreement is good for Bx. For Bz there is more of a discrepancy, especially for small pits. This is thought to be due to the poor resolution of the theoretical data, leading to errors in the numerical integration process used for predicting results for a finite coil.

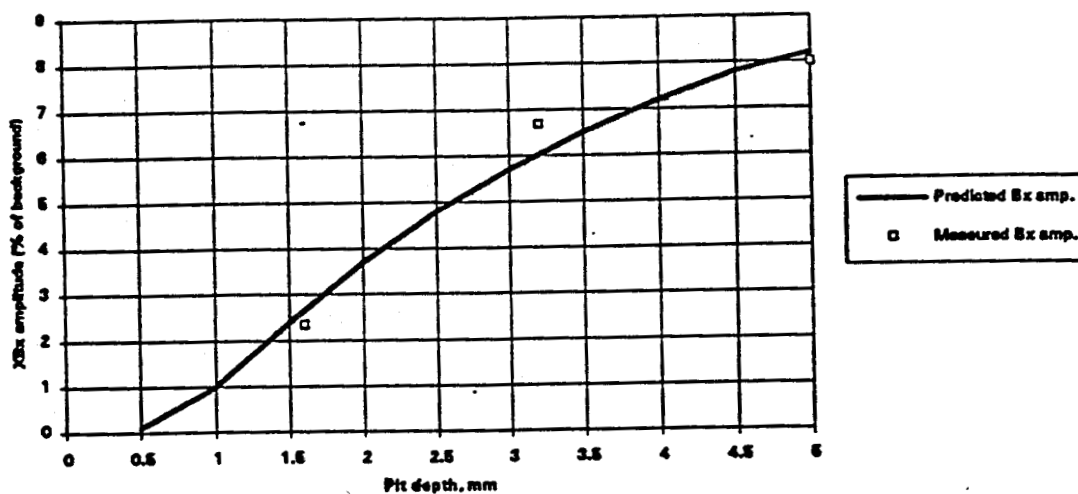


Figure 5-9A: Comparison of Measured XBx Amplitude with Prediction for Depth of Hemispherical Pits in Carbon Steel at .040" Lift Off

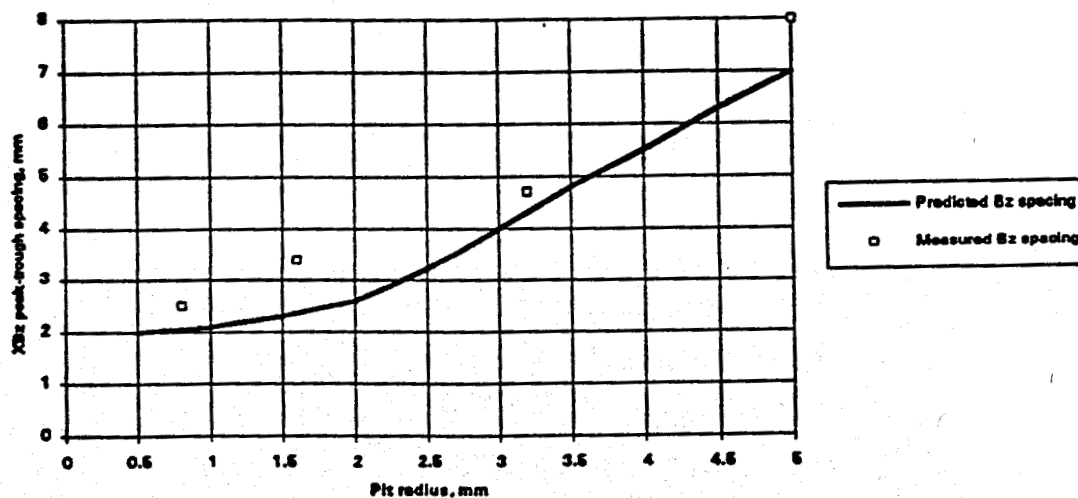


Figure 5-9B: Comparison of Measured XBz Peak Trough Spacing with Prediction for Diameter of Hemispherical Pits in Carbon Steel at .040" Lift Off

For stainless steel there is a discrepancy between measured values and the predictions of the carbon steel model, as would be expected. For example figure 5-10 illustrates stainless steel

hemispherical pit depth estimation. For the particular case of the depth of hemispherical pits the discrepancy can be eliminated by simply applying a constant factor to the measurements as shown. The diameter of hemispherical pits in stainless steel are derived in a similar way.

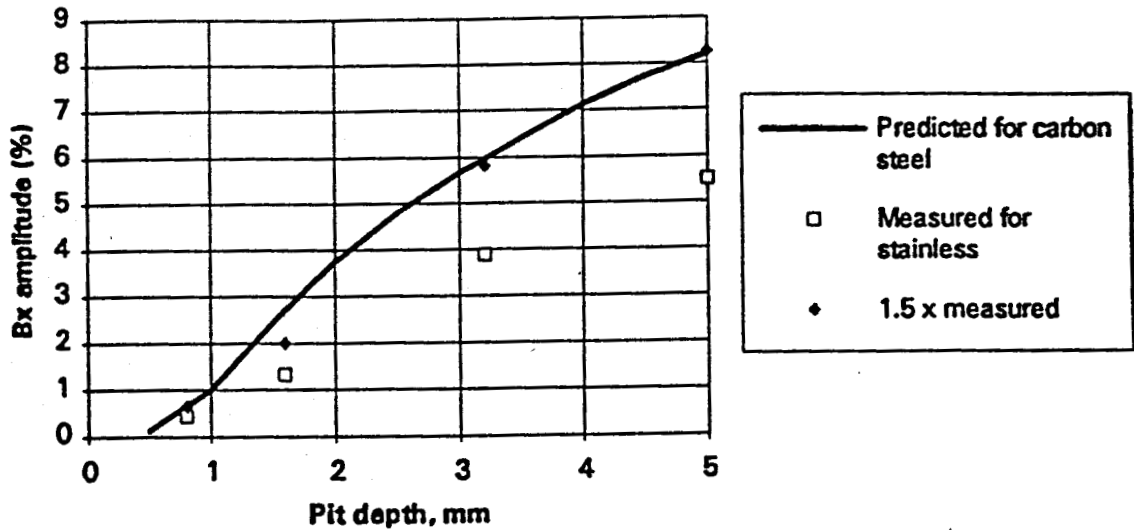


Figure 5-10: XBx Amplitudes vs Pit Depth for Hemispherical Pits in Stainless Steel

5.1.1.3 Pit Sizing (Non Hemispherical Pits)

For pits that cannot be assumed to be hemispherical, more complex correction factors are required to size in stainless and carbon steel. However the diameter of non-hemispherical carbon steel pits can still be directly derived from the model because of the very strong correlation between XBz peak-trough separation and pit diameter. In stainless steel the XBz peak-trough distance is generally larger than the pit diameter for, in contrast to carbon steel where the opposite is true. Figure 5-11 shows measurements made on a selection of pits of different widths and depths in stainless steel.

Measured XBz width v. pit width for stainless steel

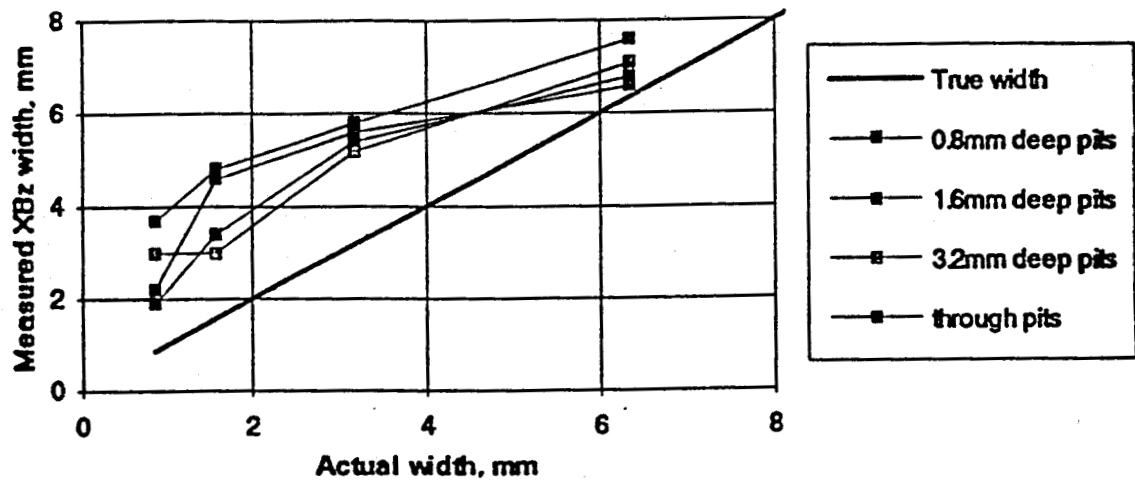


Figure 5-11: Measured XBz Width vs Pit Width for Stainless Steel

It was found that the stainless steel pit diameter (or width) can be estimated by multiplying PT (the XBz peak trough separation) by the correction factor $(1 - \exp[-(PT-2)/3])$. The diameters calculated in this way agree quite well with true pit diameters as shown in figure 5-12. There is still some scatter about the 1:1 line, however, and it may be possible with more data to improve this using a further correction factor based on calculated pit depth.

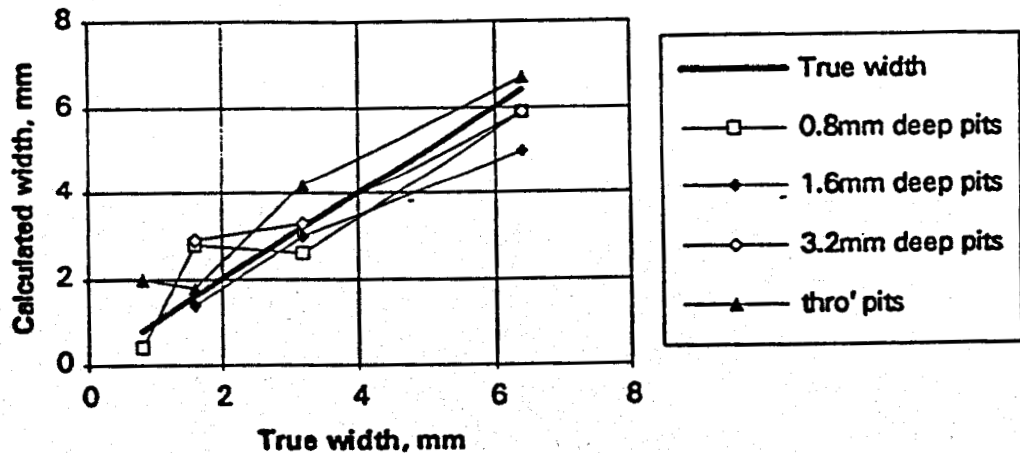


Figure 5-12: Corrected Width Estimation on Stainless Steel

The measurement of non hemispherical pit depth is more complicated for both materials because the algorithm involves both the XBx amplitude and the pit diameter calculated

earlier. It was found that pit aspect ratio (i.e. depth divided by radius) showed better correlation with XBx amplitude than pit depth alone. Plotting the measurements of XBx amplitude versus pit aspect ratio (see figure 5-13) it can be seen that the points for a given pit diameter can be fitted quite well to a straight line passing through the origin. The main deviation from a straight line is for the narrow deep pits where it is known that there will not be much increase in XBx amplitude with depth. The measurements were thus fitted using a function of the form

$$\text{depth} = \text{XBx amplitude} \cdot \text{fn}(\text{pit diameter})$$

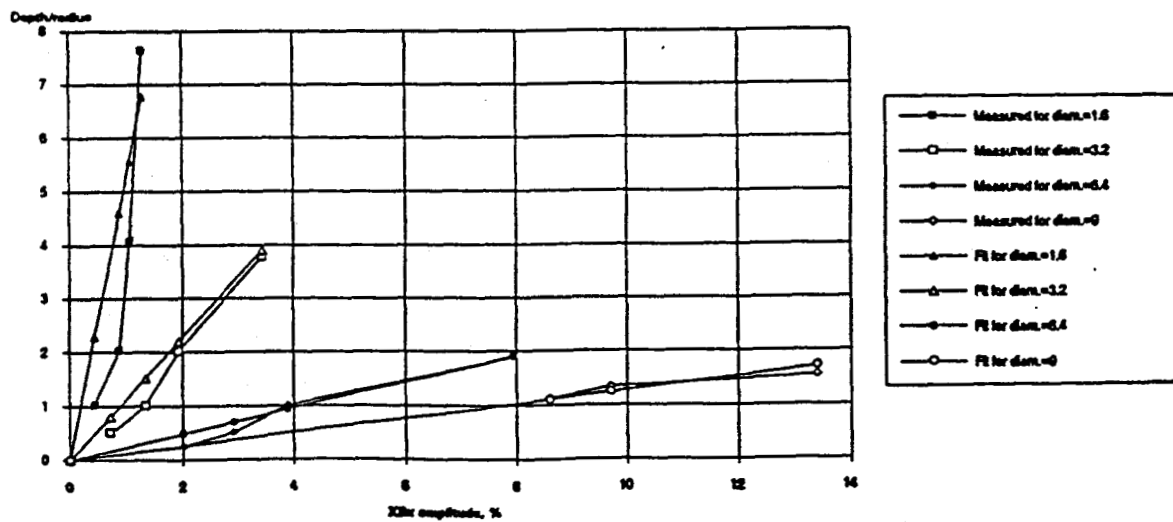


Figure 5-13: Parametric Fits to XBx Data Used for Pit Depth Sizing in Stainless Steel

A quadratic function of pit diameter (i.e. with three parameters to be determined) was used, also shown in Figure 5-13. This results in fairly accurate estimation of pit depth, but it may be possible to improve the accuracy with a more complex fit as more data is collected. If pit depth is improved it may also be worth while to go back and improve the pit diameter estimation using a correction factor based on pit depth (and thus to iterate around the two). The non hemispherical pit depth in carbon steel is estimated in a similar way.

Sensor lift-off affects the measured signal strength to some degree, causing a reduction in amplitude, and thus leading to an underestimation in depth estimation if not taken into account. This signal reduction is quite severe for Z-field data, and is greater for Bz than Bx. The reduction is least severe for the XBx data used to calculate pit depth. Pit depth is

corrected for the effect of lift-off by multiplying by an exponential function incorporating a user-entered value of lift-off. The effect of lift-off on Bz signal spacing (and hence on the estimation of pit diameter) is sufficiently small to be ignored.

Experimental Results for the Inspection of Stainless Steel

Inspection of stainless steel uses the XBx and XBz fields to detect and size defects. Figure 5-14 illustrates the screen the operator sees following an inspection of a grid of pits with the XBx fields showing. The depressions in the field over the larger pits are clearly seen. This image can be compared to the XBz field for the same inspection that has peak trough pairs over the pits (figure 5-15). Figure 5-16 illustrates the detection and sizing display. The image consists of the detection and sizing display next to a video image of the inspected area. The location, diameter and depth of each pit detected is listed in the small window. The pit location is recorded in cartesian co-ordinates relative to the end-effector coordinate system: the upper left corner of the scanning frame corresponds to the origin (0,0). As these images attest the location algorithm accurately locates the pits, typically within one pit radius of the actual position. Two diameters are shown (horizontal and vertical) to allow the representation of oval features, and the depth measurement is followed by a confidence level that is based on the feature being recognized in two field/sensor combinations (95%) and in only one (35%). The effect of changing the detection threshold is shown in Figure 5-17. If the detection threshold is set low enough to find even the shallowest .030" pits some spurious indications occur. If the threshold is set slightly higher, only genuine pits are detected and sized (as in Figure 5-16).

Pit DIA=034'	Pit DIA=062'	Pit DIA=125'	Pit DIA=250'	
+	+	+	⊕	Pit DEPTH=thru
+	+	+	⊕	Pit DEPTH=125'
+	+	+	⊕	Pit DEPTH=062'
+	+	+	⊕	Pit DEPTH=031'
			⊕	
			⊕	

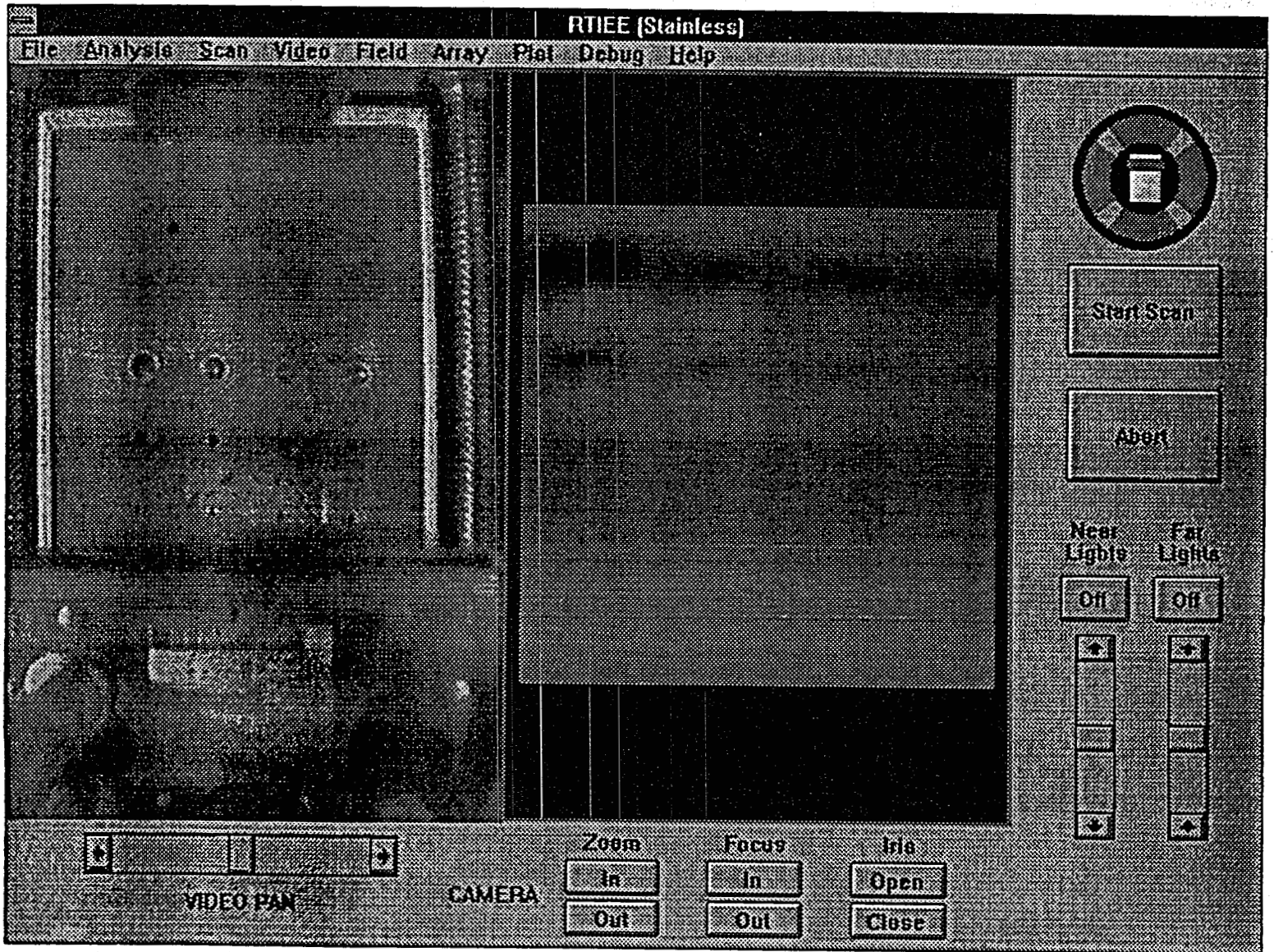


Figure 5-14: Screen Shot of Stainless Steel Inspection -XBx

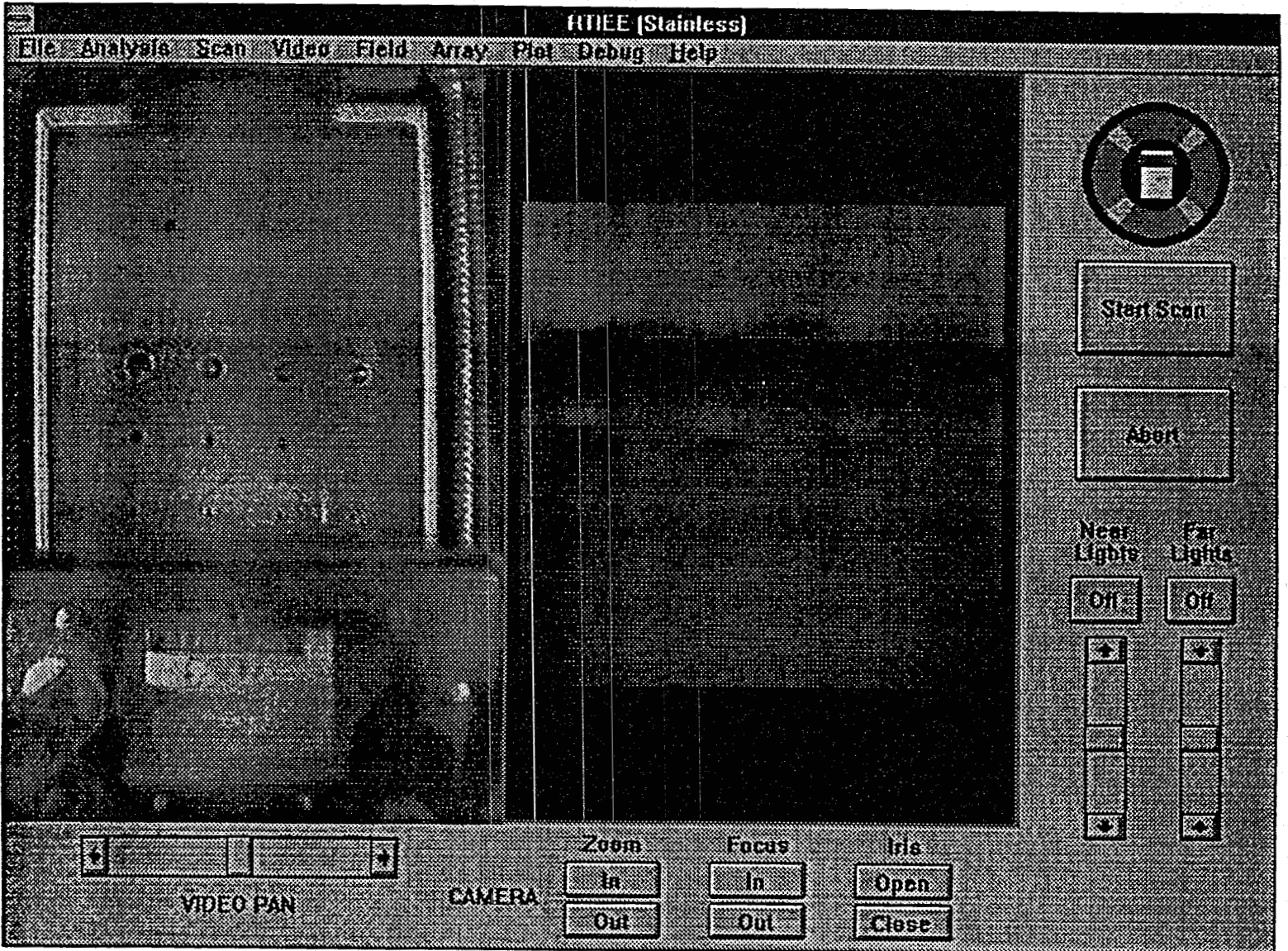


Figure 5-15: Screen Shot of Stainless Steel Inspection - XBz

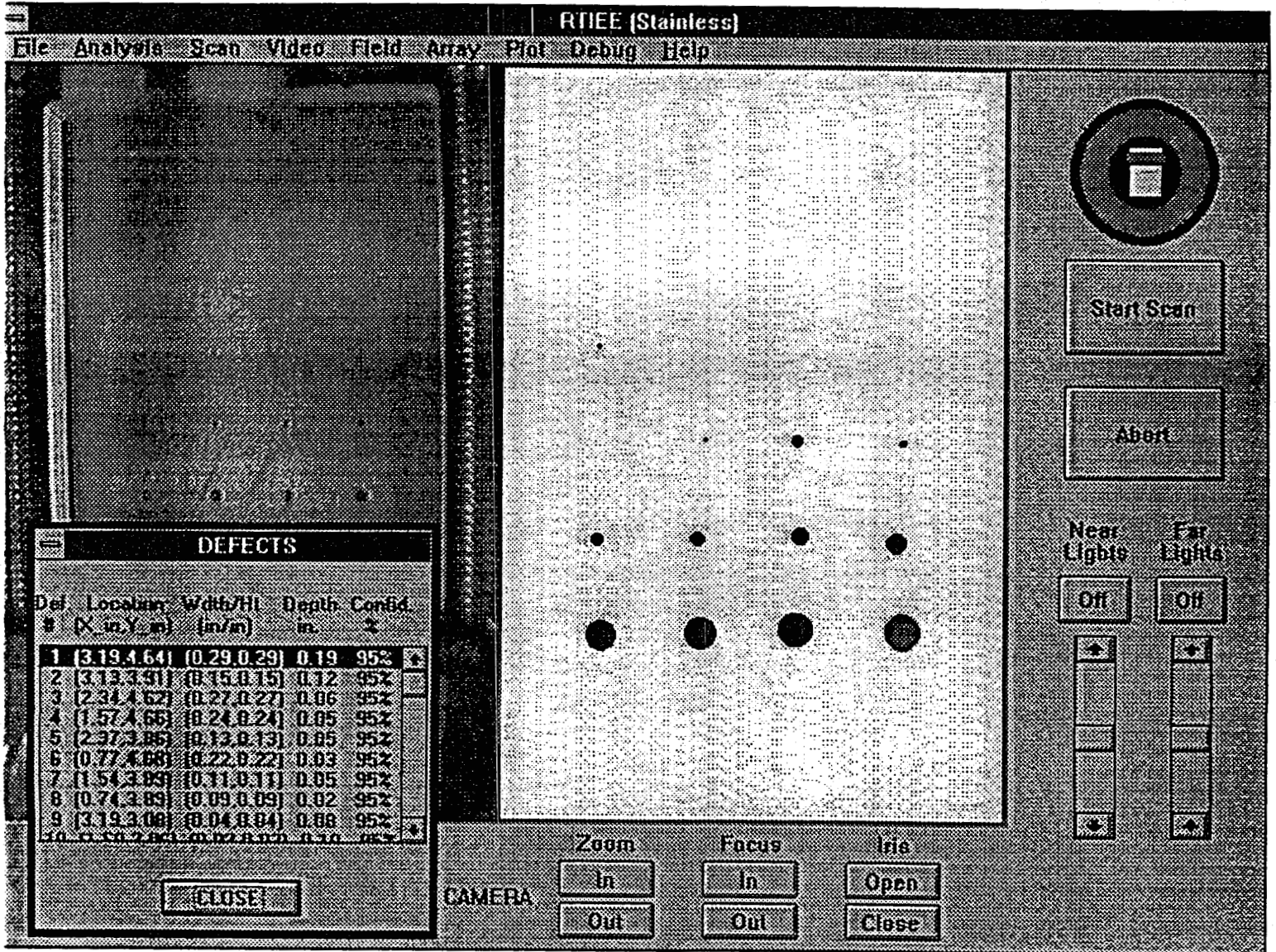


Figure 5-16: Screen Shot of Detection and Sizing Display

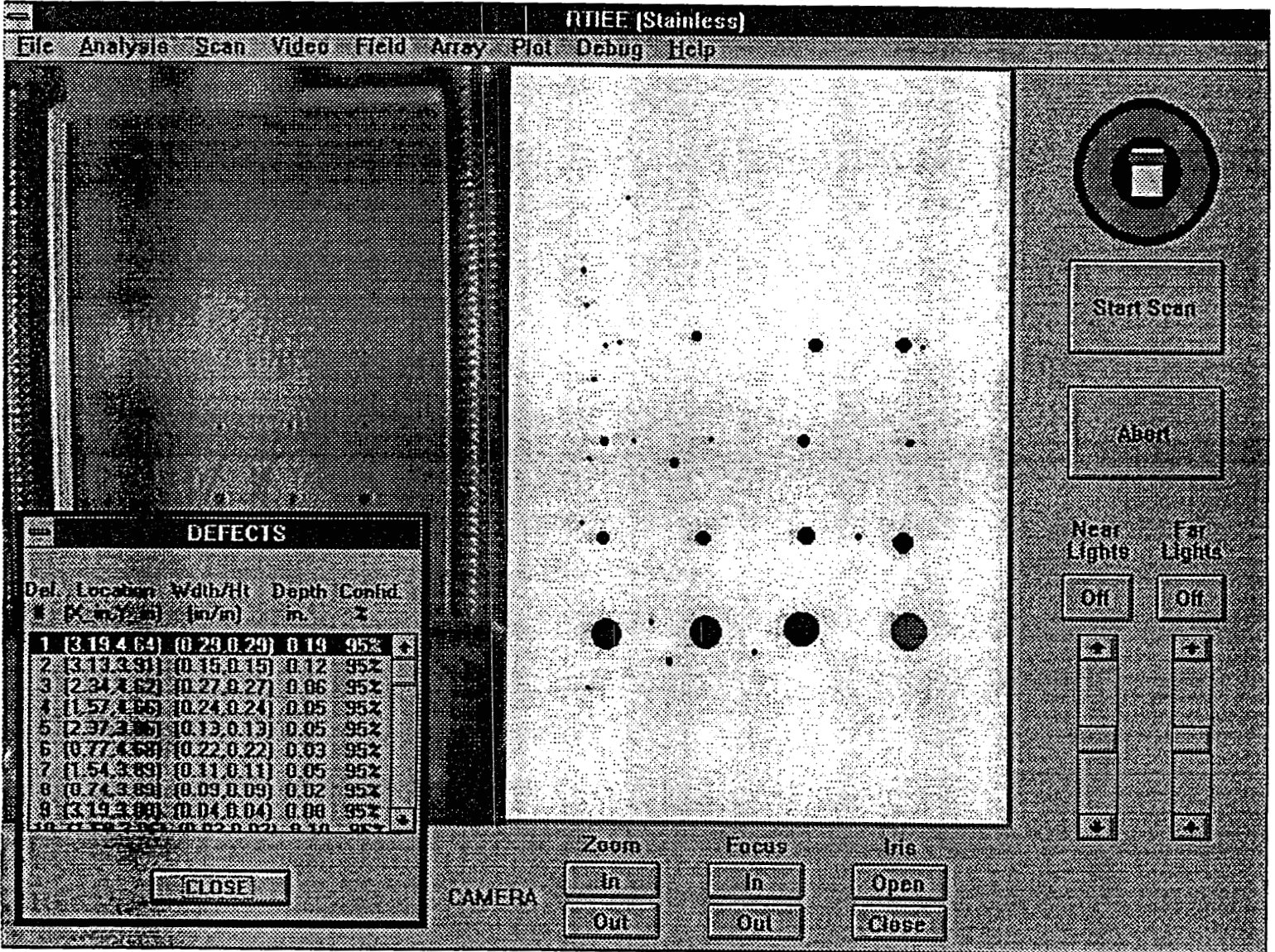


Figure 5-17: Screen Shot of Detection and Sizing Display

The stainless steel pit diameter estimation algorithms perform well, as shown in figure 5-18. Even though the depth of the pits inspected varied from 12% to 100% of the wall thickness the diameters were typically estimated to within 20% of the actual. If all pits were considered hemispherical then the depth of the features would be as accurately estimated. The depth sizing algorithms, however, attempt to estimate the depth from data in the inspections fields, as described above. On the larger pits the algorithms are reasonably accurate until the depth of the pit becomes excessive, at which point the current flow at the bottom of the feature is minimal or non-existent. Figure 5-19 illustrates this point with results from 1/4" pits and holes. The deeper holes are underestimated but as the holes become shallower the depth estimate becomes more accurate.

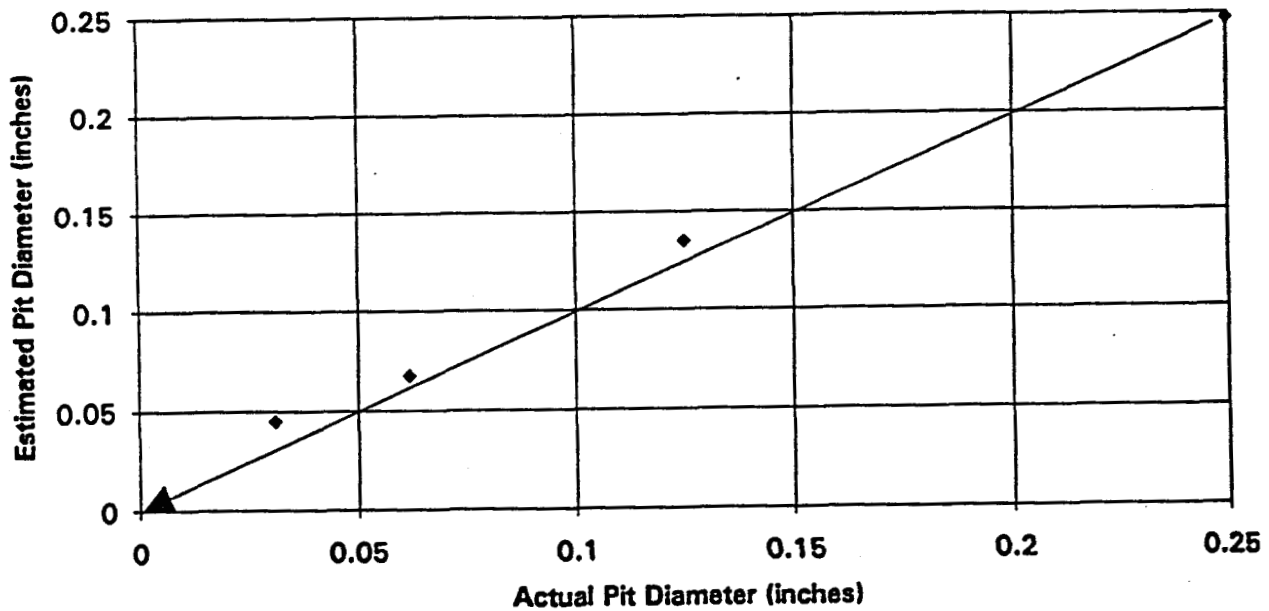


Figure 5-18: Stainless Steel Pit Diameter Estimation (average over multiple depths)

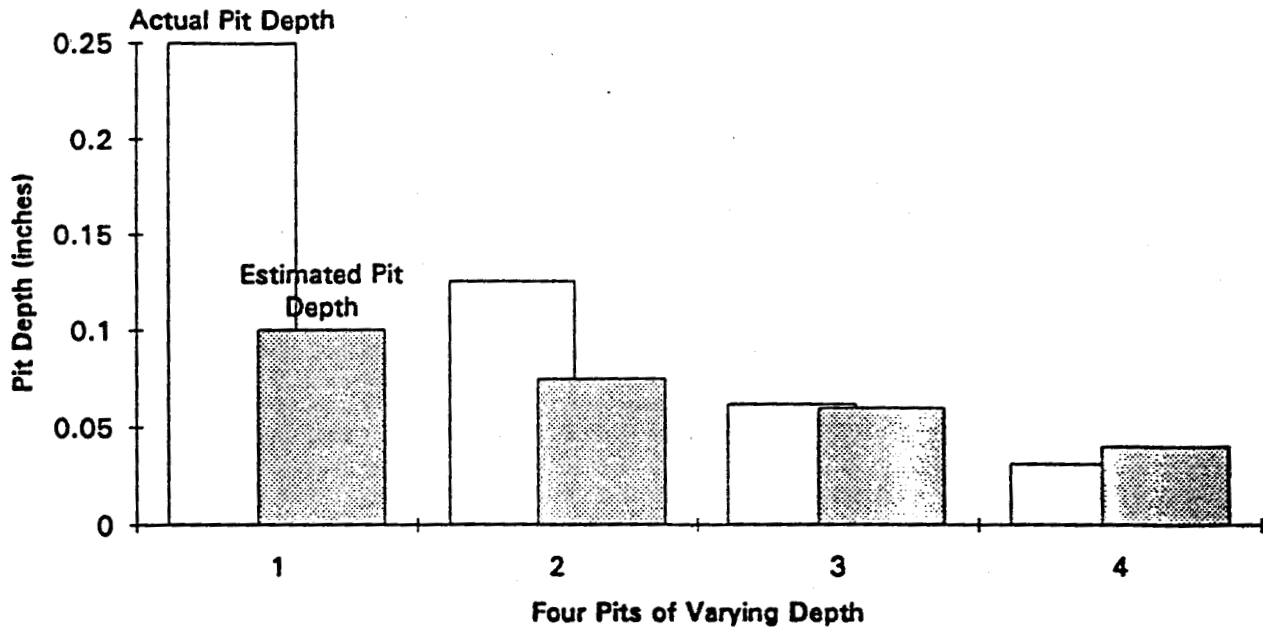


Figure 5-19: Stainless Steel Pit Depth Estimate (.25" diameter)

Experimental Results for the Inspection of Carbon Steel

Three fields are used to detect and size pits in carbon steel, XBx, XBz and ZBz. Figure 5-20 shows the results of an inspection of a grid of pits in carbon steel with the image of the ZBz field selected. As described above the ZBz field gives a strong indication of the presence of pits, in this image the .062" diameter pits are clearly seen in the normalized data. The carbon steel algorithms locate the pits with good accuracy, typically within less than the radius of the pit. Pit diameter is accurately estimated typically within 20% of actual (see figure 5-21). Pit depth is difficult to estimate in the deeper holes, more so than in stainless steel because of the thinner skin depth of AC current in carbon steel (about .005"). This lack of sensitivity of the carbon algorithms to depth is illustrated in figure 5-22. In this figure deep holes are underestimated and shallow ones over estimated.

Pit Grid in
Carbon Steel

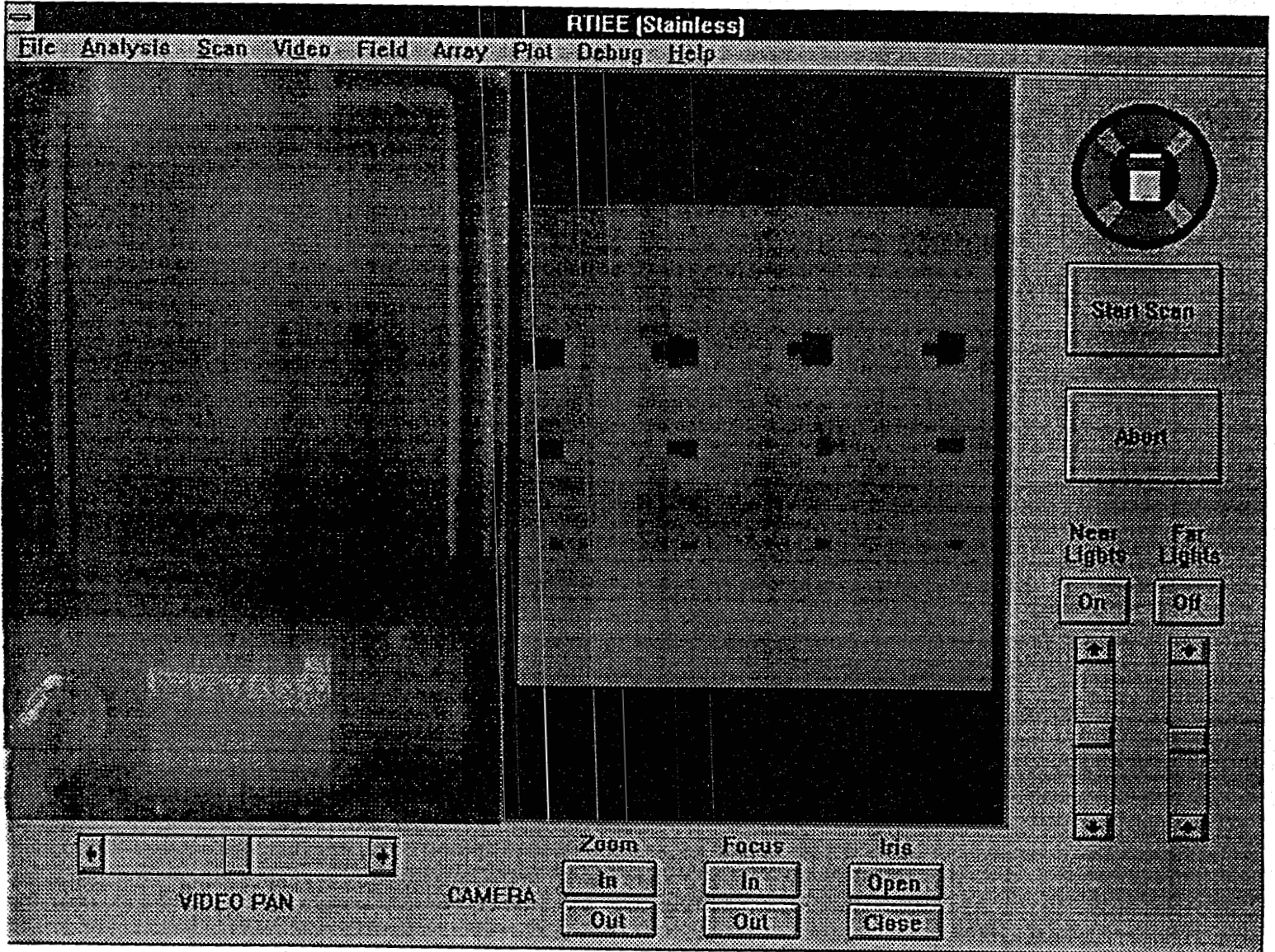
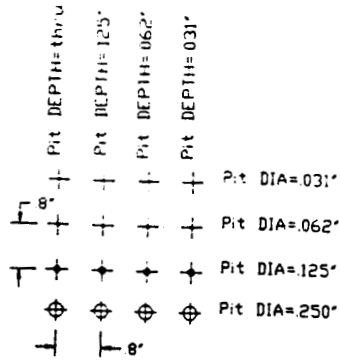


Figure 5-20: Screen Shot of Carbon Steel Inspection -ZBz

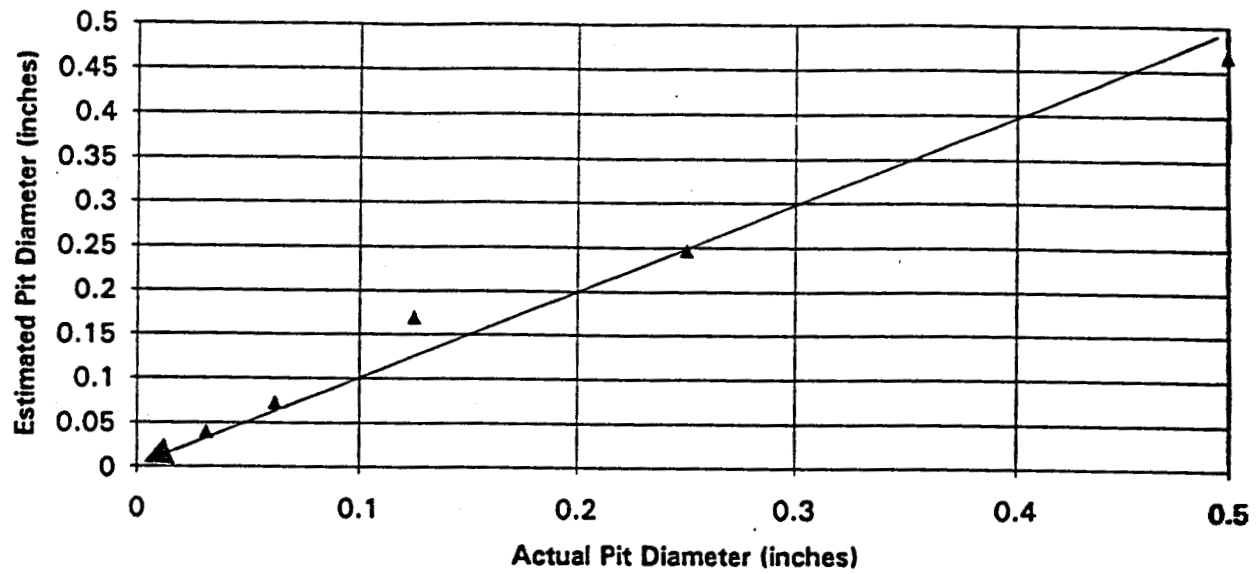


Figure 5-21: Carbon Steel Pit Diameter Estimation (average over multiple depths)

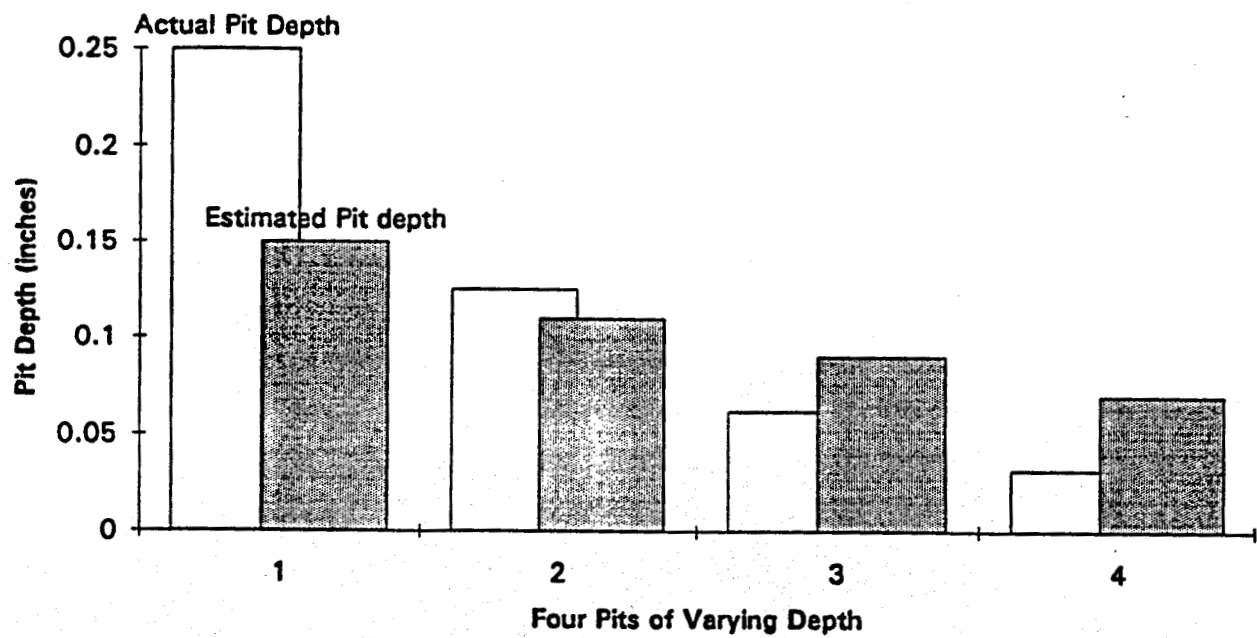


Figure 5-22: Carbon Steel Pit Depth Estimate (.5" diameter)

5.1.2 Mechanical Subsystem

The mechanical design is composed of the 4 general areas including main end effector structure, internal component support structure, compliant scanner frame, and scanner system.

The main structural design proved very successful in providing a rigid housing for the end effector as well as providing a significant level of protection for the internal components. The structure showed no degradation of any kind after repeated deployment on the OI/GE manipulator. The cylindrical stainless steel shell significantly enhanced the strength of the main body as well as providing easy access to the internal components from all directions when removed.

The internal structure was easily reconfigured to accommodate relocation and adjustment of internal components such as the camera and electronics. The internal structure also proved to be an effective heat sink for transferring heat from the internal electronic systems to the outer shell and atmosphere. The internal mounting component structure also aided in increasing the overall rigidity and impact resistance of the end effector body. The quartz lamps for the near lighting system, which were mounted inside the end effector shell on the breadboard unit, were moved to the backside of the scanner frame structure in the prototype system. Not only did this improve the near lighting quality, but also reduced the amount of heat generated within the end effector shell.

Wall pitch/yaw compliance was accomplished successfully by the use of the compression strut system. The scanner head was shown to comply up to 15 degrees in any combination of pitch or yaw with the application of only minimal force on the end effector. Further scanner head deflection caused all compression rods to begin to compress until full stroke is reached. The two optical position sensors mounted inside each compression rod served both to indicate initial compression ($>0.25"$) of the individual strut as well as to show excessive compression of the strut ($>2.0"$) which indicated excessive force being applied by the manipulator system.

During testing of the end effector system, the sensor carriage system provided smooth accurate translation of the array head. The twin ACME drive screw arrangement provided sufficient force for scanning in any orientation, but would stall if the scanner head caught on an obstruction. During the course of testing the scanner system, it was found necessary to have an accurate, and simple means of setting the standoff between the array face and the surface being scanned. This was accomplished using two 0.5" travel micrometer heads. The body of the micrometer heads were rigidly attached to the scanner carriage, one on either side of the array, and the tips of the micrometer heads were fastened to the array probe. This arrangement allowed for quick and accurate adjustment of the array probe standoff distance.

5.1.3 The Vision Subsystem

The video system performed well on the prototype system. The camera/lens combination provided both a wide angle view that included the status indicators for landing the end effector as well as a narrower field of view which was useful for surveying objects at greater distances from the end effector. The lighting system also worked as planned to provide illumination for both operations.

Improvements to the near light design include removal of significant heat away from the electronics and greatly improved glare reduction. The glare reduction is accomplished by changing the light source from two single point elements near the axis of viewing and behind the camera lens to six point sources distributed roughly 45 degrees off the inspected surface and beyond the camera lens.

A portion of the vision system's functionality is to provide the operator with the ability to survey a tank wall at a distance of up to 37.5' and identify suspected areas of corrosion. In order to evaluate the prototype's vision system resolution at various distances, 4 operators were asked to locate dark patches on a stainless plate. Distances from the plate to the end effector ranged from 0' to 45' and the patches ranged from 1.0 in² down to 0.032 in². The results are provided in the following table.

Viewing Distance	Tape Patch Size (inches)					
	1.0x1.0	.50x.50	.25x.25	.125x.125	.062x.062	.032x.032
45'	100%	100%	100%	50%	NA	NA
30'	100%	100%	100%	100%	25%	NA
20'	100%	100%	100%	75%	25%	NA
10'	100%	100%	100%	100%	100%	75%
5'	100%	100%	100%	100%	100%	100%
0'	100%	NA	NA	NA	100%	100%

5.1.4 Electronics Subsystem

The electrical subsystem performed as expected in the prototype end effector. The power distribution system meets all of the needs of the ACFM electronics as well as the scanner and lighting systems. The separate regulation provided for the AC drive electronics and signal conditioning system minimized crosstalk between the systems and prevented noise problems during data acquisition.

The 19.2kbps serial line used on the prototype end effector has provided reliable communication with the ACFM system. At 19.2kbps, the communication time accounts for only a very small fraction of the time involved in performing scan and further increases in transmission rates would not significantly affect overall scan times. The communication link

which controls the scanner and relays all compression strut data also performed as expected.

The control electronics, both in the console and the end effector itself, perform as planned during testing. The ACFM electronics responded appropriately to all commands for sensor readings and provided the necessary data for the ACFM analysis to be performed. The scanner positioning system performed well during its evaluation and provided more than adequate positioning resolution. The quadrature encoder provided verification of the scanner position and readily detected any variation from the commanded position which might be induced by debris jamming the scanner.

5.1.5 Software Subsystem

The RTIEE Software version 1.5 has been released with the end effector [March 8, 1995]. All functions of the software required to operate the RTIEE are complete. The software has been continuously tested and debugged throughout the RTIEE development as a stand alone program. It has not been rigorously tested for a Windows multi-program environment and is not intended to run with other programs concurrently under Windows. Windows is not a real time/pre-emptive system. Therefore, in order to ensure that all error checking occurs within prescribed periods (< 0.5 s) no other time-consuming programs should be running concurrently with the RTIEE software on the host machine.

The RTIEE software is scarred for inclusion into a GISC environment. Major RTIEE functions such as camera and scan functions are accessible through the internal RTIEE messaging systems. The RS-232 port functions as a bridge between the GISC environment and the RTIEE. Message commands are relayed from GISC through the RS-232 into the RTIEE message queue. Inclusion of the RTIEE into the GISC environment is contingent on the supervising GISC component containing the proper drivers necessary to command the RTIEE. Actual inclusion of the RTIEE into a GISC environment during testing was out of the scope of this project phase.

The graphical user interface using Windows provided a useful interface that will be familiar to most people who have used standard windowing software. Operators can navigate through the tools using the mouse, on screen buttons, and menus. Additional information needed by the software such as scan parameters are requested through dialog boxes. No arcane keystrokes or commands are necessary to operate the system. Utilization of the software is described in the RTIEE Owners Manual.

6.0 Conclusions

The RTIEE provides a single unit solution for visual and NDE tank inspections performed by robotic systems. It successfully incorporates a vision subsystem, lighting subsystem, fine positioning subsystem, ACFM NDE technology, and data analysis software into one integrated system. The RTIEE system has been successfully demonstrated in a series of manipulator tests using a laboratory waste tank wall mockup. During laboratory tests, operators used the RTIEE to visually identify an area of potential corrosion attack and then perform a detailed and quantifiable electro-magnetic inspection of that area with the compliant scanner frame in contact with the tank wall. The ACFM sensor and defect characterization software has proved capable of detecting and sizing pits on stainless and carbon steels to a minimum diameter of 0.030".

ACFM provides several advantages over other NDE technologies such as eddy current, ultrasonics, and X-ray:

- ACFM does not require contact with the inspection material.
- ACFM does not leave any waste products after an inspection (e.g., coupling fluid).
- ACFM uses theoretical models and therefore does not require the use of calibration blocks prior to an inspection.

The end effector has been designed for deployment by light duty manipulators such as the Schilling Titan and the DOE LDUA, and features an easy to decontaminate round stainless steel outer shell, limit switches to report overcompression of the scanner frame, and GISC compatible software to permit control by a supervisory computer.

Several DOE facilities (Idaho National Engineering Laboratory, Hanford, and Oak Ridge National Laboratory) have expressed an interest in the capability of an end effector similar to or derived from the Robotic Tank Inspection End Effector for use in quantifying corrosion damage or cracking in the steel walls of the underground waste storage tanks.

Future Work

This project has resulted in a fully functional prototype ACFM tank wall inspection end effector. This system has been evaluated on a limited number of artificially pitted sample plates. Realistically corroded tank wall plates in both stainless and carbon steel are very difficult to come by and expensive to produce. A natural development of this project would therefore be more extensive testing of the end effector, both as a pitting corrosion sensor and as a robotic tool. More realistic sample plates could be procured and used to refine both the

operational aspects of the end effector and the pit detection and sizing algorithms that quantify the inspection. This test series could form the basis of certification trials for a field deployable "tank ready" end effector.

This project developed automatic pit detection and sizing algorithms that reduced the workload of a tank wall inspector. Since a computer is not as efficient as a human operator at analyzing complex patterns in inspection data, this automation carries the possible cost of a reduction in overall accuracy. The inspection data interface could be reworked to allow a human operator to detect and size the pits manually, which would eliminate this source of inaccuracy. This effort could be combined with improvements in the methods of displaying the magnetic fields and the video data, perhaps including overlaying one on the other and then superimposing the detected pits on both images.

The prototype end effector system could form the basis of several research and development tasks that would further the technology already demonstrated. Some of these tasks are:

Demonstration of a 'Fly-By' Mode of Tank Wall Inspection

Most of the underground waste storage tanks within the DOE have steel walls; many have diameters in excess of 70' and depth about 35'. The total area to be inspected inside a tank runs to thousands of square feet, therefore regardless of how successful an inspection technique is, the cost of its use is directly related to the time required to inspect the whole of the tank. In order to perform quantifiable NDE of the tank surface, current technologies, including the RTIEE prototype, need to be held stationary over the area to be inspected; the area inspected by the RTIEE prototype is 6"x3" for every placement. With the operation of a manipulator in the tank costing up to hundreds of thousands of dollars a day, detailed inspection of the entire tank surface is obviously impractical. One operational solution to this problem, and the one adopted by the RTIEE design, is to prioritize the detailed inspections by using the vision and lighting system in the end effector to identify what looks like suspicious areas of corrosion before committing the end effector to a detailed ACFM inspection.

This operational approach is defeated when the defects in the tank wall are hard to see (such as cracking at welds), or an obscuring layer is coating the wall (such as paint or deposits). An alternative approach is to develop an NDE inspection system that can detect defects while being moved along the surface of the tank wall. If defects are detected, the operator could then choose to return to the suspect area, land the end effector, and perform a detailed inspection (accurately locating and sizing the feature). To further reduce the tank inspection time, an operator might choose to inspect only the welds between the tank wall plates where cracking is most likely. This fly-by mode of inspection is a possibility for the electromagnetic ACFM NDE technique.

Task objective: The objective of this task would be to demonstrate that an ACFM end effector could detect cracks and pits while moving past a weld bead or flat plate.

Task description: OSS would use the current prototype RTIEE end effector system in a series of developmental experiments that would culminate in a feasibility demonstration of fly-by inspection. Primary technical challenges would be the redesign of the RTIEE electronics to incorporate rapid real-time sampling of the sensor coils and rewriting of the current RTIEE control software to support this new mode of inspection. It would not be the intention of this task to upgrade the existing prototype to a fly-by unit since this expense is unwarranted until the feasibility of this mode of inspection is established. For example, the small diameter of the array coils are not ideally suited to a fly-by type inspection but should be sufficient to conduct feasibility experiments. Based on these experiments larger array coils might be recommended for use in an operational fly-by system.

An important aspect of a field deployable fly-by end effector would be real-time proximity sensing of the wall in front of the end effector. This proximity sensing could be used by a suitable manipulator controller to accurately maintain a fixed standoff from the wall during fly-by. It would not be the intention in this task to develop a proximity sensing system, a fixed standoff from the wall will be maintained by pre-recording a suitable path in the OI/GE arm or Puma arm digital controllers. Development of suitable proximity sensing will be left for other follow on projects (OSS is currently developing this capability under internal R&D funding).

Research Into and Development of a Certification Plan for an ACFM Tank Inspection End Effector

In order for any type of NDE survey to be recognized by a regulatory body and therefore be considered a valid appraisal of the integrity of a structure, the inspection must be carried out in strict adherence to an existing standard, or the inspection device, inspection procedure, and personnel training have to be approved by a certifying authority. Standards in the U.S. are published by the American National Standards Institute (ANSI) and various certifying authorities operate worldwide (Lloyds, TUV, Det Norske Veritas, American Bureau of Shipping).

It is unlikely that suitable standards exist for robotically deployed NDE devices used in underground waste storage tanks. Therefore, for the DOE to inspect their waste tanks, each inspection device they use will need to be certified separately.

Task objective: The objective of this task would be to produce a certification plan for an inspection end effector such as the ACFM RTIEE.

Task description: OSS would identify both the regulatory bodies involved and the possible

certifying authorities. OSS would establish a road map for the certification of an inspection device or process. As required OSS would study issues relating to the certification and regulation of waste storage tank inspections.

Incorporation of Crack Detection and Sizing Capability Into the Prototype RTIEE System

The prototype RTIEE's primary function was the characterization of pitting corrosion damage on steel tank walls. Cracking in the weldments between the tank wall plates is another concern for the field centers. Cracks, like pits, can be detected and sized by ACFM. The welds in the tanks may be proud of the surface by as much as ¼", which makes landing the end effector scanner frame over them a challenge. In addition, cracks, unlike pits, have a distinct preferred orientation for detection by ACFM. This dictates that the current RTIEE design maintain a preferred roll orientation relative to the crack. The RTIEE has already demonstrated the ability to detect some cracks as illustrated in figure 6-1.

Task objective: The objective of this task would be to upgrade the functionality of the prototype RTIEE to include detection and sizing of cracks in plate butt welds at any roll orientation.

Task description: OSS would redesign the prototype scanner frame to allow easy deployment over weld beads and incorporate induction coil and sensor coil changes in the sensor suite to allow the detection of cracks with any orientation of the scanner frame. The detection and sizing software would be modified to include results from the theoretical crack model and to allow an operator to discriminate between cracks and pits.

Technical Risk Reduction For a Tank Ready RTIEE

In order to deploy an end effector into a waste storage tank, several environmental issues must be addressed. The waste tank environment has three main influences on the design of an inspection end effector: RAD hardening of the design, making the end effector explosion proof, and increasing the ease with which the end effector can be decontaminated. Most of the work associated with making an RTIEE tank ready does not represent a significant technical risk. However RAD hardening the RTIEE involves both the replacement of every passive and active electrical component with a hardened equivalent, and a redesign of the electrical layout to relocate a majority of the end effector electronics external to the tank. This presents a challenge not only in redesigning the electronics cards, because the hardened components rarely have the same physical dimensions or functionality as their unhardened forebears, but in minimizing the unwanted effects of signal deterioration and noise due to the greatly increased data transfer distances.

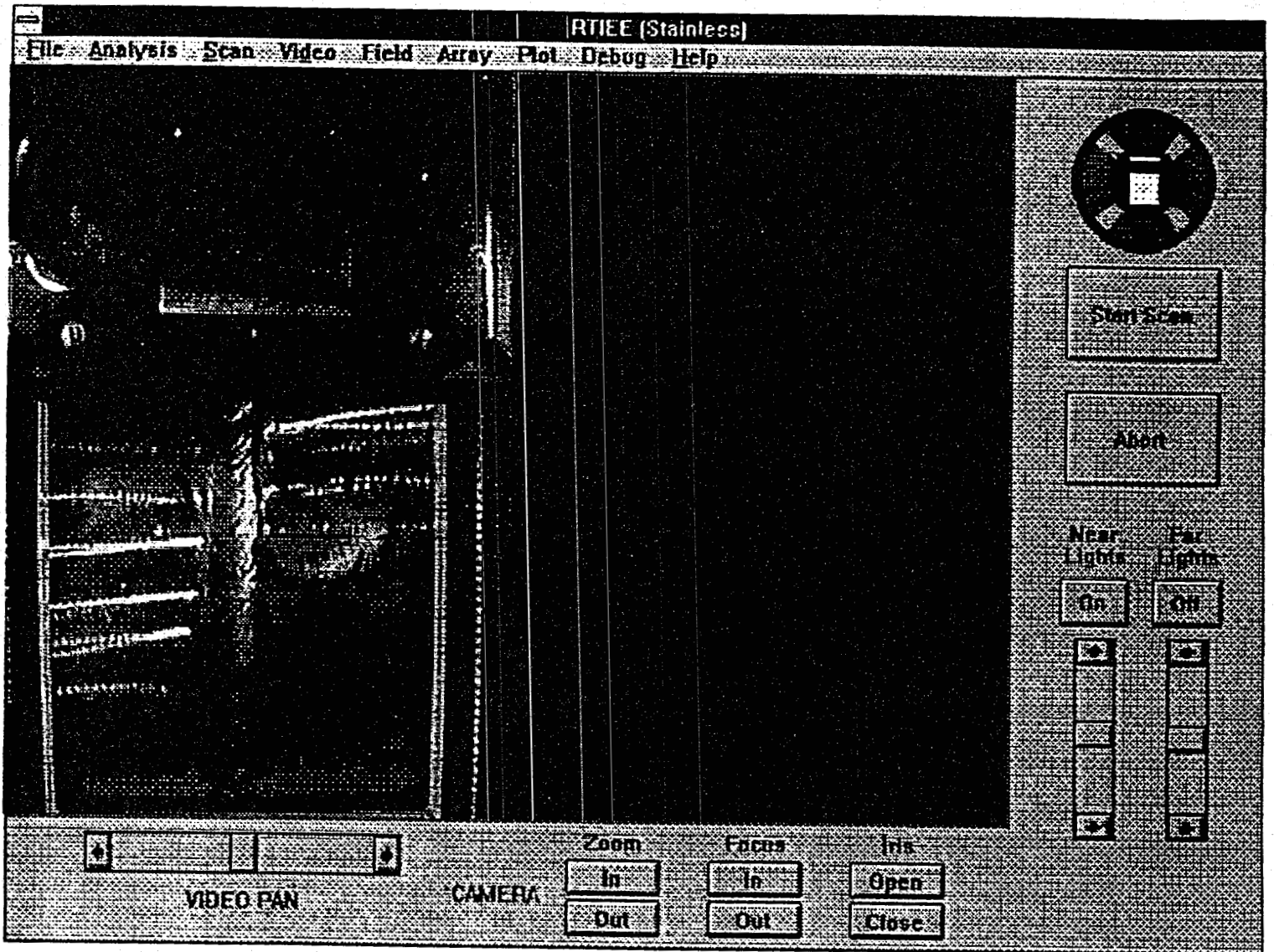


Figure 6-1: RTIEE Crack Detection in a Stainless Steel Weld

Task objective: The objective of this task would be to redesign and test a distributed electrical and electronic layout in the prototype RTIEE system to ensure that the performance of the RTIEE would not be compromised in a tank ready design. This task would not include replacing components with RAD hardened equivalents.

Task description: OSS would redesign the current prototype electronic layout to move the majority of the radiation sensitive components and the on-board processor out of the tank environment. The new design would be implemented and tests conducted to ensure no significant performance loss occurs. The umbilical length will be increased to 150' to simulate the separation of the end effector from the enclosure on top of the tank.

Production of a Tank Ready Inspection End Effector

After the successful demonstration of a prototype end effector a tank ready design can be produced (see Task 4 for a description of some of the required design changes). A significant proportion of the cost of producing a tank ready end effector is associated with the use of RAD hardened components. For example the cost of the end effector camera escalates to \$30K from \$2K if the camera must survive 1×10^6 RAD (the design life for INEL's tanks). Individual OpAmps that cost 70 cents now cost \$200. Another big cost driver is the redesign of the electronic circuitry to accommodate RAD hardened components.

Task description: The prototype system would be redesigned and rebuilt to survive a 1×10^6 RAD dosage. This tank ready design would feature a reconfigured electrical layout with a majority of electronic components relocated in the waste tank At Tank Instrument Enclosure (ATIE). All electrical components left in the end effector will be replaced by radiation hardened units with the associated board redesign and the inclusion of buffer electronics to ensure that data and control signals can be transmitted between the ATIE and end effector. The end effector would be sealed to meet NEPA explosion proofing standards. The covers and exterior surfaces would be remodelled to reduce contamination potential and improve decontamination characteristics.

Appendix B: Wall and Coating Thickness Sensor Measurement Test Summary

Reference: DE-AR21-93MC30363

Introduction

OSS has developed an electromagnetic non-destructive evaluation (NDE) sensor to measure the thickness of carbon steel, stainless steel, and aluminum. In this report the sensor was used to study carbon steel between 0.034" and 0.06" thick. This interest resulted from a focus on the waste storage in carbon steel barrels at several locations overseen by the Department of Energy. The objective of the tests summarized in this report is to be able to accurately measure the thickness of carbon steel (16-gauge and thinner) as both an inspection and a preventative measure. The sensor is intended for use as an indicator of general wall thinning of 16-gauge carbon steel waste storage drums. The ultimate goal is to package this instrument into a simple hand-held sensing device connected to a portable carrying case to perform the NDE of 55-gallon carbon steel drums in the field.

Background/Theory

The inspection system uses a pair of coils to transmit and receive changes in magnetic fields. The transmission coil is driven by a pulsed current, which produces a pulsed magnetic field in the vicinity surrounding the coil. When the coil is placed near a sample, the coil's pulsing magnetic field generates eddy currents in the sample material (in this case, a steel plate). Eddy currents are an example of the law of inertia in the electromagnetic realm (Lentz' Law). The eddy currents are, in effect, a flow of electrons, which try to maintain the balance of the fields. As a result, upon the introduction of a magnetic field, the eddy currents attempt to cancel the presence of this new magnetic field by inducing a secondary opposing magnetic field in the sample material. If the external (the field which was initially introduced due to the coil) field is introduced and then held constant, then the eddy current phenomenon will occur at the same instant as the introduction of the external field, and then the secondary field would also become constant. Because the field surrounding the coils is pulsing, the secondary field is also pulsing. This is because the magnetic field is introduced (pulse turned on) and then taken away (pulse turned off). Now, because each of these events induces an opposing magnetic field, there is also a pulsing flow of eddy currents in the sample material. The secondary pulsing magnetic field of the sample then induces another set of eddy currents in the receiving coil. The eddy currents produced in the receiving coil are then measured by means of the voltage differential between the two coils. Figure 1 shows an illustration of the eddy current phenomenon, which illustrates the opposing fields and induced current.

Because these secondary induced eddy currents in the receiving coil vary with the induced field in the sample material, experiments were performed to determine a relationship correlating the decay of these eddy currents with the thickness of the sample plate. The trend, which is discussed

in further detail in the analysis section of the report, seems to show that eddy current decay increases with material thickness.

Test Description

The Wall Thickness Sensor consists of a pair of concentric coils, one transmits and one receives. A BK Precision 10MHz Sweep/Function Generator (model 4017) produces a square wave, which is converted into a current pulse by the drive signal amplifier. The current pulse then drives the transmitter coil, creating a pulsing magnetic field. The receiving amplifier increases the signal picked up by the receiver coil and passes it on to the A/D data acquisition board. The board is combined with "Snapmaster for Windows" software to record the signal. The block diagram in Figure B-1 shows the details of the setup.

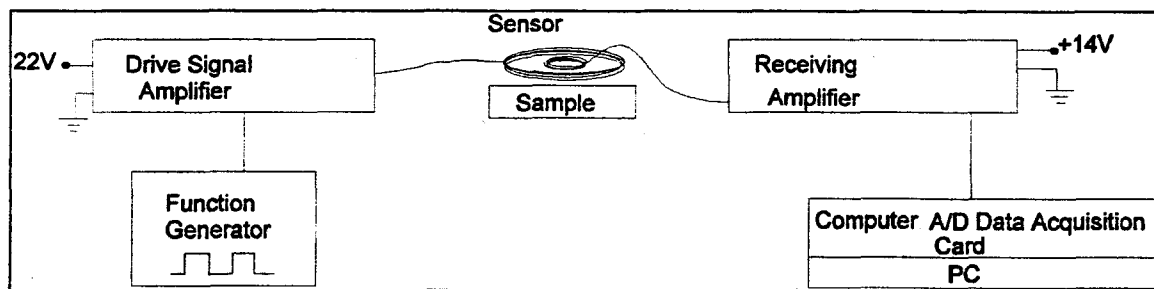


Figure B-1: Test Configuration for wall thickness measurement.

The material samples measured during the tests included carbon steel plates (1008 alloy) and a standard DOT 17-C (16-gauge) carbon steel drum. The alloy of the drum is not known, but the data collected for the drum was consistent with that taken for a rolled plate of the same thickness. The plates were 0.034", 0.046", 0.048", 0.06", 0.1" thick, and the nominal drum wall thickness is 0.06". Most of the plates are 18"x18", though some are narrower (14"x18"). Some of the plates were left flat and some were rolled to a similar radius of curvature to that of the drum to determine the effects of geometry.

Test Results

The data collected (see Figures 2 & 3) was used to develop a mathematical equation which described a relationship between the transient response decay time of the signal and the material thickness. The %-difference was calculated in order to evaluate the fit of the data. The %-difference is the delta between the measured (actual) and calculated (evaluated mathematically) thicknesses, divided by the measured value, and multiplied by 100. The largest %-difference of the data points from the model is 10%.

The effect of standoff or liftoff was also examined. Non-conductive plastic shims (Lexan, cardboard, plastic) were used to establish the standoff between the sensor and the carbon steel samples. As shown in Figure 3, the effect of standoff was negligible at distances of 0.015" and less. A standoff of 0.034" contributed an additional 5% deviation (added to the 10% already present) from the thickness model. At a standoff of 0.125", there is an additional deviation of 10% in some cases.

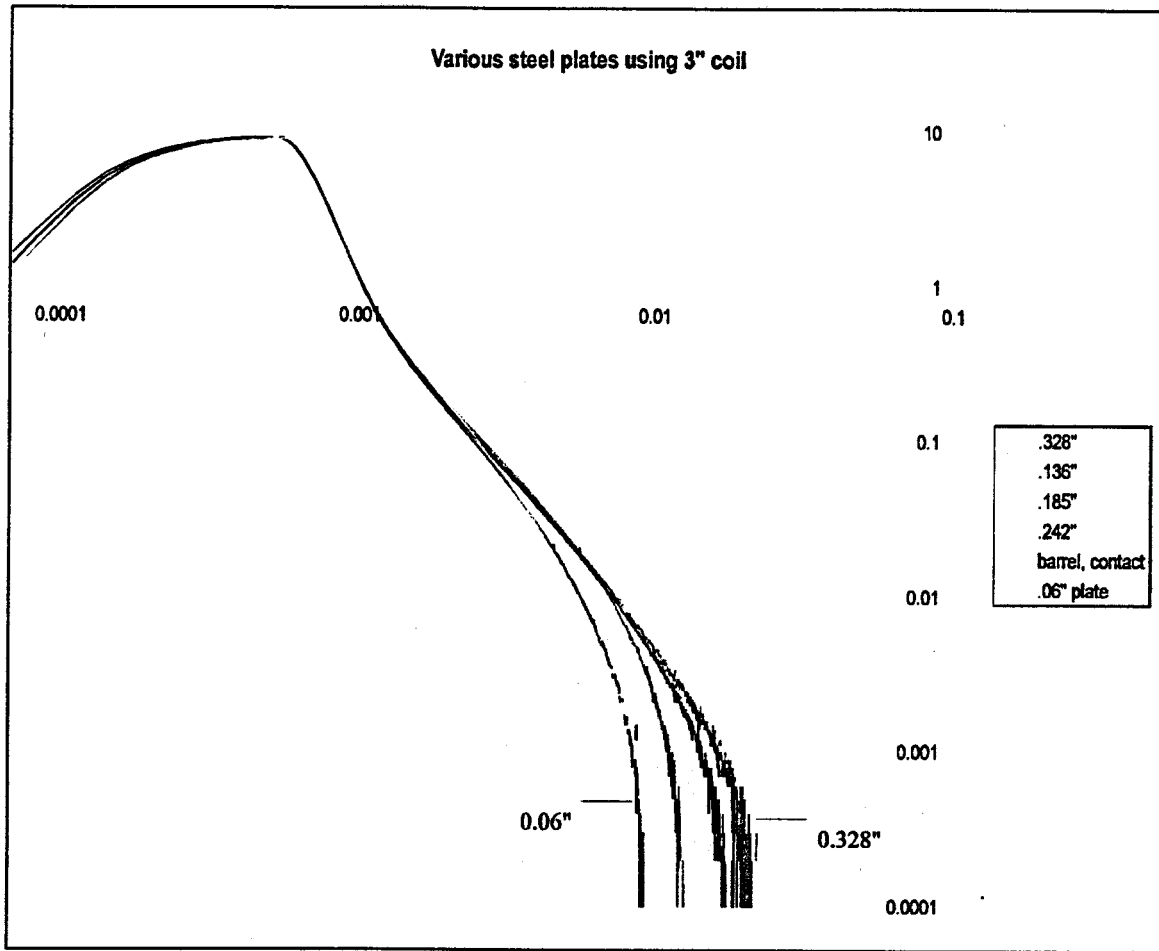


Figure B-2:

Figure B-2: Data collected using a sensor with an outer diameter of 3". The horizontal axis is log time and the vertical axis is log signal voltage. The curves shift to the right for thicker plates. In this graph, the thinnest plate (0.06") lies to the far left (along with the barrel), and the thickest plate lies to the far right.

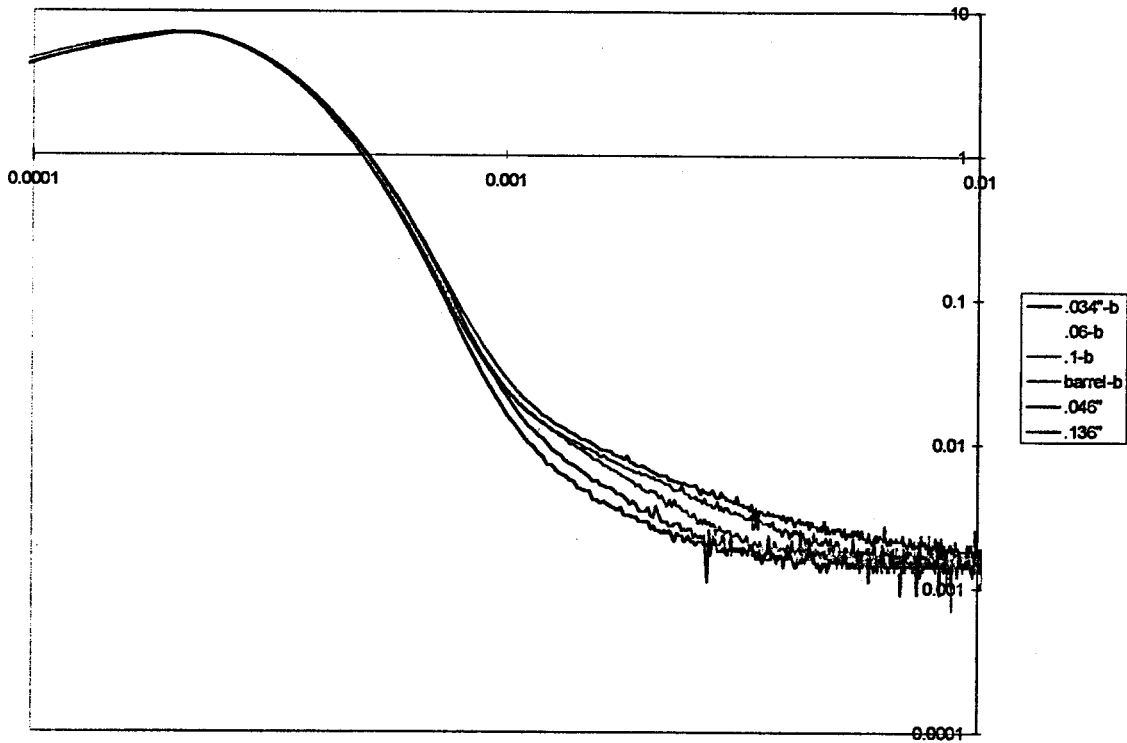


Figure B-3:

Figure B-3: Thickness data collected using a sensor with an outer diameter of 1.0". The horizontal axis is log time and the vertical axis is log signal voltage. The thinnest plate is to the left of the bottom portion of the curve and the thickest plate is the farthest curve to the right.

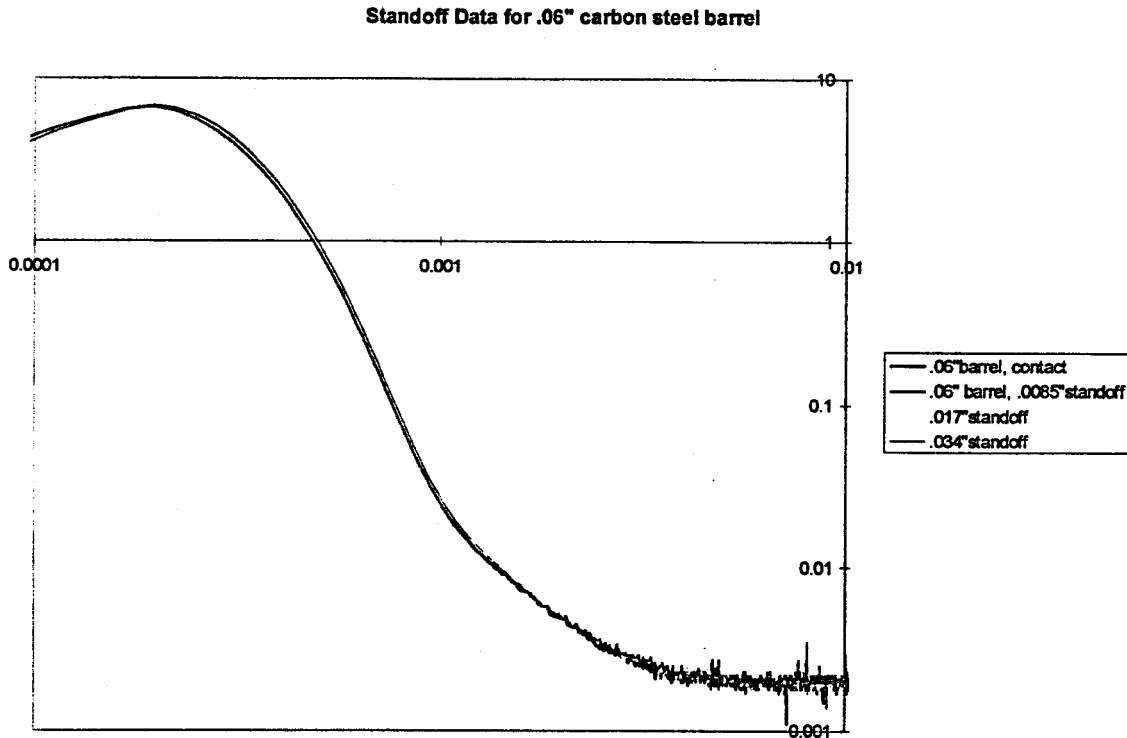


Figure B-4:

Figure B-4: Standoff sensitivity data collected using the 1.0" OD sensor. The horizontal axis is log time (msec) and the vertical axis is log signal amplitude (voltage). Note that the standoff does not significantly differ from the contact data.

Conclusions

The OSS wall thickness sensor can measure thin wall (0.03" to 0.1" thick) carbon steel with a maximum error of about 10%. On average the model tends to be very accurate around 0.06" and 0.034" (50% thinning), giving an error of 1-3%. For small standoff distances, 0.015" and less, the effects of standoff such as might be produced by surface corrosion are negligible.

Unfortunately, work on this promising technology was halted after these early tests due to a lack of interest by any DoE field sites.